Quantum memory: design and applications

Fernando Pastawski

München 2012

Quantum memory: design and applications

Fernando Pastawski

Dissertation

an der

Ludwig-Maximilians-Universität

München

vorgelegt von

Fernando Pastawski

aus Córdoba, Argentinien

München, den 4.6.2012

Tag der mündlichen Prüfung: 26.7.2012

Erstgutachter: Prof. J. I. Cirac

Zweitgutachter: Prof. H. Weinfurter

Weitere Prüfungskommissionsmitglieder: Prof. J. von Delft , Prof. T. Liedl

Abstract

This thesis is devoted to the study of coherent storage of quantum information as well as its potential applications. Quantum memories are crucial to harnessing the potential of quantum physics for information processing tasks. They are required for almost all quantum computation proposals. However, despite the large arsenal of theoretical techniques and proposals dedicated to their implementation, the realization of long-lived quantum memories remains an elusive task.

Encoding information in quantum states associated to many-body topological phases of matter and protecting them by means of a static Hamiltonian is one of the leading proposals to achieve quantum memories. While many genuine and well publicized virtues have been demonstrated for this approach, equally real limitations were widely disregarded. In the first two projects of this thesis, we study limitations of passive Hamiltonian protection of quantum information under two different noise models.

Chapter 2 deals with arbitrary passive Hamiltonian protection for a many body system under the effect of **local depolarizing noise**. It is shown that for both constant and time dependent Hamiltonians, the optimal enhancement over the natural single-particle memory time is logarithmic in the number of particles composing the system. The main argument involves a monotonic increase of entropy against which a Hamiltonian can provide little protection.

Chapter 3 considers the recoverability of quantum information when it is encoded in a many-body state and evolved under a Hamiltonian composed of known geometrically local interactions and a **weak yet unknown Hamiltonian perturbation**. We obtain some generic criteria which must be fulfilled by the encoding of information. For specific proposals of protecting Hamiltonian and encodings such as Kitaev's toric code and a subsystem code proposed by Bacon, we additionally provide example perturbations capable of destroying the memory which imply upper bounds for the provable memory times.

Chapter 4 proposes **engineered dissipation** as a natural solution for continuously extracting the entropy introduced by noise and keeping the accumulation of errors under control. Persuasive evidence is provided supporting that engineered dissipation is capable of preserving quantum degrees of freedom from all previously considered noise models. Furthermore, it is argued that it provides additional flexibility over Hamiltonian thermalization models and constitutes a promising approach to quantum memories.

Chapter 5 introduces a particular experimental realization of coherent storage, shifting the focus in many regards with respect to previous chapters. First of all, the system is very concrete, a **room-temperature nitrogen-vacancy centre in diamond**, which is subject to actual experimental control and noise restrictions which must be adequately modelled. Second, the relevant degrees of freedom reduce to a single electronic spin and a carbon 13 spin used to store a qubit. Finally, the approach taken to battle decoherence consists of inducing motional narrowing and applying dynamical decoupling pulse sequences, and is tailored to address the systems dominant noise sources.

Chapter 6 analyses **unforgeable tokens** as a potential application of these room-temperature qubit memories. Quantum information protocols based on Wiesner's quantum money scheme are proposed and analysed. We provide the first rigorous proof that such unentangled tokens may be resistant to counterfeiting attempts while tolerating a certain amount of noise.

In summary, this thesis provides contributions to quantum memories in four different aspects. Two projects were dedicated to understanding and exposing the limitations of existing proposals. This is followed by a constructive proposal of a new counter-intuitive theoretical model for quantum memories. An applied experimental project achieves record coherent storage times in room-temperature solids. Finally, we provide rigorous analysis for a quantum information application of quantum memories. This completes a broad picture of quantum memories which integrates different perspectives, from theoretical critique and constructive proposal, to technological application going through a down-to-earth experimental implementation.

Zusammenfassung

Diese Arbeit widmet sich der kohärenten Speicherung von Quanteninformation, sowie ihren potenziellen Anwendungen. Quantenspeicher sind wesentlich, wenn es darum geht das Potential der Quantenmechanik für Aufgaben der Informationsverarbeitung zu nutzen. Sie sind Voraussetzung in nahezu allen Vorschlägen zur Realisierung von Quantencomputern. Trotz der Fülle an theoretischen Methoden und Vorschlägen zu ihrer experimentellen Implementierung, steht die Realisierung eines langlebigen Quantenspeichers bis heute aus.

Einer der vielversprechendsten Ansätze zur Implementierung von Quantenspeichern ist es, Information in Quantenzuständen, die zu topologischen Phasen in Vielteilchensystemen gehören und durch einen statischen Hamiltonoperator geschützt werden, zu codieren. Während auf der einen Seite die Vorzüge dieses Ansatzes viel Beachtung gefunden haben und in zahlreichen Arbeiten diskutiert wurden, hat man auf der anderen Seite viele ebenso wichtige Einschränkungen bislang weitgehend ignoriert. In den ersten beiden Projekten dieser Arbeit untersuchen wir Schwierigkeiten, die bei dem Versuch Quanteninformation passiv durch Hamiltonoperatoren zu schützen, auftreten. Hierbei konzentrieren wir uns auf zwei unterschiedliche Modelle zur Beschreibung der äusseren Störeinflüsse.

Kapitel zwei befasst sich mit den Möglichkeiten ein System, das **lokalem depolarisierenden Rauschen** ausgesetzt ist, durch beliebige Hamiltonoperatoren passiv zu schützen. Wir zeigen, dass sich die optimale Erhöhung der Speicherzeit im Vergleich zu Einteilchenspeichern sowohl für konstante als auch zeitabhängige Hamiltonoperatoren logarithmisch zu der Teilchenzahl, aus denen das System besteht, verhält. Die Hauptursache für dieses Verhalten liegt in dem monotonen Anstieg der Entropie.

In Kapitel drei betrachten wir Systeme die einer Zeitentwicklung durch Hamiltonoperatoren, die durch bekannte lokale Wechselwirkungen und eine **beliebige hamiltonsche Störung** beschrieben werden, ausgesetzt sind. Wir leiten allgemeine Kriterien, die von der

codierten Information erfüllt werden müssen, her. Für spezifische Hamiltonoperatoren und Codierungen, wie Kitaevs torischen Code und Bacons 3D Kompas Code, beschreiben wir Beispiele von Störungen, die dazu in der Lage sind den Speicher zu zerstören. Dies impliziert eine obere Beschränkung für Speicherzeiten, die bewiesen werden können.

In Kapitel vier stellen wir ein Konzept vor, mit welchem Entropie, die dem System durch Rauschen zugeführt wurde, durch manipulierbare Dissipation kontinuierlich extrahiert werden kann. Gleichzeitig wird dabei die Akkumulation von Fehlern unter Kontrolle gehalten. Wir zeigen, dass manipulierbare Dissipation die Quanteneigenschaften von all den von uns betrachteten Modellen für Rauschen erhält.

In Kapitel fünf betrachten wir eine konkrete Realisierung von kohärentem Speichern. Hier geht es um eine konkrete physikalische Anwendung in einem NV-Zentrum, in der experimentelle Kontrollmöglichkeiten und realistische Bedingungen für das Rauschen in Betracht gezogen und adäquat modelliert werden müssen. Der Bewegungsfreiheitsgrad ist in diesem System auf nur einen Elektronenspin und einen Kohlenstoff-13 Kernspin beschränkt. Das Konzept, das wir hier zur Bekämpfung von Dekohärenz vorschlagen, besteht aus Bewegungsmittelung und dynamischen Entkopplungs-Pulssequenzen und ist auf das System und seine vornehmlichen Quellen für Rauschen optimiert.

Solch ein Quantenspeicher für Quantenbits in NV-Zentren, der bei Raumtemperatur funktionsfähig ist, stellt unsere Motivation für Kapitel sechs dar. Dort stellen wir Konzepte vor, welche die Realisierung fälschungssicherer Sicherheitslösungen mit derartigen Quantenbits erlauben. Basierend auf Wiesners Quantengeld-Schema entwickeln wir neue Quanteninformations-Protokolle. Wir stellen hier den ersten rigorosen Beweis vor, dass derartige unverschränkte Sicherheitslösungen gegen Fälschungsversuche sicher wären und außerdem eine bestimmte Menge an Rauschen tolerieren könnten.

Zusammenfassend liefert diese Doktorarbeit einen Beitrag zu Quantenspeichern aus vier verschiedenen Perspektiven. Zwei Projekte sind dem Verständnis und den Limitierungen von bestehenden Konzepten gewidmet. Dann stellen wir ein neuartiges, kontraintuitives, theoretisches Konzept zur Realisierung eines Quantenspeichers vor. In Kollaboration mit einer experimentellen Arbeit ist der Rekord von kohärenten Speicherzeiten bei Raumtemperatur gebrochen worden. Außerdem stellen wir eine rigorose Beschreibung von Quanteninformationsanwendungen für Quantenspeicher vor.

Contents

PhD Publications

This thesis is based on the following publications, which resulted from research conducted during the author's PhD. Some copyrighted material from these articles is reproduced with permission of APS, AAAS, PNAS and Rinton editorial.

1. *How Long Can a Quantum Memory Withstand Depolarizing Noise?*
   Fernando Pastawski, Alastair Kay, Norbert Schuch, and J. Ignacio Cirac
   Phys. Rev. Lett. **103**, 080501 (2009). (See chapter 2) as well as the original published article appended to this thesis with permission of APS.

2. *Limitations of Passive Protection of Quantum Information*
   Fernando Pastawski, Alastair Kay, Norbert Schuch, and J. Ignacio Cirac
   Quant. Inf. and Comp. **10**, (7&8) 0580-0618 (2010). (See chapter 3)

3. *Quantum memories based on engineered dissipation*
   Fernando Pastawski, Lucas Clemente, and J. Ignacio Cirac
   Phys. Rev. A **83**, 012304 (2011). (See chapter 4)

4. *Room-Temperature Quantum Bit Memory Exceeding One Second*
   Peter C. Maurer, Georg Kucsko, Christian Latta, Liang Jiang, Norman Y. Yao, S. Bennett, Fernando Pastawski, D. Hunger, N. Chisholm, M. Markham, D. Twitchen, D. J. Ignacio Cirac, and Mikail D. Lukin
   Science **336** 1283-1286 (2012). (See chapter 5) as well as the original published article appended to this thesis with permission from AAAS.

5. *Unforgeable Noise-Tolerant Quantum Tokens*
   Fernando Pastawski, Norman Y. Yao, Liang Jiang, Mikhail D. Lukin, and J. Ignacio Cirac arXiv:1112.5456 (2011). (See chapter 6)

Chapter 1

Introduction

Quantum mechanics is the well established physical theory describing the world below the Planck scale. With the advent of integrated circuits and Moore's law [92] predicting a doubling in their transistor density every two years, it soon became clear that it would eventually become necessary to seriously take quantum effects into account. In this context, some ideas of quantum computing and quantum information unavoidably began to emerge in the 1970' and early 1980' in the minds of physicists and computer scientists such as Charles H. Bennett, Paul A. Benioff, David Deutsch and Richard P. Feynman [17, 15, 40, 33]. It was time to move on from the models of billiard ball computing and embrace the era of quantum information.

While it became clear early on [33] that a quantum computer would be at least as powerful as a classical one, expected advantages of a quantum computer were apparently limited to simulating quantum-mechanical systems [40] in addition to solving a few relatively contrived mathematical problems. There was also no pressing urge from the microelectronics industry to better understand the workings of quantum information. This all changed with the break-through result of Peter Shor [112], who in 1994 proposed an algorithm by which a quantum computer could factor large numbers in a time exponentially faster than most practical classical algorithms. If implemented, Shors algorithm could be used to crack mainstream cryptographic codes such as RSA [107] for which the difficulty of factoring is essential. Since then, quantum computation has received a huge amount of attention, not only from the scientific community, but from the whole world.

Ironically, in their seminal work of 1984, Charles Bennett and Gilles Brassard [16] had already proposed a quantum key distribution scheme, which could potentially substitute RSA

allowing for cryptographically secure private communication even in a world with quantum computers. However, contrary to popular belief, this was not the first cryptographic protocol relying on the quantum nature of information. Stephen Wiesner[129], had been ahead of his time in proposing the use of bank notes which were impossible to duplicate due to the quantum character of the state defining them, a topic which we will get back to in the last chapter of this thesis.

As illustrated, quantum computing and quantum information are both of technological and fundamental appeal. This brings us to the topic of this thesis, quantum memories, which are expected to play a central role in the implementation of quantum information technologies. They are required to perform entanglement swapping and are thus crucial for long-distance quantum key distribution. They are necessary in almost all models of quantum computation, where it is ubiquitous to have data wait. Finally, the quality of a quantum memory constitutes a benchmark for the degree of coherent quantum control achievable within a system and may be used to compare different technologies.

This thesis is devoted to the understanding and design of quantum memories and their applications. We present the five projects in the subsequent chapters with these general goals in mind. The first two (chapters 2 and 3) explore existing proposals for many-body quantum memories exposing their limitations and understanding their virtues. The following two (chapters 4 and 5) propose implementations of quantum memories, first paying attention to scaling in an abstract many-body context and later concentrating on a concrete experimental quantum optics setting, namely Nitrogen-vacancy centers. Inspired by record coherence times, in the chapter 6, we propose an application consisting of tokens impossible to counterfeit.

The main contributions of this thesis are to the field of many-body quantum memories (chapters 2 , 3 and 4). In order to better understand these contributions, it is convenient to set the context in terms of pre-existing developments such as fault-tolerant quantum computation [47] and topological quantum memory [73, 32, 74].

The theory of fault-tolerant quantum computation [47] proves that it is possible to simulate an ideal circuit model quantum computer using only imperfect (yet sufficiently good) single and two qubit gates, initialization of ancillary qubits and measurements. Quantum memories may be seen as representing the most trivial computation, the identity. In particular, one should be able to compute the identity function within universal models of quantum

computation such as the fault tolerant circuit model. In practice however, the experimental requirements imposed by fault tolerant quantum computation have up to now proven prohibitively difficult to achieve. This has motivated ongoing research to find alternative routes to both quantum computing and quantum memory.

Topological quantum computing and quantum memory, a revolutionary idea introduced by Kitaev in 1997 [73, 32, 74], promises to attain fault-tolerance by means of an alternate route, more akin to physics than to circuit engineering. At the core of this approach is the independence of an anyonic quasi-particle picture from specific microscopic details of the defining Hamiltonian. During the time of this thesis and the period preceding it many of the claims pertaining to these proposals have been rigorously proven, and some of the folklore that has arisen from it has been dissipated. The contributions of chapter 2 and 3 have been partly responsible for this.

The toric code [74] is the most simple and hence the most widely popularized representative for the topological approach to fault tolerance. It is associated to two related, yet distinct, concepts both involving physical qubits placed on the edges of a 2d lattice on a torus. First, the toric code refers to a stabilizer **quantum error correcting code** accommodating two logical qubits. As such, it enjoys desirable properties such as

- **Geometrically local check operators**: Only quantum measurements involving groups of four nearest neighbour qubits are needed in order to diagnose physical errors.
- **Large code distance**: The minimal number of single qubits that must be acted upon in order to go from one logical state to an orthogonal one is proportional to the perimeter of the torus. [1]
- **High error threshold**: The code is capable of correcting random flip and phase errors on up to $\approx 11\%$ of the qubits in the limit of large torus.

Second, the **toric-code Hamiltonian** is obtained from interpreting the Hermitian stabilizer operators as local Hamiltonian terms acting on groups of two-level systems. The resulting Hamiltonian enjoys the following properties:

- **Geometrically local interaction**: Geometrically local terms in the Hamiltonian can be associated to geometry local effective interactions.

[1] By perimeter, we mean the minimal number of edges to non-trivially wind around the torus.

- **Degenerate ground state**: Information can be thought of as being accommodated in a 4-fold degenerate ground space.[2]

- **Robust degeneracy**: For a weak geometrically local yet extensive perturbation, the degeneracy of the ground space is approximately preserved.

- **Energy gap**: An energy gap suggests that excitations out of the ground space could be thermally suppressed.

These two related notions of toric code have regretfully led to some confusion among part of the quantum information community. The wide-spread belief that implementing a toric code Hamiltonian would guarantee a quantum memory to be protected against any form of local noise is a paragon example of such misconception. Results provided in this thesis have been crucial in rigorously elucidating limitations of Hamiltonian protection models and proposing alternatives to overcome them.

In particular, chapter 2 provides a definite proof that no Hamiltonian may by itself provide significant protection against depolarizing noise. We consider a system which is subject to both a unitary evolution generated by a Hamiltonian and the dissipative effect of local depolarizing noise over the constituent particles. The motivation behind choosing a local depolarizing noise model can be traced to infrequent yet highly energetic interactions capable of randomizing the state of single components. For this noise model the approach towards a maximally mixed steady state may not be postponed by a Hamiltonian. Entropy accumulates at an unavoidable rate, and all that can be achieved by a Hamiltonian is to transfer it into irrelevant degrees of freedom. We show that the optimal protection afforded by a constant Hamiltonian only marginally increases the lifetime of quantum information from constant to logarithmic in the number of system constituents.

Along similar lines, chapter 3 studies the degree of protection that may be afforded by a protecting Hamiltonian against Hamiltonian perturbations and perturbative coupling to an environment. Contrasting with the previous chapter, possible evolutions are unitary yet our ignorance of the specific perturbation applied and/or entanglement with the environment lead to effective loss of information. We show that an encoding through an error correcting

[2]The degeneracy of the ground space only depends on the genus of the surface represented by the lattice, hence the name topological.

code with a finite error threshold is a necessary condition for information to withstand such perturbed evolutions. This justifies the assumption of an initial encoding and final decoding of information before and after the free evolution of a many body system. We go on to describe adversely chosen Hamiltonian perturbations which are capable of destroying information "protected" by the toric code Hamiltonian even if the final state is decoded using the underlying error correcting code. Finally, we show that either time dependent perturbations or weak coupling to an energetic environment are sufficient to erase information from a large class of protecting Hamiltonians and codes.

In chapter 4 we propose engineered dissipation as an alternative capable of protecting quantum information against a wider variety of noise. In the spirit of protecting Hamiltonians, we consider the engineering of a constant Liouvillian to protect encoded information. The hope, is that by imposing a constant dynamics one may sidestep the requirement of fast time dependent external control. The advantage with respect to protecting Hamiltonians is that Liouvillians are capable of extracting entropy from the system. We provide numerical and analytical evidence that such dissipative protection can protect information against depolarizing noise. However, the challenge of simplifying the required Liouvillians to forms which are also geometrically local and experimentally realistic remains open.

The first chapters of this thesis (2, 3 and4) study protecting Hamiltonians and dissipative dynamics focusing on the thermodynamic limit for the number of particles used to encode quantum information. In contrast, chapter 5 considers the opposite extreme, where quantum information is stored in a single ^{13}C nuclear spin. The system of choice is the Nitrogen-Vacancy (NV) center, whose physics is similar to that of an isolated atom. Here attention is directed at identifying leading decoherence sources and using available control to suppress them to the highest degree achievable. As a result of the simultaneous combination of multiple decoupling techniques it was possible to achieve an experimental spin coherence time of approximately two seconds, a time unprecedented among room temperature solid state qubits.

In the case of these qubit memories one of the implicit requirements for quantum computation may actually be missing. Indeed, the approach taken and the chosen parameter regime do not allow the coherent transfer of the stored qubit into another quantum system, i.e. the memory system can become classically correlated during measurement but not entangled.

This excludes the possibility of performing general quantum computation or implementing entanglement-based protocols. A naturally arising question is how such a qubit with long coherence can be applied. While magnetometry is likely to be the most immediate technological application, it turns out that the initialization, coherent storage and measurement of single quantum bits is also sufficient for certain protocols which we will discuss.

Among the protocols realizable with prepare and measure qubits, is the original proposal of Wiesner [129], which exploits the impossibility of cloning quantum information to devise money tokens which are immune to forgery. In Wiesner's scheme, a quantum bank-note consists of a large number of qubits, each prepared in a secret pure state only known to the issuing bank. In contrast to classical objects, the destructive nature of quantum measurements forbids the reproduction of the quantum-banknotes even by the holder of a perfect specimen. Recently, extensions to Wiesner's original "quantum money" protocol have attracted significant attention, mainly focussing on resolving the pending issue of making the money tokens publicly verifiable [1, 86, 94, 38, 39, 85]. One particular extension resolves the issue of public authentication of quantum tokens by requiring a classical public communication channel with the bank[44].

Under assumptions of ideal measurements and decoherence-free memories such security can be quantitatively guaranteed by providing a bound on the success probability of any counterfeiting attempt which is exponentially small in the number of qubits employed. These results are a relatively straightforward generalization of optimal cloning[128] to pure product states. However, in any practical situation, noise, decoherence and operational imperfections abound. Furthermore, in non-scalable qubit memories such as for the ^{13}C nuclear spins in NV-centers, there is no single system parameter with which the storage fidelity can be made to systematically converge to 1. These reasons motivate the development of secure "quantum money"-type primitives capable of tolerating realistic infidelities, which is the main original contribution presented in chapter 6.

In order to tolerate noise, the verification of quantum tokens must condone a certain finite fraction of qubit failures; naturally, such a relaxation of the verification process enhances the ability for a dishonest user to forge quantum tokens. While the definition of such a protocol adapted to tolerate noise is straightforward, providing proofs for the security of such protocols under counterfeiting attacks is significantly more involved. We provide such rigorous proofs

and determining tight fidelity thresholds under which the security of the protocol can be guaranteed. This is done for a natural relaxation of Wiesner's original protocol [129] as well as for a simplified version of Gavinsky's protocol [44] which allows for public verification provided a classical communication channel with the issuing bank.

This last project provides a suitable closure to this thesis. It demonstrates that new quantum information applications will become available as soon as we achieve long time coherent storage. It thus provides additional motivation to the work of previous chapters and further reserach along those lines.

Chapter 2

Hamiltonian memory model under depolarizing noise

In this chapter, we investigate the possibilities and limitations of passive Hamiltonian protection of a quantum memory against depolarizing noise. Without protection, the lifetime of an encoded qubit is independent of N, the number of qubits composing the memory. In the presence of a protecting Hamiltonian, this lifetime can increases at most logarithmically with N. We construct an explicit time-independent Hamiltonian which saturates this bound, exploiting the noise itself to achieve protection.

2.1 Introduction

A cornerstone for most applications in quantum information processing is the ability to reliably store qubits, protecting them from the adversarial effects of the environment. Quantum Error Correcting Codes (QECC) achieve this task by encoding information in such a way that regular measurements allow for the detection, and subsequent correction, of errors [111, 3, 47, 48]. An alternative approach uses so-called *protecting Hamiltonians* [74, 11], which permanently act on the quantum memory and immunize it against small perturbations. Presumably, its most attractive feature is that, in contrast to QECC, it does not require any regular intervention on the quantum memory, encoding and decoding operations are only performed at the time of storing and retrieving the information. Whereas this approach may

tolerate certain types of perturbation [32, 9], it is not clear if it is suitable in the presence of depolarizing noise, something which QECC can deal with.

We give a complete answer to this question. More specifically, we consider the situation where a logical qubit is encoded in a set of N physical qubits and allowed to evolve in the presence of depolarizing noise and a protecting Hamiltonian. The goal is to find the strategy delivering the longest lifetime, τ, after which we can apply a decoding operation and reliably retrieve the original state of the qubit. By adapting ideas taken from [4], it is established that the lifetime cannot exceed $\log N$. An analysis of the case in which no protecting Hamiltonian is used presents markedly different behaviour depending on whether we intend to store classical or quantum information. Finally, we construct a static protecting Hamiltonian that saturates the upper bound $\tau \sim O(\log N)$. To this end, we first show how to achieve this bound using a time–dependent Hamiltonian protection which emulates QECC. We then introduce a clock gadget which exploits the noise to measure time (similar to radiocarbon dating) thus allowing us to simulate the previous time dependent protection without explicit reference to time.

We consider a system of N qubits, each of which is independently subject to depolarizing noise at a rate r. The total state evolves as

$$\dot{\rho}(t) = -i[H(t), \rho(t)] - r\left[N\rho(t) - \sum_{n=1}^{N} \mathrm{tr}_n(\rho(t)) \otimes \frac{\mathbb{1}_n}{2}\right], \tag{2.1}$$

where the sub-index n in the identity indicates the position it should take in the tensor product. Note that the defined dynamics is Liouvilian and may also be explicitly expressed in terms of Lindblad operators as

$$\dot{\rho}(t) = \mathcal{L}(t)\rho(t) = -i[H(t), \rho(t)] + r/4\left[\sum_{n=1}^{N} \sum_{L\in\{\sigma_x^{(n)},\sigma_y^{(n)},\sigma_z^{(n)}\}} L\rho(t)L^\dagger - \frac{1}{2}\left\{L^\dagger L, \rho\right\}_+\right], \tag{2.2}$$

where $\{\sigma_x, \sigma_y, \sigma_z\}$ are the Pauli matrices and the supra-index (n) indicates in which of the physical qubit they act on.

We shall allow for an arbitrary encoding of the initial state as well as a final decoding procedure to recover the information. In this sense, the relevant memory channel will be defined defined as

$$\Lambda_t = \mathsf{Dec}_t \circ e^{\mathcal{L}t} \circ \mathsf{Enc} \tag{2.3}$$

where Enc and Dec_t are arbitrary encoding and decoding operations from/into a two level system. A standard benchmark for the quality of a quantum memory will be the average

channel fidelity [98] given by

$$\overline{F}(\Lambda_t) = \int d\psi \, \langle\psi| \, \Lambda_t(|\psi\rangle \langle\psi|) \, |\psi\rangle \,, \tag{2.4}$$

where the average is taken respect to the unitary invariant Haar measure over pure qubit states.

2.2 Protection limitations

Using purely Hamiltonian protection, a survival time of $\tau \sim O(\log N)$ is the maximum achievable. Intuitively, this is due to the fact that the depolarizing noise adds entropy to the system, while any reversible unitary operation (i.e., Hamiltonian evolution) will never be able to remove this entropy from the system. Rather, in the best case, it can concentrate all the entropy in a subsystem, keeping the remaining part as pure as possible. This entropic argument was first presented in [4], where the authors investigated the power of reversible computation (both classical and quantum) subject to noise in the absence of fresh ancillas. To this end, they considered the *information content* $I(\rho) = N - S(\rho)$ of the system, with N the number of qubits and $S(\rho) = -\operatorname{tr}(\rho \log_2 \rho)$ the von Neumann entropy. The information content upper bounds the number of classical bits extractable from ρ, and thus ultimately also the number of qubits stored in ρ.

While the original statement about the decrease of $I(\rho)$ is for discrete-time evolution, it can be straightforwardly generalized to the continuous time setting of Eq. (2.1), where it states that

$$\frac{dI(\rho)}{dt} \leq -rI(\rho) \tag{2.5}$$

In order to prove 2.5 we consider the channel described by $e^{\mathcal{L}\Delta t}$ in the limit of small Δt and perform a Trotter decomposition which splits the Hamiltonian and dissipative terms of the Liouvillian. The Hamiltonian term is seen to preserve the entropy and hence the information content of any state whereas according to [4], the depolarizing term can be seen to increase the entropy by at least $(1 - e^{-r\Delta t})I(\rho) \approx r\Delta t I(\rho)$. We may then integrate inequality 2.5 to bound $I(\rho(t)) \leq e^{-rt} I(\rho(0)) \leq e^{-rt} N$ which implies that the information content of the system is smaller than ε bits after a time $\frac{\ln N/\varepsilon}{r}$. Finally, having the information content of all evolved states be smaller than one implies severe bounds on the average fidelity $\overline{F}$, even when allowing for a final decoding step.

Having established an upper bound for the scaling of τ with N, let us analyze whether this bound can be reached under different circumstances. We start out with the simplest case where we use no Hamiltonian protection (i.e., $H = 0$) and show that τ is independent of N; that is, no quantum memory effect can be achieved. For that, we note that the effect of Eq. (2.1) on each physical qubit may be expressed in terms of a depolarizing channel

$$\mathcal{E}_t(\rho) = \lambda(t)\rho + (1 - \lambda(t))\frac{\mathbb{1}}{2}$$

where $\lambda(t) = e^{-rt}$. For $t \geq t_{\mathrm{cl}}$, where $\lambda(t_{\mathrm{cl}}) = \frac{1}{3}$, the resulting channel is entanglement breaking [59]. This remains true if one incorporates encoding and decoding steps on the full system. This is, the map $\mathsf{Dec} \circ E_t^{\otimes N} \circ \mathsf{Enc}$ which incorporates encoding and decoding from/into a two level system remains entanglement breaking with respect to any other system. According to [59], the average fidelity [98] for any entanglement breaking channels is upper-bounded by 2/3. Thus, we may say that the lifetime τ is smaller than $t_{\mathrm{cl}} = \ln 3/r$, which is independent of N.

The previous argument does not apply to classical information, for which an optimal storage time logarithmic in N may be achieved. The classical version of Eq. 2.1, taking $H(t) \equiv 0$, is a system of N classical bits subject to bit flipping noise (each bit is flipped at a rate $r/2$). In this case, encoding in a repetition code, and decoding via majority voting, yields an asymptotically optimal information survival time $O(\log N)$. Using optimal estimation [89] and this classical protocol in the encoding phase, the bound 2/3 for the average channel fidelity may be asymptotically reached. An intuitive way to see this is to consider an encoding which produces N copies of a single observable (say σ_z) from the original qubit. This observable may be restored as reliably as a classical memory whereas complementary observables (say σ_y and σ_x) are effectively guessed leading to an average fidelity of 2/3.

2.3 Time dependent protection

We will now use the ideas of QECC to build a simple circuit based model that reaches the upper bound on the protection time. This model assumes that unitary operations can be performed instantaneously, which is equivalent to having a time–dependent protecting Hamiltonian with unbounded strength; we will show how to remove both requirements later on. Instead of using a repetition code, we encode the qubit to be protected in an l level

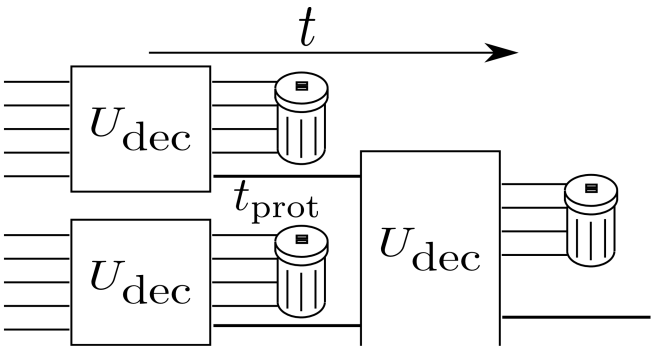

Figure 2.1: Decoding a nested QECC. The "discarded" qubits carry most of the entropy and are not used further.

concatenated QECC [3, 47, 48] (i.e., l levels of the QECC nested into each other), which requires $N = d^l$ qubits, where d is the number of qubits used by the code. Each level of the QECC can provide protection for a constant time $t_{\mathrm{prot}} < t_{\mathrm{cl}}$, and thus, after t_{prot} one layer of decoding needs to be executed. Each decoding consists of a unitary U_{dec} on each d-tuple of qubits in the current encoding level; after the decoding, only one of each of the d qubits is used further (Fig. 2.1). The total time that such a concatenated QECC can protect a qubit is given by $t_{\mathrm{prot}} l = t_{\mathrm{prot}} \log_d N \sim O(\log N)$, as in the classical case.

2.4 Time-independent protection

In the following, we show that the same $\log N$ protection time which we can achieve using a time-dependent protection circuit can also be obtained from a time-independent protecting Hamiltonian. The basic idea of our construction is to simulate the time-dependent Hamiltonian presented before with a time independent one. To this end, a clock is built which serves as control. The time-independent version performs the decoding gates conditioned on the time estimate provided by the clock. In order to obtain a clock from (2.1) with a time-independent H, we will make use of the noise acting on the system: we add a number, K, of "clock qubits" which we initialize to $|1\rangle^{\otimes K}$ and let the depolarizing noise act on them. The behavior of the clock qubits is thus purely classical; they act as K classical bits initialized to 1 which are being flipped at a rate $r/2$. Thus, the polarization k, defined by the number of "1" bits minus the number of "0" bits has an average expected value of $\bar{k}(t) = Ke^{-rt}$ at time

t. Conversely, this provides the time estimate

$$\tilde{t}(k) = \min\left(\frac{\ln(K/k)}{r}, t_{\max}\right). \tag{2.6}$$

Particular realizations of this random process of bit flips can be described by a polarization trajectory $k(t)$. *Good trajectories* are defined to be those such that

$$|k(t) - \bar{k}(t)| < K^{1/2+\varepsilon} \tag{2.7}$$

for all $0 \leq t \leq t_{\max}$. For appropriate parameters $t_{\max}$ and $0 < \varepsilon < \frac{1}{2}$, the following theorem states that almost all trajectories are good and can provide accurate time estimates.

Theorem 2.4.1 (Depolarizing clock) *For $K \geq 16$, good trajectories have a probability*

$$P\left[k(t) \text{ good traj.}\right] \geq 1 - K\frac{rt_{\max} + \exp[-3K^{2\varepsilon}/8]}{\exp[K^{2\varepsilon}/8]} \ . \tag{2.8}$$

Furthermore, for any good trajectory $k(t)$, the time estimate $\tilde{t}$ returned by the clock will differ from the real time t by at most

$$\frac{\delta}{2} := \frac{1}{rK^{1/2-\varepsilon}} e^{rt_{\max}} \geq |\tilde{t}(k(t)) - t| \ . \tag{2.9}$$

Note that the theorem does not simply state that any time evolution will be outside (2.7) for an exponentially small amount of time (which is easier to prove), but that there is only an exponentially small number of cases in which (2.7) is violated *at all*. Although the former statement would in principle suffice to use the clock in our construction, the stronger version of the theorem makes the application of the clock, and in particular the error analysis, more transparent and will hopefully lead to further applications of the clock gadget.

Proof. To prove the theorem, note that each of the bits undergoes an independent exponential decay, so that the total polarization is the sum of K identical independent random variables. We can thus use Hoeffding's inequality [58] to bound the probability of finding a polarization far from the expected average value $\bar{k}(t)$,

$$\mathbf{Pr}\left[|k(t) - \bar{k}(t)| \geq K^{1/2+\varepsilon}\right] \leq 2e^{-\frac{K^{2\varepsilon}}{2}} \ . \tag{2.10}$$

This already implies that most of the trajectories violate (2.7) for no more than an exponentially small amount of time. To see why (2.10) implies that most trajectories are good trajectories, we bound the average number of times a trajectory leaves the region (2.7) of

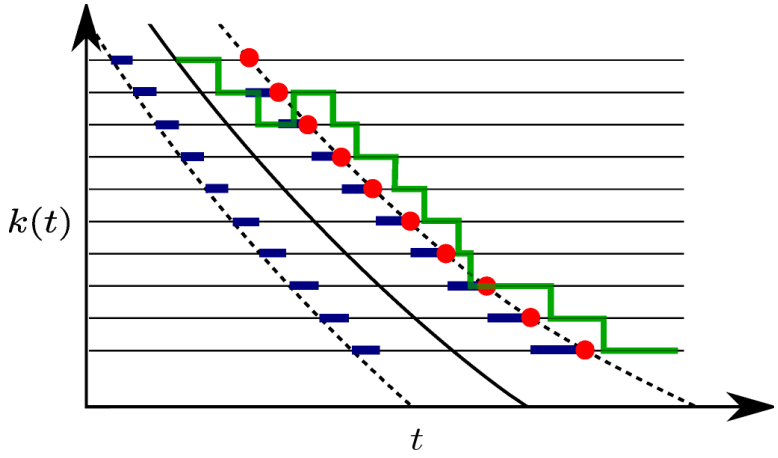

Figure 2.2: A step-like trajectory in green illustrates the two ways of leaving region (2.7) of good trajectories (dashed lines): either a spin flip can take the polarization out of the marked region (thick blue), or polarization may leave region (2.7) as time passes without a spin flip (red dots).

good trajectories. Since a non-good trajectory must leave (2.7) at least once, it is also an upper bound on the probability of non-good trajectories. Hence, it suffices to consider the average rate $R(t)$ at which processes leave (2.7), and integrate over t to obtain a bound on the probability of trajectories which are not good.

The rate at which a process leaves the set of good trajectories has two sources, as illustrated in Fig. 2.2: First, the system can undergo a spin flip, thus leaving the region defined by (2.7) vertically (rate R_v), and second, it can leave it horizontally if the time t passes the maximum time allowed by (2.7) for the current value $k(t)$ of the polarization (rate R_h). A vertical leave can occur only if $|k(t) - \bar{k}(t)| \geq K^{1/2+\varepsilon} - 2 \geq K^{1/2+\varepsilon}/2$, provided $K \geq 16$ (a spin flip changes $k(t)$ by ± 2). Eqn. (2.10) thus gives an average bound

$$R_v(t) \leq Kre^{-K^{2\varepsilon}/8} \ .$$

A horizontal leave can only occur at discrete times extremizing (2.7),

$$t \in \mathcal{T} = \{t : \bar{k}(t) + K^{1/2+\varepsilon} \in \mathbb{N}\} \ ,$$

and the probability of a trajectory fulfilling $k(t) = \bar{k}(t) + K^{1/2+\varepsilon}$ may again be bounded using (2.10), such that

$$R_h(t) \leq 2e^{-K^{2\varepsilon}/2} \sum_{\tau \in \mathcal{T}} \delta(t - \tau) \ .$$

The inequality (2.8) follows immediately by integrating $R_h(t) + R_v(t)$ from 0 to $t_{\max}$.

Assuming that $k(t)$ corresponds to a good trajectory, the accuracy of the time estimate (2.6) may be bounded by applying the mean value theorem to $\bar{k}$:

$$|\tilde{t}(k(t)) - t| = \frac{|\bar{k}(\tilde{t}(k(t))) - \bar{k}(t)|}{|\bar{k}'(t_{\text{interm}})|} \leq \frac{K^{\varepsilon}}{r\sqrt{K}} e^{r t_{\max}} \ .$$

■

2.4.1 Clock dependent Hamiltonian

Let us now show how the decoding circuit can be implemented using the clock gadget. The circuit under consideration consists of the decoding unitaries $U_{\text{dec}}^{l,k}$ (decoding the k'th encoded qubit in level l, acting on d qubits each); after a time interval t_{prot} (the time one level of the code can protect the qubit sufficiently well), we perform all unitaries $U_{\text{dec}}^{l,k}$ at the current level l—note that they act on distinct qubits and thus commute. Each of these unitaries can be realized by applying a d-qubit Hamiltonian $H_{\text{dec}}^{l,k}$ for a time $t = t_{\text{dec}}$. Thus, we have to switch on all the $H_{\text{dec}}^{l,\cdot}$ for $t \in [t_l, t_l + t_{\text{dec}}]$, where $t_l = l\, t_{\text{prot}} + (l-1) t_{\text{dec}}$.

In order to control the Hamiltonian from the noisy clock, we define clock times $k_{l,\text{on}} = \lfloor \bar{k}(t_l) \rfloor$ and $k_{l,\text{off}} = \lceil \bar{k}(t_l + t_{\text{dec}}) \rceil$, and introduce a time-independent Hamiltonian which turns on the decoding Hamiltonian for level l between $k \in [k_{l,\text{on}}, k_{l,\text{off}}]$,

$$H = \sum_l \left(H_{\text{dec}}^{l,1} + \cdots + H_{\text{dec}}^{l,d^{L-l}} \right) \otimes \Pi_l \ . \tag{2.11}$$

The left part of the tensor product acts on the N code qubits, the right part on the K clock (qu)bits, and

$$\Pi_l = \sum_{k=k_{l,\text{on}}}^{k_{l,\text{off}}} \sum_{w_x = (k+N)/2} |x\rangle \langle x| \, ,$$

where x is an N-bit string with Hamming weight w_x. The initial state of the system is, as for the circuit construction, the product of the encoded qubit in an l-level concatenated code and the maximally polarized state $|1\rangle^{\otimes K}$ on the clock gadget.

2.4.2 Error analysis

We now perform the error analysis for the protecting Hamiltonian (2.11). In order to protect the quantum information, we will require that the error probability per qubit in use is bounded by the same threshold p^* after each decoding step is completed (i.e. at $t = t_l + t_{\text{dec}} + \frac{\delta}{2}$). We will restrict to the space of good trajectories, since we know from the clock theorem that this accounts for all but an exponentially small fraction, which can be incorporated into the final error probability.

We will choose K large enough to ensure that the error $\frac{\delta}{2} \geq |\tilde{t} - t|$ in the clock time satisfies $\delta \ll t_{\text{prot}}, t_{\text{dec}}$. In this way, we ensure that the decoding operations are performed in the right order [1] and with sufficient precision. We may thus account for the following error sources between $t_l + t_{\text{dec}} + \delta/2$ and $t_{l+1} + t_{\text{dec}} + \delta/2$:

i) *Inherited errors* from the previous rounds which could not be corrected for. By assumption, these errors are bounded by $p_{\text{inher}} \leq p^*$.

ii) Errors from the *depolarizing noise* during the free evolution of the system. The system is sure to evolve freely for a time $t_{\text{prot}} - \delta$, i.e., the noise per qubit is bounded by $p_{\text{evol}} \leq 1 - \exp[-r(t_{\text{prot}} - \delta)] \leq r(t_{\text{prot}} - \delta)$.

iii) Errors during the *decoding*. These errors affect the *decoded* rather than the encoded system and stem from two sources: On the one hand, the time the Hamiltonian is active has an uncertainty $t_{\text{dec}} \pm \delta$, which gives an error in the implemented unitary of not more than $\exp[\delta \|H^{k,l}_{\text{dec}}\|] - 1$. On the other hand, depolarizing noise can act during the decoding for at most a time $t_{\text{dec}} + \delta$. In the worst case, noise on any of the code qubits during decoding will destroy the decoded qubit, giving an error bound $d(1 - \exp[-r(t_{\text{dec}} + \delta)]) \leq dr(t_{\text{dec}} + \delta)$. Thus, the error on the decoded qubit is

$$p_{\text{dec}} \leq \exp[\|H^{k,l}_{\text{dec}}\|\delta] - 1 + dr(t_{\text{dec}} + \delta) \ .$$

Since the noise is Markovian (i.e. memoryless), the clock does not correlate its errors in time. In summary, the error after one round of decoding is at most $B(p_{\text{inher}} + p_{\text{evol}}) + p_{\text{dec}}$, which we require to be bounded by p^* again. Here, $B(p)$ is a property of the code, and returns the error probability of the decoded qubit, given a probability p of error on each of the original qubits; for example, for the 5-qubit perfect QECC [80], $B(p) \leq 10p^2$.

[1] The noisy clock has the potential to run backwards in time within its accuracy.

We will now show that it is possible to fulfil the required conditions by appropriately defining the control parameters. First, we choose $p^* \leq 1/40$ to have the QECC [80] work well below threshold. We may take $t_{\text{prot}} := \frac{p^*}{r}$ and $t_{\text{dec}} := \frac{p^*}{4dr}$. To minimize imprecision in the implemented unitaries, the decoding Hamiltonians are chosen of minimal possible strength, $\|H^{k,l}_{\text{dec}}\| \leq \frac{2\pi}{t_{\text{dec}}}$. Finally we take $\delta := \frac{p^* t_{\text{dec}}}{8\pi}$. Inserting the proposed values in the derived bounds, it is straightforward to show that $B(p_{\text{inher}} + p_{\text{evol}}) + p_{\text{dec}} < p^*$.

The number of code qubits required is $N := d^l$, with $l := \lceil \frac{\tau}{t_{\text{prot}}+t_{\text{dec}}} \rceil$. The required clock lifetime $t_{\max} = \tau$ and precision δ are guaranteed by taking $\varepsilon = 1/6$ and $K := (\frac{2e^{r\tau}}{r\delta})^3$ in the clock theorem. For any fixed r and p^*, this allows a lifetime $\tau \sim O(\log(N + K))$.

2.5 Conclusions

In this chapter, we have considered the ability of a Hamiltonian to protect quantum information from depolarizing noise. While without a Hamiltonian, quantum information is destroyed in constant time, the presence of time-dependent control can provide protection for logarithmic time, which is optimal. As we have shown, the same level of protection can be attained with a time-independent Hamiltonian. The construction introduced a noise-driven clock which allows a time dependent Hamiltonian to be emulated without explicit reference to time.

Since depolarizing noise is a limiting case of local noise models, it is expected that the time-independent Hamiltonian developed here can be tuned to give the same degree of protection against weaker local noise models, although these models may admit superior strategies. For instance, noise of certain forms (such as dephasing) allows for storage of ancillas, potentially yielding a linear survival time by error correcting without decoding. In the case of amplitude damping noise, the noise itself distills ancillas so that the circuit can implement a full fault-tolerant scheme, which gives an exponential survival time, assuming that one can redesign the clock gadget to also benefit from these properties.

Whether the same degree of protection can be obtained from a Hamiltonian which is local on a 2D or 3D lattice geometry remains an open question[2]. However, intuition suggests this

[2] A first step is to incorporate the notion of boundedness. By controlling each decoding unitary in a given round from a different clock (which does not affect the scaling properties), a constant bound to the sum of Hamiltonian terms acting on any given finite subsystem can be shown.

might be impossible; the crucial point in reversibly protecting quantum information from depolarizing noise is to concentrate the entropy in one part of the system. Since the speed of information (and thus entropy) transport is constant due to the Lieb-Robinson bound [83], the rate at which entropy can be removed from a given volume is proportional to its surface area, while the entropy increase goes as the volume. It thus seems impossible to remove the entropy sufficiently quickly, although this argument is not fully rigorous, and the question warrants further investigation.

Chapter 3

Hamiltonian memory model under Hamiltonian perturbations

In this chapter, we study limitations on the asymptotic stability of quantum information stored in passive N-qubit systems. We consider the effect of small imperfections in the implementation of the protecting Hamiltonian in the form of Hamiltonian perturbations or weak coupling to a ground state environment. We thus depart from the usual Markovian approximation for a thermal bath by concentrating on models for which part of the evolution can be calculated exactly. We prove that, regardless of the protecting Hamiltonian, there exists a perturbed evolution that necessitates a final error correcting step for the state of the memory to be read. Such an error correction step is shown to require a finite error threshold, the lack thereof being exemplified by the 3D XZ-compass model [11]. We go on to present explicit weak Hamiltonian perturbations which destroy the logical information stored in the 2D toric code in a time $O(\log(N))$.

3.1 Introduction

Quantum information processing promises exciting new capabilities for a host of computational [114, 28, 56] and cryptographic [16, 37] tasks, if only we can fabricate devices that take advantage of the subtle and very fragile effects of quantum mechanics. The theory of quantum error-correcting codes (QECCs) and fault-tolerance [113, 3, 47, 48] assure that this

fragility can be overcome at a logical level once an error rate per element below a certain threshold is achieved. However, providing a scalable physical implementation of computational elements with the required degree of precision and control has proven to be a task of extreme difficulty. Thus, one might hope to design superior fault-tolerant components whose robustness is enforced in a more natural way at a physical level.

A first step in this daunting task is to concentrate not on universal quantum computation, but on one sub-protocol within this; the storage of quantum information. Thus, the aim is to find systems naturally assuring the stability of quantum information, just like magnetic domains in a hard disk provide stable storage of classical information. The quest for such a passive quantum memory was pioneered by Kitaev [74], who introduced the toric code as the first many body protecting Hamiltonian. The promising conjunction of properties shown by his proposal has fueled a search, which is yet to provide a definitive result.

For families of protecting Hamiltonians, such as Kitaev's toric code [74, 32], a constant energy gap γ separates the degenerate ground space, used for encoding, from low energy excited states. Furthermore, the stabilizer representation of these Hamiltonians naturally associates it with a QECC, which permits an error threshold without the use of concatenation [32]. A perturbation theoretic expansion of local errors V in the Hamiltonian must then cancel to orders increasing with the distance of the associated QECC. Recently Bravyi et al. [21, 20] have used this to rigorously prove that under the effect of sufficiently weak yet extensive perturbations, the energy splitting of the degenerate ground space decays exponentially with the system size. Together with previous results by Hastings and Wen [57], this guarantees the existence of perturbed logical operators and local observable. Additionally, it also implies that it takes this splitting an exponentially long time to implement logical rotations on the perturbed ground space (e.g. a phase gate). A non trivial condition being that encoding is actually performed onto the perturbed ground space.

However, such perturbation theoretic results must be applied with caution. The most important limitation probably arises from the fact that they deal with a closed quantum system whereas actual noise may be better modeled by perturbative coupling to an environment. Even if local observables can be adapted for to a high degree of accuracy [57], the global eigenstates of the system may change and become very different. Within our understanding, the possibility of adapting encoding and decoding protocols relies on the perturbation

being characterized, something that seems unrealistic for such many-body systems[1]. This is why we consider an uncharacterized perturbation introduced through a quench. By this we mean that encoding is performed according to the ideal (unadapted) code-space of the unperturbed Hamiltonian as will the decoding and order parameters considered. This allows us to derive no-go, or limitation, results from the exact analysis of adversarially engineered noise instances. However, it must be noted that error correction to the perturbed encoding may be performed without explicit knowledge of the perturbation. This is for example the case, for the self-correcting mechanism which is based on energy dissipation.

The first systematic study of limitations of passive quantum memories can be atributed to Nussinov and Ortiz [99], finding constant (system size independent) bounds for the auto-correlation times. They study the effect of infinitesimal symmetry breaking fields on topological quantum order at finite temperature [100]. More recently, Alicki et. al. have presented results supporting the thermal instability of quantum memories based on Kitaev's 2D toric code [8] and the stability of its 4D version [9] when coupled to a sufficiently cold thermal environment. They analyse the evolution of correlation functions for the case of Markovian dynamical semigroup [7]. Chesi et al. [26] have made progress in providing a general expression giving a lower bound for the lifetime of encoded information. The approach taken in these articles is thermodynamic in nature and has the advantage of allowing the derivation of positive results. A weak coupling Markovian approximation to an environment at thermal equilibrium is assumed, thus neglecting any memory effects from the environment. In a previous article [103], we considered a Hamiltonian system subject to independent depolarizing noise (corresponding to the infinite temperature limit of the above approach) and proved that $O(\log N)$ is the optimal survival time for a logical qubit stored inside N physical qubits.

Our current approach directly deals with Hamiltonian perturbations and environment couplings without going through a Markovian approximation for the environment. Thus, approximations needed for a Markovian description of a bath are not required and do not pose an issue. A comparative advantage of our approach is the capability of exactly dealing with certain weak but finite perturbations and couplings, and providing restricted no go results.

To falsify claims of protection against any possible noise of a certain class (such as weak

[1] A possible exception to this is given by proposals of adiabatic state preparation [54].

local perturbations to the Hamiltonian), it suffices to consider an adversarial noise instance within such a class. In such a noise model, different perturbations and environments are not assigned probabilities; a perturbation is simply considered possible if it adheres to certain conditions. There is a range of different conclusions that one may reach from such an analysis of noise instances. One may simply provide upper bounds on how fast a passive memory may be erased by a perturbation complying to a certain noise class. We may prove or extrapolate requirements for a memory model to protect against the given noise class. We may find that a class of noise is unreasonable by showing that it invalidates a memory model which we expect to work (i.e. a magnetic domain). An intermediate scenario arises when we consider the noise class to be reasonable but expect a certain notion of typicality for which the considered instance is not representative. Such a typicality condition would then be needed explicitly to provide proof of robustness for the memory model.

We consider the effect of relatively weak yet unknown perturbations of an N qubit local protecting Hamiltonian and coupling to an ancillary environment starting out in its ground state. We show that as the number N of physical subsystems used grows, it is impossible to immunize a quantum subspace against such noise by means of local protecting Hamiltonians only. We further show that if one wishes to recover the quantum state by means of an error correction procedure, the QECC used must have some finite error threshold in order to guarantee a high fidelity; this result is applied to the 3D XZ-compass model [11] which is shown not to have such a threshold. In the case of the 2D toric code [74], we propose Hamiltonian perturbations capable of destroying encoded information after a time proportional to $\log(N)$, suggesting that some form of macroscopic energy barrier may be necessary. Weak finite range Hamiltonian perturbations are then presented which destroy classical information encoded into the 2D Ising model; in this case interactions involving a large, yet N independent, number of qubits are required. Finally, we consider time dependent Hamiltonian perturbations and coupling to an ancillary environment with a high energy density; here we provide constructions illustrating how these more powerful models may easily introduce logical errors in constant time into information protected by any stabilizer Hamiltonians, and even certain generalizations. Drawing from practical experience with classical memories, the one likely conclusion here is that general time dependent Hamiltonian perturbations are not a relevant noise model to consider, as it is in general too powerful to protect against.

3.1.1 Noise model motivation

A prerequisite to assess protecting Hamiltonians is a precise definition of the noise model they will be expected to counter. Our aim is to understand the protection lifetime they provide to (quantum) information as well as to identify the properties a good protecting Hamiltonian should have. In order to be able to make such predictions, we will study noise models admitting a mathematically tractable description while striving to keep our choices physically motivated.

The most elementary way in which the Hamiltonian evolution of a closed system can be altered is by including a small perturbation V to the Hamiltonian H. A simple physical interpretation for such a perturbation is to associate V to imperfections in the implementation of the ideal protecting Hamiltonian H. Furthermore, Hamiltonian perturbations extending beyond the system under experimental control are modeled by a weak coupling between the system and an environment. We focus on families of protecting Hamiltonians satisfying certain locality and boundedness conditions, and naturally extend similar restrictions on the perturbations and couplings considered.

Let us first introduce some definitions. A family of protecting Hamiltonians $\{H_N\}$ is parametrized by a natural number N which in most cases, will simply be the number of physical subsystems (particles) on which H_N acts. A Hamiltonian H is called "k-local" when it can be represented as a sum

$$H = \sum_i T_i, \tag{3.1}$$

with at most k physical subsystems participating in each interaction term T_i. The interaction strength of a physical subsystem s in a k-local Hamiltonian H is given by the sum $\sum_i |T_i|$ of operator norms over those interaction terms T_i in which the physical subsystem s participates. A family of k-local Hamiltonians is called "J-bounded" if, for every Hamiltonian H_N in the family, the largest interaction strength among the physical subsystems involved is no greater than J. Finally, a family of Hamiltonians will be D-dimensional if the physical subsystems involved can be arranged into a D-dimensional square lattice, such that all interaction terms are kept geometrically local.

We will concentrate on families of k-local, J-bounded protecting Hamiltonians, with $J > 0$, and $k, J \sim O(1)$. Furthermore, the specific Hamiltonians treated in this chapter admit an embedding into 2, 3 or 4 spatial dimensions and we may assume such embeddings also when

dealing with generic protecting Hamiltonians.

The families of Hamiltonian perturbations $\{V_N\}$ which we will consider will be $\tilde{J}$-bounded, with the strength $\tilde{J}$ small in comparison to J. The perturbations will be taken to be $\tilde{k}$-local, with $\tilde{k}$ possibly different, and even larger, than k. This allows, for example, taking into consideration undesired higher order terms which may arise from perturbation theory gadgets [19]. Allowed perturbations should also admit a geometrically local interpretation under the same arrangement of subsystems as the protecting Hamiltonian.

When considering coupling to an environment, an additional set of physical subsystems will be included as the environment state. A family of local environment Hamiltonians $\{H_N^{(E)}\}$ will be defined on these additional subsystems. The coupling between system and environment will be given by a family of weak local Hamiltonian perturbations $V_N^{(SE)}$, acting on both system and environment.

$$\tilde{H}_N = H_N^{(S)} \otimes I_N^{(E)} + I_N^{(S)} \otimes H_N^{(E)} + V_N^{(SE)} \tag{3.2}$$

Finally, it should be possible to incorporate the additional physical subsystems from the environment while preserving the number of spatial dimensions required for the Hamiltonian. To simplify notation, the sub-index N shall in general be dropped.

The engineering of k-body interactions is increasingly difficult as k grows [130, 19]. This is why we limit our study to families of k-local Hamiltonians (i.e. k independent of N). It is under such criteria that we exclude proposals such as quantum concatenated-code Hamiltonians [12], for which the required degree of interactions would grow algebraically with the number of qubits.

The J-bounded condition guarantees that the rate of change for local observables remain bounded. This is a necessary condition to certifiably approximate a Hamiltonian through perturbation theory gadgets [19]. There, constant bounds are imposed both on the norm of each interaction as well as on the number of interactions in which each subsystem participates. The J-bounded condition also leaves out systems with long range interactions, as, for those systems, the total interaction strength of individual physical subsystems diverges as the system size grows. Such long range interacting systems are physically relevant, and may lead to protecting Hamiltonian proposals [27, 53]. However, we abstain from treating such models for which our notion of weak perturbation seems inappropriate.

Each physical subsystem may independently be subject to control imprecision. Such is the case for weak unaccounted "magnetic field" acting on every component of the system or a weak coupling of each component to an independent environment. Thus, relevant physical scenarios involve perturbations with extensive operator norm (i.e. scaling with the number of subsystems). The $\tilde{J}$-bounded condition encapsulates these scenarios and seems to better describe what we understand by a weak perturbation.

Finally, it is expected that scalable physical implementations should be mapped to at most three spatial dimensions. This would rule out the 4D toric code Hamiltonian [32], a proposal which was otherwise shown to provide increasing protection against weak local coupling to a sufficiently cold thermal bath [9]. As would occur with an actual physical embedding, we expect that the perturbations considered may be included into the same geometrical picture as the protecting Hamiltonian they affect.

3.1.2 Outline of results

In the following sections, we analyze the problem of obtaining increased protection for quantum information by means of an encoding and a protecting Hamiltonian acting on an increasing number of physical subsystems. We consider the effect of adversarial noise models consisting of local Hamiltonian perturbations and/or a weakly coupled environment. The aim is to examine the assumptions and limitations of memory schemes based on Hamiltonian protection with a growing number of physical subsystems as quantified by the survival time of stored information.

We will prove in complete generality that the survival of information should be associated to a subsystem and not to a particular subspace. The figure of merit considered here is $S(t) = \mathsf{tr}\left(|\psi(0)\rangle\langle\psi(0)|\,\rho(t)\right)$, the overlap between initial and evolved state after a constant time t. For arbitrary protecting Hamiltonians we provide a completely general construction involving a weakly coupled environment starting in its ground state (Sec. 3.2.2) which yields an exponentially small (in N) upper bound on $S(t)$ after a constant time. For gapped Hamiltonians, a proof proceeding without reference to an environment (Appendix 3.A) can provide an upper bound to the time averaged overlap which is close to $\frac{1}{2}$. We thus infer that the information should be associated to a subsystem.

Having found that subspaces can not provide robust encoding, we consider protecting

Hamiltonians together with a recovery operation $\mathcal{R}$, which can be thought of as applied on read-out. This provides the formal means to project information from a logical subsystem onto a code subspace and leads to a more robust figure of merit given by $S_{\mathcal{R}}(t) = \mathsf{tr}\left(\rho(0)\mathcal{R}(\rho(t))\right)$. Although throughout the chapter, we assume $\mathcal{R}$ to be an unperturbed error correction procedure associated to an encoding, it is important to emphasize that other means may allow keeping information in a logical subsystem. In particular, self-correcting Hamiltonians advocate the use of a local thermalizing coupling as a way of continuous error correction at finite temperature. This is, while an unperturbed order parameter may be shown to be inadequate for the storage of information, it may be possible for a robust yet implicit logical subsystem to arise by including genuine dissipation.

In (Sec. 3.3), a weak coupling construction like that of (Sec. 3.2.2) shows that information content of the 3D XZ-compass model [11] can be destroyed in constant time by a zero temperature environment, despite of a final recovery operation $\mathcal{R}$. From a broader perspective, the structure of our proof strongly suggests that the underlying QECC defining the recovery operation $\mathcal{R}$ must have a strictly positive error threshold.

We continue by considering the effect of Hamiltonian perturbations on the 2D toric code [74]. The recovery mechanism $\mathcal{R}$ is then taken as the composition of a fixed syndrome measurement followed by a correction operation pairing the detected anyons. It is shown (Sec. 3.4) that, although the underlying QECC has an error threshold, it is not protected against combinations of unknown weak local Hamiltonian perturbations, even after a final round of error correction is considered. Our claim is based on adversarial weak local perturbations that are capable of destroying the stored information in a time logarithmic in N. This is stronger than previous results [67] in that, the noise model requires no interaction with the environment and the information is destroyed exponentially faster.

In a similar manner, we consider perturbations on the 2D Ising Hamiltonian (Sec. 3.5), which is often used as an example of self-correcting classical memory. Here, Hamiltonian perturbations may transform (classical) code states into an ambiguous state in constant time. While the number $\tilde{k}$ of bodies in perturbation terms is required to grow as the overall perturbation strength decreases, it shows no dependence on the size N of the system. In this model, any sequence of local errors connecting the two classical code states must go through states with a macroscopic amount of extra energy, showing that this property alone is not sufficient

to give protection against this family of perturbations. There are two possible implications of this result. First we may think that since ferromagnetic domains seem to be quite stable, our choice of perturbation may not be significant in that it is by no means typical. On the other hand, although the lifetime obtained is independent of N, this independence is only found for very large N in terms of the perturbation strength, possibly allowing to reconcile this model with experience and hinting that in practice, information lifetime scaling with N may be unnecessary.

Beyond the Hamiltonian perturbation model and coupling to a ground state environment, we consider more aggressive noise models (Sec. 3.6) in which the environment can introduce large amounts of energy. The models considered are time dependent Hamiltonian perturbations and weak Hamiltonian coupling to an environment starting in a high energy state. For such noise models, even the information storage capabilities of the 4D toric code and any local ferromagnetic Ising model, proposals shown to be stable under Markovian thermal coupling, are completely destroyed. We thus argue that requiring robustness against an adversarial noise model of such a class is asking for too much and is not a prerequisite for practical quantum or classical memories.

One might expect that the results presented here are not limited to the task of designing a quantum memory. Rather, they tell us about the difficulty of keeping a state and its time evolution confined within a specific subspace of the system, under the effect of Hamiltonian noise. Such considerations arise in other settings, such as in the models of adiabatic and topological quantum computation. We will outline some of these connections in Sec. 3.7.

3.2 Subsystems instead of subspaces

We start our examination of passive quantum memories by proving that regardless of the choice of encoding subspace and protecting Hamiltonian the weak coupling to an environment can, in constant time, exponentially reduce the fidelity with the evolved state. By this, we wish to convey that a more robust figure of merit is required. Such figures are in general derived from associating the information to a logical subsystem.

First, we propose weak local perturbations showing an exponentially decreasing overlap between perturbed and unperturbed eigenstates. For general local Hamiltonians and states, we consider a local coupling V of the system with a γ-bounded environment initialized in its

ground state. Averaging over such couplings V, we are able to derive an exponentially small upper bound $\langle S(t_f)\rangle_V \leq [1-\sin^2(2\varepsilon)]^N$ for the overlap between initial and evolved system states at a time $t_f = \frac{\pi}{\gamma}$.

3.2.1 Eigenstate susceptibility to perturbations

Consider a k-local Hamiltonian H, decomposable into k-body interaction terms T_i as described in (3.1). We choose a perturbation V such that the initial and final Hamiltonians are related by a composition of local unitary transformations,

$$\tilde{H} = H + V = \mathcal{U} H \mathcal{U}^\dagger, \text{ with } \mathcal{U} = \bigotimes_{l=1}^{N} e^{i\varepsilon P_l}, \tag{3.3}$$

where P_l are normalized local Hermitian operators. Taking this definition, V can be written as

$$V = \sum_i \mathcal{U} T_i \mathcal{U}^\dagger - T_i, \tag{3.4}$$

and thus is also k-local. Furthermore, if $2k\varepsilon \ll 1$, it is justified to call V a perturbation with respect to H, since all terms are small with respect to those of H.

Degeneracies in H are assumed to be infinitesimally lifted to ensure uniquely defined eigenvectors. The overlap between eigenvectors $|\psi_i\rangle$ of H and the perturbed eigenvectors $\mathcal{U}|\psi_i\rangle$ is then given by $F_{\mathcal{U}} = |\langle\psi_i|\mathcal{U}|\psi_i\rangle|^2$.

By averaging over all possible directions P_l, we effectively obtain an independent qubit depolarization.

$$\int \mathcal{U}^\dagger |\psi_i\rangle\langle\psi_i| \mathcal{U} dP_1 \dots dP_N = \Delta_{\lambda(\varepsilon)}^{\otimes N}(|\psi_i\rangle\langle\psi_i|) \tag{3.5}$$

Here, $\Delta_\lambda(\rho) = \lambda\rho + (1-\lambda)\frac{I}{2}$ is the qubit depolarizing channel and $\lambda(\varepsilon) = 1 - \frac{3}{2}\sin^2(\varepsilon)$. We may then denote $\langle F\rangle_{\mathcal{U}}$ as average of the overlap $F_{\mathcal{U}}$ over all local rotations $\mathcal{U}$ having a given strength ε. This average is expressed in terms of the depolarizing channel as

$$\langle F\rangle_{\mathcal{U}} = \langle\psi_i|\, \Delta_{\lambda(\varepsilon)}^{\otimes N}\left(|\psi_i\rangle\langle\psi_i|\right)|\psi_i\rangle\,. \tag{3.6}$$

A result of King [72], known as multiplicativity of the maximum output p-norm for the depolarizing channels, states that

$$\max_{|\phi\rangle} \left|\Delta_\lambda^{\otimes N}\left(|\phi\rangle\langle\phi|\right)\right|_p \leq \left(\max_{|\phi\rangle} \left|\Delta_\lambda\left(|\phi\rangle\langle\phi|\right)\right|_p\right)^N. \tag{3.7}$$

For qubit subsystems and for $p = \infty$, Eq. (3.7) bounds the overlap of $\Delta_\lambda^{\otimes N}(|\phi\rangle\langle\phi|)$ with any single pure state, leading to

$$\langle F\rangle_{\mathcal{U}} \leq \left(\frac{1+\lambda}{2}\right)^N = \left(1 - \frac{3}{4}\sin^2(\varepsilon)\right)^N . \tag{3.8}$$

Not only does this imply the existence of specific rotations such that F becomes exponentially small as the number of subsystems N grows, but that this is true for most rotations $\mathcal{U}$. While this is already known under the name of Anderson's orthogonality catastrophe (see, for example [10, 124]), we re-derive it for completeness and as an opportunity to introduce techniques needed throughout the rest of the chapter.

3.2.2 State evolution in coupled Hamiltonians

In this section, we consider a weak Hamiltonian perturbation coupling the system to a "cold" environment. The environment is assumed to start in its ground state, corresponding to a cold environment assumption. Averaging over a specific family of such perturbations instances V, an exponentially small bound on the overlap between the initial state and the evolved state is obtained. This bound, $\langle S(t_f)\rangle_V \leq [1-\sin^2(2\varepsilon)/3]^N$, is obtained after a constant evolution time $t_f = \frac{\pi}{\gamma}$, inversely proportional to the strength of the environment Hamiltonian.

Suppose that we start with a state $|\psi_0\rangle$ "protected" by an N qubit system Hamiltonian H_S. We can introduce a simple environment, composed of $2N$ qubits, each of which starts in its ground state, $|0\rangle$, and which is defined by its Hamiltonian

$$H = H^{(S)} \otimes I^{(E)} + I^{(S)} \otimes H^{(E)} \tag{3.9}$$

$$H^{(E)} = \gamma \sum_{i=1}^{N} |1+\rangle\langle 1+|_i^{(E)} - |00\rangle\langle 00|_i^{(E)} . \tag{3.10}$$

When necessary, we take the supraindices (S), $(E1)$ and $(E2)$ to denote the system, the first, and second components of the environment respectively. While both environment components will interact with the system, it is the presence of both which will allow a simple interpretation of the induced decoherence as a probabilistic application of local errors.

We again use the trick of considering a perturbed Hamiltonian $\tilde{H} = \mathcal{U} H \mathcal{U}^\dagger$ which results from the weak local rotations $\mathcal{U} = \bigotimes_{j=1}^N U_j$ of the decoupled Hamiltonian H. The rotation elements will involve both system and environment components, $U_j = e^{i\varepsilon P_j^{(S)} \otimes X_j^{(E1)}}$, where the operators $P_j^{(S)}$ are taken to be Pauli-like operators on site j of the system.

The perturbation $V = \mathcal{U}H\mathcal{U}^\dagger - H$ must be decomposable into small local terms. Such a decomposition for V is given in terms of the decomposition $H^{(S)} = \sum_i T_i$ into at most k-body terms. Each perturbation term $V_i = \mathcal{U}T_i\mathcal{U}^\dagger - T_i$ has an operator norm no greater than $2\varepsilon k\,|T_i|$ and involves up to $2k$-body interactions[2]. The perturbation required to rotate the environment Hamiltonian terms involve at most 3-body terms and a total norm bounded by $2\varepsilon\gamma$.

The initial state, $|\psi_0\rangle\,|00\rangle^{\otimes N}$ will thus evolve into $e^{-it\mathcal{U}H\mathcal{U}^\dagger}\,|\psi_0\rangle\,|00\rangle^{\otimes N}$. The survival probability is then $S(t) = \langle\psi_0|\,\rho_S(t)\,|\psi_0\rangle$, where $\rho_S(t) = \mathsf{tr}_E\,(\rho(t))$, and

$$\rho(t) = \mathcal{U}e^{-itH}\mathcal{U}^\dagger\,|\psi_0\rangle\langle\psi_0|\otimes|00\rangle\langle 00|^{\otimes N}\,\mathcal{U}e^{itH}\mathcal{U}^\dagger. \tag{3.11}$$

Here, $\mathcal{U}$ may be explicitly decomposed as

$$\begin{aligned}\mathcal{U} &= \exp(i\varepsilon\textstyle\sum_j P_j^{(S)}\otimes X_j^{(E1)})\\ &= \textstyle\sum_{\mathbf{p}}\cos(\varepsilon)^{N-w(\mathbf{p})}(i\sin(\varepsilon))^{w(\mathbf{p})}P_{\mathbf{p}}^{(S)}\otimes X_{\mathbf{p}}^{(E1)},\end{aligned} \tag{3.12}$$

where $\mathbf{p}$ denotes a binary vector indicating the sites on which rotations are applied in $P_{\mathbf{p}}^{(S)}$ and $w(\mathbf{p})$ is the weight of the bit string $\mathbf{p}$ (number of non identity factors in $P_{\mathbf{p}}^{(S)}$).

Now consider a time $t_f = \frac{\pi}{\gamma}$ such that e^{-it_fH} transforms components of the environment from $|10\rangle$ to $|11\rangle$, while leaving components in state $|00\rangle$ unaltered. At such a time t_f, substituting $\mathcal{U}$ into expressions (3.11) allows explicitly tracing over the environment to yield

$$\begin{aligned}\rho_S(t_f) = \sum_{\mathbf{p},\mathbf{q}}&\cos^2(\varepsilon)^{2N-w(\mathbf{p})-w(\mathbf{q})}\sin^2(\varepsilon)^{w(\mathbf{p})+w(\mathbf{q})}\times\\ &P_{\mathbf{p}}e^{-it_fH^{(S)}}P_{\mathbf{q}}\,|\psi_0\rangle\langle\psi_0|\,P_{\mathbf{q}}e^{it_fH^{(S)}}P_{\mathbf{p}}.\end{aligned} \tag{3.13}$$

Thus, $\rho_S(t_f)$ may be considered as the density matrix resulting from the independent probabilistic application of the local unitary rotations prescribed by $\mathcal{U}$ on $|\psi_0\rangle\langle\psi_0|$, followed by the evolution under the unperturbed system Hamiltonian, followed by a second round of random application of the local rotations prescribed by $\mathcal{U}$. Defining

$$\mathcal{E}_{R,p}(\rho) = pR\rho R + (1-p)\rho, \tag{3.14}$$

and the Hamiltonian evolution

$$\mathcal{H}_t(\rho) = e^{-iH^{(S)}t}\rho e^{iH^{(S)}t}, \tag{3.15}$$

[2]For $\varepsilon k \ll 1$, a further decomposition of such terms can be provided in which subterms involving $k+b$ bodies are of strength $O(\varepsilon^b)$, guaranteeing that the strength of terms decays exponentially with the number of bodies involved.

we can take $p = \sin^2(\varepsilon)$ and define $\rho_{virt} := \left(\bigotimes_{i=1}^{N} \mathcal{E}_{P_i,p}\right) |\psi_0\rangle\langle\psi_0|$, so that we can express $S(t_f)$ as

$$S(t_f) = \mathsf{tr}\left(\rho_{virt} e^{-it_f H_S} \rho_{virt} e^{it_f H_S}\right). \tag{3.16}$$

This is the overlap between a density matrix and its own unitary evolution, and can be upper bounded by

$$S(t_f) \leq \mathsf{tr}\left(\rho_{virt}^2\right). \tag{3.17}$$

In turn, using the fact that P_i are Pauli-like operators we may rewrite it as

$$S(t_f) \leq \langle\psi_0| \left(\bigotimes_{i=1}^{N} \mathcal{E}_{P_i,2p(1-p)}\right) (|\psi_0\rangle\langle\psi_0|) |\psi_0\rangle. \tag{3.18}$$

Averaging over the Pauli-like operators, we obtain

$$\langle S(t_f)\rangle_V \leq \langle\psi_0| \Delta_{\lambda(\varepsilon)}^{\otimes N}(|\psi_0\rangle\langle\psi_0|) |\psi_0\rangle, \tag{3.19}$$

which is the overlap at time t_f averaged over the proposed family of weak perturbative couplings. Here $\Delta_\lambda(\rho)$ is again the depolarizing channel, and $\lambda(\varepsilon) = \text{is } 1 - \frac{4}{3}2p(1-p)$. Using Eq. (3.8), we obtain

$$\langle S(t_f)\rangle_V \leq [1 - \frac{4}{3}p(1-p)]^N, \tag{3.20}$$

which by substituting p for $\sin^2(\varepsilon)$ yields

$$\langle S(t_f)\rangle_V \leq [1 - \sin^2(2\varepsilon)/3]^N. \tag{3.21}$$

By averaging over different possible weak couplings, we obtain an overlap between initial and evolved states which is exponentially decreasing in N.

The norm γ of Hamiltonian terms in the environment should be bounded, since it is in part these terms which are rotated by $\mathcal{U}$ to introduce a weak coupling between system and environment. Thus, the proposed evolution time $t_f = \frac{\pi}{\gamma}$ is constant. Furthermore, if one considers an environment of N semi-infinite chains of coupled two level systems (such as Heisenberg chains), it is possible to ensure that the overlap with the initial state is small for all times larger than $t \sim \frac{\pi}{\gamma}$, rather than have the recurrences that arise from the discrete spectra of the described model.

In appendix (3.A), the evolution of an unperturbed eigenstate is considered under the effect of pure Hamiltonian perturbations (no environment). In this case, a constant rate of

change in the system state is guaranteed by an energy gap γ in the system Hamiltonian. If an initial state belongs to an energy band separated from the rest of the Hilbert space by such an energy gap γ, we provide an upper bound on the time averaged overlap $\langle S(t')\rangle_{t'\in[0,t]} \leq \frac{1}{2} + \frac{1}{2\gamma t}$ between initial and evolved state.

3.2.3 Discussion

We were able to show after a constant time t_f, an exponentially large degradation of the overlap $S(t_f)$ in terms of N. If we are to find a benchmark by which to evaluate a memory scheme, we expect that the memory improves as more resources are dedicated to its implementation. It is now clear that many-body quantum states are inherently unstable with respect to the uncorrected overlap, i.e. $S(t)$ is not the appropriate benchmark.

The fact that we may count on N physical subsystems to implement a quantum memory should not exclude using only one of them and ignoring whatever noisy evolution is affecting the others. This corresponds to considering an overlap reduced to the relevant subsystem and not on the whole state. Already such a simple idea guarantees that information storage quality is non-decreasing with N.

One may further generalize this by realizing that the relevant subsystem need not correspond to an actual physical subsystem. This corresponds to providing a new decomposition for the physical Hilbert space which allows factoring out a logical subsystem. The resulting benchmark is $S_{\mathcal{R}}(t) = \mathsf{tr}\left(\rho(0)\mathcal{R}(\rho(t))\right)$, quantifying the quality of the information recoverable from the evolved state and not of the state itself. Here, $\mathcal{R}$ may be thought of as an operation zeroing the irrelevant subspace, which may also be interpreted as the recovery super-operator of a QECC. Conversely, given the recovery operation $\mathcal{R}$ of a QECC, one may define the corresponding logical subsystem. Robust error corrected logical observables[3] can analogously be defined via the extension provided from the code space to the whole Hilbert space by the recovery operation $\mathcal{R}$. In the following sections, we shall consider protecting Hamiltonians toghether with such error correcting codes and robust logical observables.

[3] Alicki et al. [9] use the name dressed observables, whereas Chesi et al. [26] use the self-explanatory name of error corrected logical operators, which we will adopt.

3.3 Error threshold required

A desirable property for a quantum memory is that any sequence of local operators mapping between different logical code-states should have energy penalties which grow with the system size. It has been shown that this happens for schemes in four dimensions, such as the 4D toric code [32]. Seeking to provide such an example in three spatial dimensions, Bacon proposed the 3D XZ-compass model [11], a scheme based on subsystem error correcting codes [77] and requiring only 2-body nearest neighbour interactions. Furthermore, mean field arguments suggest that this model might show such an increasingly large energetic barrier.

However, we will show that the zero temperature (local, but non-Markovian) environment construction of the previous section is capable of giving a false read-out from the code after constant time. A recovery operation $\mathcal{R}$ is assumed on read-out, and taken to be the unadapted version of the associated error correcting code. We show that the shortcoming is inherent to the choice of recovery procedure $\mathcal{R}$ by illustrating that the same flaw is present for the 4D toric code if one assumes an alternative recovery protocol similar to the one considered for the 3D XZ-compass model. This failure is a general feature of recovery protocols not having a local error threshold (i.e. those which are unable to handle errors on a constant fraction of randomly chosen sites).

For the 3D XZ-compass model, quantum information is first encoded into the groundspace of a 2-local Hamiltonian H_S defined on a $N \times N \times N$ arrangement of two level systems (where N is an odd number).

$$H_S = -\lambda \sum_{i,j=1}^{N} \sum_{l=1}^{N-1} (X_{l,i,j} X_{l+1,i,j} + X_{i,l,j} X_{i,l+1,j} + Z_{i,l,j} Z_{i,l+1,j} + Z_{i,j,l} Z_{i,j,l+1}) . \tag{3.22}$$

This is not a stabilizer code but a subsystem code. This means that a recovery operation need not correct certain errors which have no effect on the logical observables, and information may be preserved even if the recovered state is different.

First, note that pairs of planes of operators $\hat{Z}_l = \prod_{i,j} Z_{i,j,l} Z_{i,j,l+1}$ and $\hat{X}_l = \prod_{i,j} X_{l,i,j} X_{l+1,i,j}$ commute with the Hamiltonian H for all l. This also holds for logical operators, which consist of products along a single plane $\bar{Z} \equiv \bar{Z}_l = \prod_{i,j} Z_{i,j,l}$ and $\bar{X} \equiv \bar{X}_l = \prod_{i,j} X_{l,i,j}$ operators respectively, for an arbitrarily chosen l. In the ground space, the choice of l is irrelevant, since the operators $\hat{Z}_l, \hat{X}_l$ all have $+1$ eigenvalues. Provided N is odd, $\bar{X}$ and $\bar{Z}$ anti-commute,

giving a qubit algebra. In the presence of errors (outside of the ground space), the error corrected logical observables will be defined as the majority vote among plane observables

$$\bar{Z}_{ec} = \mathsf{maj}_l \bar{Z}_l \quad \bar{X}_{ec} = \mathsf{maj}_l \bar{X}_l \tag{3.23}$$

where maj stands for a majority vote among the ± 1 eigenvalued commuting operators. Measuring all pairs of adjacent planes $\hat{Z}_l$ allows a majority vote error correction scheme to be performed on the value of the $\bar{Z}_l$ plane observables without extracting whether the corrected state yields $+1$ or -1 values for all such planes.

Considering a perturbation on the system plus an environment, as presented in section 3.2.2. By explicitly developing the final expectation values for the observables of interest ($\mathsf{tr}[\bar{Z}_{ec}\rho_S(t_f)]$ and $\mathsf{tr}[\bar{X}_{ec}\rho_S(t_f)]$), it can be seen that the information stored in the code will not be reliable after a time t_f. For this, we can pick up from the evolved state of the system in Eq. (3.16)

$$\rho_S(t_f) = \left(\bigotimes_{i=1}^{N} \mathcal{E}_{P_i,p}\right) \circ \mathcal{H}_{t_f} \circ \left(\bigotimes_{i=1}^{N} \mathcal{E}_{P_i,p}\right) |\psi_0\rangle\langle\psi_0| \,. \tag{3.24}$$

Since all plane observables ($\bar{X}_l$ and $\bar{Z}_l$) of a given type mutually commute, and also do so with the Hamiltonian, we can independently consider the probability of each plane observable having suffered a flip. If the P_i in Eq. (3.14) are taken to be single X or Z rotations, they will anticommute with overlaping $\bar{Z}_l$ or $\bar{X}_l$ plane observables respectively, changing their value upon an odd number of applications. Taking the P_i to be simple Z operators, the probability of flipping the value of an $\bar{X}_l$ plane observables by applying $\bigotimes_{i=1}^{N^3} \mathcal{E}_{P_i,p}$ once is given by

$$\begin{aligned} p_{\text{plane}*} &= \sum_{i \in odd}^{i \leq N} \cos^{2N^2-2i}(\varepsilon) \sin^{2i}(\varepsilon) \binom{N^2}{i} \\ &= \frac{1-\cos^{N^2}(2\varepsilon)}{2}, \end{aligned} \tag{3.25}$$

which is exponentially close to $1/2$. Since all observables involved commute with the system Hamiltonian, the probability of observing any result configuration will be preserved by $\mathcal{H}_{t_f}$. Finally, a second round of errors $\bigotimes_{i=1}^{N^3} \mathcal{E}_{P_i,p}$ will again flip the observed value for each plane with a probability $p_{\text{plane}*}$. The final independent probability of flipping the value of each plane is

$$p_{\text{plane}} = 2p_{\text{plane}*}(1 - p_{\text{plane}*}) = \frac{1-\cos^{2N^2}(2\varepsilon)}{2}. \tag{3.26}$$

The proposed correction scheme is equivalent to a majority voting among such planes. Thus, if more than half the planes suffer such an error, the majority vote will fail. The probability for incorrectly measuring the error corrected logical observable $\bar{X}_{ec}$ on read-out is then

$$p_{\text{logic}} = \sum_{i=(N+1)/2}^{N} p_{\text{plane}}^{i}(1-p_{\text{plane}})^{N-i}\binom{N}{i}. \tag{3.27}$$

Given that $\frac{1}{2}[1-\cos^{2N^2}(2\varepsilon)] \leq p_{\text{plane}} \leq \frac{1}{2}$, we have that

$$\frac{1}{2}[1-N\cos^{2N^2}(2\varepsilon)] \leq p_{\text{logic}} \leq \frac{1}{2}. \tag{3.28}$$

Assuming ε to be a small constant independent of N, the probability p_{logical} will exponentially approach $1/2$ for large N. We conclude that the encoding is not robust against the error model posed by local coupling to a cold adversarial environment.

The problem lies in the error correction mechanism rather than the protecting Hamiltonian itself. This becomes apparent if one applies a similar analysis to the 4D Toric code. There, the suggested noise model does not present a problem, since the usual error correction [32] of the 4D toric code has an error threshold. That is, provided the probability of per-site error, $p = \sin^2\varepsilon$ is below this threshold, there exist error correction criteria which succeed with a probability approaching 1 exponentially with N. On the other hand, we could consider a majority voting version of error correction in this setting, where we measure hyperplanes of X operators, and apply a majority vote to choose the correct result. In this case, an analysis completely analogous to that of the 3D XZ-compass code would hold proving such a read-out technique unreliable. We conclude that the error correction procedure of the 3D XZ-compass code does not allow sufficient resolution to use any potentially topological properties of the encoded quantum information.

The errors introduced by $\bigotimes_{i=1}^{N}\mathcal{E}_{P_i,p}$ are sufficiently general to suggest a necessary criterion for Hamiltonian protection of information from weak coupling to a cold environment. Even if we consider the first round of errors and the Hamiltonian evolution as part of the encoding procedure, information should still be able to withstand the probabilistic application of arbitrary local errors. This means that the information, either quantum or classical, should be encoded in such a way as to provide a finite error threshold in the thermodynamic (large N) limit.

3.4 Limitations of the 2D toric code

We will now show how local Hamiltonian perturbations are capable of introducing uncorrectable errors in Kitaev's 2D toric code Hamiltonian. The introduction of such errors will strongly rely on the lack of string tension on the toric code, suggesting a macroscopic energy barrier may be a necessary requirement. A brief introduction to the toric code Hamiltonian is provided in appendix 3.B, and is recommended to the unfamiliar reader.

Logical operations in the 2D toric code can be realized by creating a pair of anyons, propagating them so as to complete a non-trivial loop, and finally annihilating them. It is roughly such a scheme that will be followed by the perturbations we develop here. Repeating techniques from section 3.2, we may consider the initial state as containing a superposition of local errors which are interpreted as neighboring anyon pairs. A perturbation construction due to Kay [67] allows the deterministic propagation of such anyon pairs along predefined adversarial paths on the lattice. Syndrome measurement allows restricting to a probabilistic picture where error strings corresponding to anyon propagation paths are present with a predefined probability. It is finally the recovery procedure which may possibly complete these errors into logical operations by selecting an incorrect anyon matching.

A family of weak local perturbations capable of probabilistically introducing distant anyon pairs will first be presented. As before, the initial state $|\psi(0)\rangle$ is assumed to be a ground state of the unperturbed Hamiltonian H, in this case an $N \times N$ toric code as in Eq. (3.63). After a time t_f proportional to the maximum desired anyon propagation distance D, unperturbed syndrome read-out on $|\psi(t_f)\rangle$ will probabilistically detect distant (as well as local) anyon pairs. Our construction will then be applied to produce a simple set of $O(N)$ distance anyons such that no syndrome based error correction may be reliably applied. Later, shorter yet more elaborate anyon propagation paths will require explicit analysis of the error correcting probability of different anyon pairing protocols. In this context, we find weak Hamiltonian perturbations are capable of introducing logical errors with a large probability ($\approx \frac{1}{2}$) in a time t_f logarithmic in the system size N.

3.4.1 Probabilistic introduction of distant anyons

Kay [67] showed that local errors (anyons) in the 2D toric code, and other local stabilizer Hamiltonians lacking string tension, can be propagated into logical errors corresponding to

almost complete loop operators by a local Hamiltonian perturbation P. While in his work the initial presence of the anyons was assumed, here, anyons will be introduced with a certain amplitude by a generalization of the Hamiltonian perturbation P.

Consider introducing perturbations of the form $V = \mathcal{U}(H + P)\mathcal{U}^\dagger - H$, where $\mathcal{U} = \bigotimes_i U_i$ decomposes into weak local unitary rotations, and P is, as in [67], a weak local perturbation capable of deterministically propagating anyons in a given time t_f. The perturbed Hamiltonian

$$\tilde{H} = \mathcal{U}(H + P)\mathcal{U}^\dagger \tag{3.29}$$

induces a time evolution which can be written as

$$|\psi(t)\rangle = e^{-it\tilde{H}} |\psi(0)\rangle = \mathcal{U}e^{-it(H+P)}\mathcal{U}^\dagger |\psi(0)\rangle . \tag{3.30}$$

In this context, $\mathcal{U}$ and P are chosen such that:

1. By applying small Z rotations on connecting edges qubits, pairs of neighbouring vertex anyon are created by $\mathcal{U}^\dagger$ with amplitude $O(\varepsilon)$.

2. Each of the anyons is deterministically propagated by P along a predefined path. Thus, local excitation pairs become strings of errors defining new positions for the anyon pair.

3. Finally, $\mathcal{U}$ is unable to remove anyon pairs created by $\mathcal{U}^\dagger$ after at least one of them has been propagated. Moreover, $\mathcal{U}$ may create additional anyon pair with amplitude $O(\varepsilon)$.

Propagation paths for each anyon are not allowed to overlap but are otherwise completely independent. The propagation of the i-th anyon along its path $\ell^{(i)}$ may be attributed to a specific component P_i of $P = \sum_i P_i$. In turn, each component P_i admits a decomposition

$$P_i = \sum_{j=1}^{|\ell^{(i)}|} J_j^{(i)} \; T_{\ell_{j-1}^{(i)}, \ell_j^{(i)}}, \tag{3.31}$$

in terms of local interaction terms $T_{p,q}$, where $\ell_j^{(i)}$ are the anyon locations along the path ℓ. As in [67], the scalar coefficients $J_j^{(i)}$ are chosen to implement a perfect state transfer [29, 66, 68] and each term $T_{p,q}$ implement a swap among vertex anyons on p and q. If p and q are neighboring vertices, $T_{p,q}$ is defined as

$$T_{p,q} = Z_s \frac{(\mathbb{1} - A_p A_q)}{2}, \tag{3.32}$$

where A_p and A_q are the vertex stabilizer operators corresponding to p and q respectively (appendix 3.B) and Z_s is a Z rotation on physical site s corresponding to the edge connecting p and q. Furthermore, by allowing p and q to be next nearest neighbors, it is possible to have crossing anyon paths $\ell^{(j)}$, $\ell^{(i)}$ without having them overlap in the anyon locations used. If vertices p and q are not neighbors, the same effect is obtained by substituting Z_s in (3.32) for a tensor product of Z operators along an edge path $\overline{pq}$ from p to q,

$$T_{p,q} = \bigotimes_{s\in\,\overline{pq}} Z_s \, \frac{(\mathbb{1} - A_p A_q)}{2}. \tag{3.33}$$

The distance D is the maximum number of steps among the different anyon propagation paths $D = \max_i \left|\ell^{(i)}\right|$. It will be taken as $D = N/2-1$ in section (3.4.2) and as $D = O(\log N)$ in section (3.4.4). Fixing the strength of perturbation terms in P as $J_j^{(i)} = \frac{\varepsilon}{D}\sqrt{j(\left|\ell^{(i)}\right|+1-j)}$ allows the perturbation P to remain ε-bounded while allowing simultaneous perfect anyon transfer in a time $t_f = \frac{D\pi}{2\varepsilon}$. Similarly to previous sections, by taking the rotations $U_j = e^{i\varepsilon Z_j}$ as ε weak, the final perturbation required V will also be composed of $O(\varepsilon)$ strength interactions involving at most 8 bodies each.

The quantum state before measurement at time t_f is given in Eq. (3.30). Expanding $\mathcal{U}^\dagger$ from $U_j = e^{i\varepsilon Z_j}$, we get

$$|\psi(t_f)\rangle = \mathcal{U} e^{-i(P+H)t_f} \bigotimes_j (\cos\varepsilon \mathbb{1}_j - i\sin\varepsilon Z_j)\,|\psi(0)\rangle\,, \tag{3.34}$$

where the index j ranges over sites of non trivial action for $\mathcal{U}$. The state $|\psi(0)\rangle$ is a ground space eigenstate of H, and assuming the locations j on which $\mathcal{U}$ acts are non neighboring, each Z_j will increase the energy respect to H by γ. Furthermore since the energy of a state respects to H depends only on anyon number and P is anyon number preserving, we have $[H, P] = 0$, allowing us to write

$$|\psi(t_f)\rangle = \mathcal{U} e^{-iPt_f} \bigotimes_j (\cos\varepsilon \mathbb{1}_j - ie^{-i\gamma t_f}\sin\varepsilon Z_j)\,|\psi(0)\rangle\,. \tag{3.35}$$

Since all the propagations in P commute and correspond to exact transfer of each anyon created by $\mathcal{U}^\dagger$ precisely at time t_f , we may write

$$|\psi(t_f)\rangle = \mathcal{U} \prod_j (\cos\varepsilon \mathbb{1} - ie^{-i\gamma t_f}\sin\varepsilon \bigotimes_{i\in\ell\ell^{(j)}} Z_i)\,|\psi(0)\rangle \tag{3.36}$$

where $\ell\ell^{(j)}$ is the path given by the union of $\{j\}$ and the two propagation paths $\ell^{(j+)}$ and $\ell^{(j-)}$ of P corresponding to the each of the two anyons created by Z_j. By expanding $\mathcal{U}$, we obtain

$$\begin{aligned} |\psi(t_f)\rangle = \prod_j \Bigg[& \cos^2\varepsilon \mathbb{1} - ie^{-i\gamma t_f} \sin\varepsilon\cos\varepsilon \bigotimes_{i\in\ell\ell^{(j)}} Z_i \\ & + i\cos\varepsilon\sin\varepsilon Z_j + \sin^2\varepsilon e^{-i\gamma t_f} Z_j \bigotimes_{i\in\ell\ell^{(j)}} Z_i \Bigg] |\psi(0)\rangle \,. \end{aligned} \tag{3.37}$$

The state $|\psi(t_f)\rangle$ described by Eq. (3.37) corresponds to a coherent quantum superposition of applying different error paths. For such unitary evolutions, initially orthogonal states will remain orthogonal and thus fully distinguishable. However, there are at least two mechanisms which lead us to consider a mixed density matrix as the final state. The first, is due to the fact that the actual perturbation applied is not known, and can for instance be taken probabilistically among the family of perturbations described. The second, is unperturbed syndrome measurement $\mathcal{M}$, which is the first step of a quantum error correction procedure to recover the initial state.

Syndrome measurement $\mathcal{M}$ will probabilistically project the state $|\psi(t_f)\rangle$ into a subspace consistent with a fixed anyon distribution. This is the first step of the recovery operation $\mathcal{R} = \mathcal{C} \circ \mathcal{M}$, the sequential application of unperturbed syndrome measurement $\mathcal{M}$ followed by a syndrome dependent correction operation $\mathcal{C}$. Analysis of different correction strategies $\mathcal{C}$ need only focus on the resulting mixed state $\mathcal{M}(|\psi(t_f)\rangle\langle\psi(t_f)|)$. Since for any anyon configuration there is at most one combination of operators yielding it in Eq. (3.37), the state $|\psi(t_f)\rangle\langle\psi(t_f)|$ is reduced to a probabilistic application of these operators on $|\psi(0)\rangle\langle\psi(0)|$. Again, taking $\mathcal{E}_{R,p}(\rho) = pR\rho R + (1-p)\rho$, one may verify that

$$\mathcal{M}(|\psi(t_f)\rangle\langle\psi(t_f)|) = \bigcirc_j \mathcal{E}_{Z_j,p} \mathcal{E}_{\bigotimes_{i\in\ell\ell^{(j)}} Z_i,p}(|\psi(t_f)\rangle\langle\psi(t_f)|) \tag{3.38}$$

with $p = \sin^2\varepsilon$. Note that the order of application is arbitrary, since the $\mathcal{E}_{R,p}$ superoperators commute. Thus, one may consider independent probabilities p for observing each anyon pair created by $\mathcal{U}^\dagger$ and propagated by P (or unpropagated anyon pairs created by $\mathcal{U}$). Hence, when instantiating the Hamiltonian perturbation described on a certain set of anyon propagation paths, one need only deal with the independent probabilities of measuring propagated and unpropagated anyon pairs.

3.4.2 Simple error loops in $O(N)$ time

The aim of this subsection is to provide a simple ensemble of perturbations, employing the above construction in such a way that resulting anyon configurations are provably ambiguous, by which we mean that a single anyon configuration could have, with equal likelihood, originated from logically inequivalent errors. This means that for such configurations, the anyon pairing recovery procedure $\mathcal{C}$ can do no better than guessing, and will complete a logical error with a 50% probability for any possible choice of $\mathcal{C}$.

Case	Probability	Errors	Anyons
A	$(1-p)^2$	$\ldots III \ldots III \ldots$	$\ldots 0000 \ldots 0000 \ldots$
B	$p(1-p)$	$\ldots ZZZ \ldots ZIZ \ldots$	$\ldots 0000 \ldots 0110 \ldots$
C	$(1-p)p$	$\ldots IZI \ldots III \ldots$	$\ldots 0110 \ldots 0000 \ldots$
D	p^2	$\ldots ZIZ \ldots ZIZ \ldots$	$\ldots 0110 \ldots 0110 \ldots$

Figure 3.1: Two hollow dots indicate positions where a pair of vertex anyons may be created by $\mathcal{U}^\dagger$ and/or by $\mathcal{U}$ with probability p. Anyons created by $\mathcal{U}^\dagger$ are propagated by P along the darkening path. A table is provided indicating the probability of possible error configurations and their corresponding syndrome observables (1 (0) representing anyon presence (absence)).

Let us first consider weakly perturbing only in the vicinity of a single row. The joint effect of many such perturbations, will then be shown to produce further degradation of stored information. So, $\mathcal{U}^\dagger$ introduces a single Z error (neighboring anyon pair) on a physical start site s of the row with probability p. The paths for the perturbation P are chosen such that both of the produced anyons propagate along the row in opposite directions up to final neighboring locations which are diametrically opposite s (see figure 3.1). For ε weak perturbations, this requires no more than $O(N/\varepsilon)$ time. Finally, with probability p, $\mathcal{U}$ may introduce an error at site s or counter an element of the propagated error chain. As can be seen from the figure, if the anyon introduction site s is chosen uniformly at random, there are observable anyon configurations which occur with probability $2p(1-p)$, which are completely ambiguous (e.g. cases B and C are indistinguishable under exchange of initial site s). However, if such a syndrome is measured, the correction protocol has a 50% chance of completing a horizontal Z loop on the lattice, which is equivalent to applying a completely dephasing channel on one of the encoded qubits with probability $2p - 2p^2$.

By applying such a perturbation family to $i \leq N$ rows of the lattice, the probability of not having such a logically dephasing action take place becomes $(1-2p+2p^2)^i$, which may be made arbitrarily small for large N (i.e. an odd number of horizontal Z loops is completed with a probability exponentially close to $1/2$). Completely analogous string like perturbations exist for any of four logical operators defining the 2-qubit algebra associated to the ground space. Again, by simultaneously considering such perturbations on a sufficiently large set of parallel lines these operators too will be completed with a probability exponentially close to $1/2$. Furthermore, by allowing anyons to hop directly to next nearest neighbors (i.e. Eq. (3.33)), it becomes possible to simultaneously introduce perpendicular yet commuting loop operations as a result of anyon removal.

Simultaneously introducing the four logical operators independently with probability exponentially close to $\frac{1}{2}$, would yield a state exponentially close to a maximal mixture over the code space. Our proof requires terms from different perturbation paths to commute, indicating a possible obstacle to achieving this. In practice however, given that different anyons follow roughly ballistic trajectories with a relatively small spread, this does not pose an issue. In appendix 3.C, we show how it is possible to select the set of anyon trajectories in the perturbation such that the order of anyon crossing is well defined (exponentially well in N). In turn, this implies an exponentially small deviation from the result of performing such anyon propagations in order, resulting in a state exponentially close to a maximal mixture on the four dimensional code-space.

Finally, it is worth mentioning that exactly the same perturbation construction may be applied to the protecting Hamiltonian proposed by Chesi et al. [27] which presents long range repulsive interactions among anyons. However, it must be made clear that the resulting perturbation will, like the unperturbed Hamiltonian, also involve long range interactions. In the case that has been studied numerically, which introduces a constant energy penalty for every arbitrarily distant pair of anyons, our perturbation construction provides exactly the same result for the information lifetime as for the original TC Hamiltonian.

3.4.3 Localization in 2D stabilizer codes

In the perturbations constructed to introduce logical errors in the toric code, there is a strong use of the energy degeneracy of subspaces with the same number of anyons. The strengths

of the different stabilizer terms in the 2D toric code manifest as strengths of local magnetic fields in the effective Hamiltonian of the propagation [67]. However, having exactly the same strength for all local Hamiltonian terms is not an essential feature of the 2D toric code or of stabilizer Hamiltonians in general.

In the unperturbed picture of stabilizer Hamiltonians, excitations are completely localized. However, when different excitations live in a degenerate energy space, perturbations may be very effective at propagating them. In the spirit of Anderson localization, different stabilizer term strengths may be randomly chosen from some range $\gamma_{\text{upper}} > \gamma_{\text{lower}} > 0$, with the hope of protecting against anyon propagation terms.

However, for each such random instance, a specific Hamiltonian perturbation may "smooth" this distribution to take on, at random, only a finite number of discrete energy values, separated by ε, the strength of the perturbation. The number of such possible values is given by $\lceil \frac{\gamma_{\text{upper}} - \gamma_{\text{lower}}}{\varepsilon} \rceil$, which is therefore also the average spacing between sites of the same energy. Hence, by selecting propagation terms of a similar size, the hopping scheme can route around the uneven energy landscape and introduce a logical error. Thus, the argument is unable to guarantee protection against any constant sized perturbation. Nevertheless, it may be that the perturbation terms necessary to break the code should involve a larger number of bodies, which would definitely be an improvement.

In the case of the 2D toric code [67], and all other 2D local stabilizer Hamiltonians [22, 69], there are always logical operations with string like support. This means that, albeit with some possible energetic smoothening, the scheme presented in section 3.4.2 can be adapted to introduce logical errors in arbitrary 2D stabilizer Hamiltonians, meaning that the asymptotic lifetime which 2D $N \times N$ stabilizer codes may guarantee against weak local perturbations cannot be more than $O(N)$.

3.4.4 Logical errors in $O(\log N)$ time

In the previous section, we gave a rigorous upper bound of $O(N)$ on the information lifetime of the toric code. This bound coincides with the one provided by Kay in [67], which required initial anyons in the system to be introduced by an unspecified environment. In this subsection, we provide an exponentially tighter bound by concentrating on specific choices for error correction protocols. We argue that it is possible for a Hamiltonian perturbation to introduce

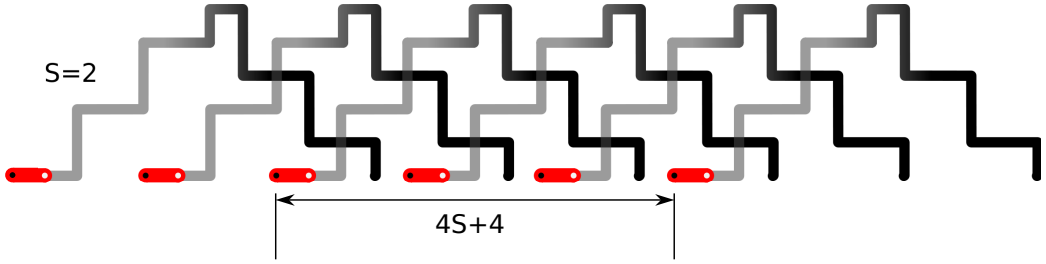

Figure 3.2: Anyon pairs corresponding to each thick red edge may be created by $\mathcal{U}^\dagger$. After a time t_f, the right anyon from each pair introduced will be propagated a distance $4S+2$ to the right introducing Z errors along the darkening paths. Finally, $\mathcal{U}$ acting on the same red segment may move an unpropagated anyon one position to the right or create a neighboring anyon pair on it. The number of big steps (or equivalently of crossings) during the upward propagation is given by S, which in the case of the figure is 2.

ambiguous distributions of anyon configurations in a time logarithmic in N, i.e. after a time $t_f \sim O(\log N)$, error correction succeeds with probability not much higher than $1/2$. Figure 3.2 schematically presents one such perturbation, indicating where anyon pairs should be introduced, and paths P_k along which they should propagate. The fact that the trajectories have only simple crossings allows them to be implemented by weak local Hamiltonian perturbation terms involving at most 8 bodies, as obtained from Eq. (3.33), with p, q being next nearest neighbors. Furthermore, the trajectory length is no more than twice the distance at which the anyon pair is finally separated.

The length of anyon propagation trajectories is $8S+4$, where

$$S = \left\lceil \frac{\ln N}{2p} \right\rceil , \tag{3.39}$$

and each has $2S$ simple crossings with other trajectories. The time required to perform such a propagation by fixed strength local perturbations is proportional to S (i.e. logarithmic in N).

A relevant property of such a perturbation is that anyons observed when performing unperturbed error correction after an evolution time t_f are always collinear. The anyon type and line direction may be chosen to coincide with any of the logical operations, translating to the fact that any logical error may be introduced. This also has the desirable effect of simplifying the analysis of anyon matching criteria. There are only two logically inequivalent

anyon matchings on the line, which are the two perfect matchings in which each anyon is paired with one of its two nearest neighbors (i.e. right or left). The point is that one matching will be logically equivalent to the actual trajectories performed by the anyons, canceling any errors introduced, whereas the other will complete the actual paths into a logical error. A simple criterion to determine which case we are dealing with is to count how many times the actual trajectories, together with the anyon matching, cross a vertical line or any homologically equivalent curve. An odd number of crossings means that a logical error has been completed, whereas an even number of crossings means that the proposed pairing has been successful at error correcting.

We study the success probability of two apparently reasonable matching criteria. The first minimizes the furthest distance among paired anyons. The second, for which a polynomial algorithm is known [122], consists of minimizing the sum of distances among paired anyons. Proofs and numerics will be provided for the large N regime given by $N \gg 4S + 2$ which convey a high logical error rate.

Anyon matching that minimizes L_∞

Let us first consider minimizing the furthest distance among paired anyons. This is the L_∞ norm of the vector with components given by the individual distances among anyons paired by the matching. We will prove that the probability of introducing a particular logical error is close to $1/2$ by considering two disjoint scenarios. The first is the very unlikely scenario in which, on syndrome measurement, two consecutive anyons are measured at a distance $\geq D$ (by consecutive, we mean no additional anyons were measured in the interval between them). The second is composed of anyon distributions consistent with the measurement of a fixed pair of consecutive anyons at a distance $\leq D$. For such distributions, the number of activated anyon paths passing completely over the fixed pair is shown to be odd with probability very close to $1/2$.

Let us first bound the probability of observing two consecutive anyons at a distance greater than D in the syndrome measurement for the evolved state. Given a fixed region of length D, at least $\lfloor D/4 \rfloor$ different potential anyon paths start and end in it. Furthermore, assuming $D < 4S$, the probabilities for not measuring anyons in this region are independent and are $1 - p$ for each end of an anyon path and $(1 - p)^2$ for each start of an anyon path, since both

$\mathcal{U}$ and $\mathcal{U}^\dagger$ could have created anyons in this case. The anyon-free region can begin in any of N locations of the full loop. Thus, regardless of correlations, the probability of having D consecutive anyon-free sites is upper bounded by $N(1-p)^{3\lfloor D/4 \rfloor}$.

Assume now that a pair of consecutive anyons is measured at a distance no greater than D. There are at least $\lfloor (4S-D)/4 \rfloor$ potential anyon paths going over this region, each with independent probability p of being observed. On syndrome read-out, the number of such paths that is activated is odd with a probability approaching $1/2$ at least as fast as $\frac{1}{2}(1 \pm (1-2p)^{\lfloor (4S-D)/4 \rfloor})$. Since the L_∞ norm correction completes a logical error if the most distant consecutive anyon pair is covered by an odd number of activated anyon paths, then by inserting $S = \lceil \frac{\ln(N)}{2p} \rceil$ and $D = \lceil \frac{8\ln(N)}{5p} \rceil$, we get a probability lower bound for logical errors which approaches $1/2$ as $1/2(1 - N^{-1/5})$.

Anyon matching that minimizes L_1

Let us now consider the anyon pairing criterion that minimizes the total sum of distances among paired anyons. Since all anyons are found on a loop of length N, this criterion will always choose a pairing with total distance no greater than $N/2$. Thus it will successfully error correct if and only if the total distance of regions of the loop covered an odd number of times by observed anyons is no greater than $N/2$. By taking S to be $\lceil \frac{\ln N}{2p} \rceil$, we expect to find roughly half of the sites flipped. To see this, note that, on average, each site is covered approximately $S\varepsilon$ times. Moreover, the probability of each site being covered an odd number of times is $\frac{1}{2}[1-(1-2p)^S]$. For small p and the chosen value of S, the average number of sites covered an odd number of times is approximated by $\frac{N}{2} - \frac{1}{2N}$. Furthermore, we expect the actual number of such sites to approximately follow a normal distribution around this value, which would imply that logical errors are completed with a probability close to $\frac{1}{2}$. However, since the flipping of different nearby sites are highly correlated events, it is not clear how to go about proving this. Instead, computer simulations (Fig. 3.3) provide very strong numerical evidence.

3.4.5 Discussion

We have proven that Hamiltonian perturbations can completely destroy the information stored in the 2D toric code in a time proportional to N. The only assumptions are that the precise

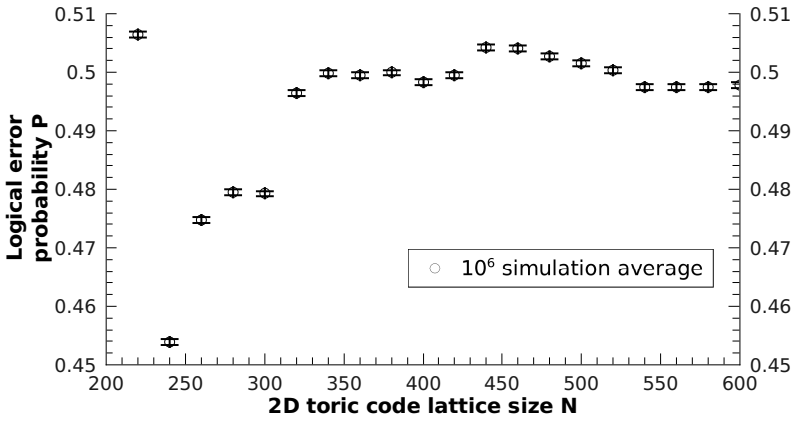

Figure 3.3: The average probability of error for L_1 correction after the system evolves for a time t_f under the described Hamiltonian perturbation. Here, anyon pairs arise, and evolve to distances of $\lceil 20 \ln(N) \rceil$, with a probability of 10%, all collinear on a line of length N. Each point represents an average over 10^6 random samples, with error bars representing the magnitude of estimated statistical errors.

Hamiltonian perturbation is unknown, and that recovery begins by performing unperturbed syndrome measurements. A simple family of Hamiltonian perturbations with associated probabilities, was used to justify that the introduction of logical errors in $O(N)$ time is fully independent from the correction protocol used. This approach remains applicable for arbitrary 2D stabilizer codes, even when the stabilizer terms are of uneven strength.

Furthermore, we have argued that logical errors may be introduced by weak local perturbations in a time logarithmic with the system size. In particular, two apparently reasonable anyon pairing schemes were shown to provide an unreliable recovery mechanism against weak local perturbations acting for $O(\log N)$ time.

A fully general proof, including all possible error correction strategies based on syndrome measurement is currently lacking for the $O(\log N)$ error introduction. The generality of the $O(N)$ construction is obtained by considering a family of different perturbations which could produce the same syndrome outcomes through topologically inequivalent error paths. It may be fruitful to apply such an approach for a general proof of logical errors produced in $O(\log N)$ time.

3.5 Limitations of the 2D Ising model

In present day classical computers, magnetic domains are widely used to provide passive safekeeping of classical information. The Ising model is usually used to elucidate the origin of such long lived magnetized states as a collective effect arising from microscopic local 2-body interactions

$$H_{Ising} = -J \sum_{\langle i,j \rangle} Z_i Z_j. \tag{3.40}$$

In two and higher spatial dimensions, the nearest neighbor Ising model presents a finite temperature phase transition between a disordered phase and an ordered magnetized phase. However, it has long been known that such a system looses its asymptotic bistability under the bias produced by even the weakest of magnetic fields [106, 30, 51]

$$\tilde{H}_{Ising} = -J \sum_{\langle i,j \rangle} Z_i Z_j + \varepsilon \sum_j Z_j. \tag{3.41}$$

Such studies consider the dynamics of minority droplets in a 2D Ising model as given by phenomenological equations or the Metropolis algorithm. For a Metropolis algorithm in which such a systematic magnetic field ε is included, there is only one stable phase parallel to the field. The anti-parallel phase becomes metastable, with a lifetime exponential in J/ε. Dependence of the information lifetime on lattice size N appears only for the small $N \leq 4J/\varepsilon$ and will thus not appear if one first takes the limit for large N.

In this section we consider storing one bit of classical information subject to a quantum evolution of a perturbed 2D Ising Hamiltonian. The observable on which the classical bit is encoded is assumed to be the overall direction for magnetization $\bar{Z} = \mathsf{maj}_j Z_j$. The perturbations may conceptually be split into two parts, Z parallel magnetic fields which introduce additional degeneracies to the Hamiltonian, and transverse magnetic fields or many body terms which couple the new ground states, introducing a hopping between them. The perturbation terms considered will not show support or intensity growing with N, and they will be capable of introducing logical errors to the unperturbed logical observable $\bar{Z}$ in a time also independent of N.

3.5.1 Hamiltonian perturbation proposal

Consider dividing the $N \times N$ 2D periodic lattice with a chessboard pattern of squares of $M \times M$ spins where $M > 4J/\varepsilon_{\max}$ and J is, again, the nearest neighbor Ising coupling constant and $\varepsilon_{\max}$ is the greatest local perturbation strength one expects the Hamiltonian to protect information against. For simplicity, we assume $N = 2nM$, where n is an integer. Consider alternately introducing $\pm\varepsilon Z_j$ magnetic fields in the lattice site j belonging to white/black squares of the chessboard pattern respectively. The value ε is chosen homogeneously for each square such that the energy difference, $2\varepsilon M^2$, from fully field parallel and anti-parallel configurations of each square exactly matches the maximum energy difference for border Ising terms $8MJ$. For $N \gg J/\varepsilon$ such a perturbation is always possible.

The point is that now, the ground space of the system acquires a much higher degeneracy, i.e. between $2^{2n^2+1} - 1$ and 2^{4n^2}. Each black square could be fully magnetized parallel to its preferred field direction or parallel to the direction of its four neighboring squares if it is opposite. By taking one spin variable for each square, the ground states may be identified with those of a 2D $n \times n$ anti-ferromagnetic Ising model with magnetic field. Three important ground states are the two fully magnetized lattice configurations and the checkerboard configuration in which all spins are fully aligned to their local magnetic field. The gap of these ground states with respect to low lying exited states is 2ε, which is the energy penalty of flipping a corner lattice site of a square that is fully oriented in the direction of the field but anti-parallel to the two neighboring squares adjacent to the stated corner.

A flipping term for each square of the chessboard should be of the form $\alpha \bigotimes_j X_j$, where the j is taken over all the M^2 sites in the square. Such terms can be introduced either on all black squares or all white squares. This would respectively couple one of the two fully magnetized configurations with the checkerboard configuration, achieving a full swap of state in a time $t_{\text{flip}} = \frac{\pi}{\alpha}$. This evolution is exact when such M^2-body terms of norm α are allowed, which implies that a proof of Hamiltonian stability will not only require assuming sufficiently weak perturbation terms but also a specific bound for the number of bodies on which such terms act.

Let us now focus on the magnitude of α. This is the coefficient for a many body term, in which the size of the support scales like $M^2 = (4J/\varepsilon)^2$, independent of N. One may consider obtaining such a term from the M^2-th order degenerate perturbation theory expansion of fields

of the form $\varepsilon_2 \sum_j X_j$. For perturbation theory to be strictly valid, one needs $M^2\varepsilon_2 < \varepsilon$. Even then, this small magnitude must be taken to the M^2-th power to obtain the first non vanishing expansion term. The time required to flip all spins in a plaquette is then proportional to:

$$\alpha \approx \varepsilon_2 \left(\frac{\varepsilon_2}{\varepsilon}\right)^{M^2} \approx \varepsilon M^{-2(M^2-1)} = \varepsilon \left(\frac{\varepsilon}{4J}\right)^{\frac{32J^2}{\varepsilon^2}+2}. \tag{3.42}$$

This expression has no dependence on N and the same perturbation can be introduced in all squares of a given color to yield a fixed flip time. Furthermore, we note that the state of those chessboard squares which are not perturbed is fixed and may be traced out exactly. Hence, the second set of perturbations applied are fully independent and degenerate perturbation theory may be rigorously applied.

3.5.2 Discussion

Although the flip time shows no dependence on N, it grows faster than exponentially in terms of $4J/\varepsilon$. It may well be that for magnetic domains, describable by such a 2D Ising Hamiltonian as Eq. (3.40), the ratio $4J/\varepsilon$ is sufficiently large to provide a lifetime longer than would be experimentally verifiable. More importatntly, we are dealing with an extremely simplified model, with the particularity of neglecting any long range interactions of actual physical systems and more importantly, dissipative terms in the form of decoherence which would dissallow the coherent evolution and thus help in preserving the classical information.

The fact that the perturbation is unknown means that if such a checkerboard state is observed on read-out, information is not recoverable. Such schemes may clearly be generalized to higher dimensions and to deformations of the checkerboard pattern. The existence of such perturbations elucidates important limitations for statements one may formally prove about the classical memory reliability of the Ising model, and therefore what conclusions one might draw about the presence of a macroscopic energy barrier (string tension) which the 2D Ising model certainly possesses. However, it is not clear that these arguments can be applied, for instance, to the 4D toric code since it is a feature of classical memories, but not quantum ones, that local fields can split degeneracies.

3.6 Aggressive noise models

In previous sections, we explored the effects of Hamiltonian perturbations on quantum memories, and particularly on the 2D toric code. We also considered examples of local cold environments perturbatively coupled to a system, as illustrated by Secs. 3.2.2 and 3.3. The only energy available in these scenarios was due to local perturbations on the system plus environment. Intuitively, a small but constant energy density proportional to ε was allowed. While this energy is potentially $O(N^d)$ for a d spatial dimension lattice of N^d qubits, it is difficult to concentrate it in specific regions in order to generate logical errors. In comparison, stabilizer codes only require $O(N^{d-1})$ energy to implement a logical gate through local rotations.

More aggressive noise models may locally introduce large amounts of energy into the system while keeping perturbation magnitudes weak. Such an example is provided by weak yet time dependent Hamiltonian perturbations. These are relevant when one considers effective protecting Hamiltonians in the interaction picture [23]. Another possibility is to consider the weak coupling of the system to an environment which starts in a high energy state. Noise constructions for these models shall be presented in this section.

In calling such noise models aggressive, we convey the fact that we do not expect "reasonable" Hamiltonian protection schemes to guarantee a long lifetime against such models. Thus, their study may help identify required restrictions on the noise model in order to allow for provably robust Hamiltonian protected memory models. Furthermore, it may provide insight regarding potentially fruitful proof techniques.

3.6.1 Time-varying Perturbations

When considering Hamiltonian perturbations, we assumed that we were unable to determine the new ground space due to the perturbation, and thus encoded in the original ground state space. One might consider an intermediate setting where encoding can be achieved in the perturbed code-space, perhaps due to an adiabatic evolution such as proposed by [54], or by a precise characterization and compensation of the perturbations present at the start of the storage time. However, in real experiments, stray fields responsible for perturbations may fluctuate in time. Again, if one can track adiabatic changes in the perturbations, the proof of Hastings and Wen [57] continues to hold because Lieb-Robinson bounds apply to time-varying

local Hamiltonians, and we can therefore adapt the final error correction step as well. Instead, we proceed assuming it is impossible to precisely learn this time variation.

Adiabatically varying perturbations

One extreme case to consider is that the perturbation varies adiabatically, so that the system remains in its ground state space. If we do not apply error correction, then we are concerned with how long it takes before the initial and final ground states have a small overlap. We shall assume that the original Hamiltonian H of N qubits has an energy gap γ, and we will consider the time-varying perturbation

$$V = \mathcal{U}(t) H \mathcal{U}^\dagger(t) - H$$

where, as before,

$$\mathcal{U}(t) = \prod_{j=1}^{N} e^{-it\varepsilon X_j/T}$$

and T is the total time of the evolution, i.e. small local rotations are gradually introduced. At any time $0 \leq t \leq T$, the effective Hamiltonian $\mathcal{U}(t) H \mathcal{U}^\dagger(t)$ has the same energy gap as H, which means that the adiabatic condition is satisfied for $T \sim 1/\text{poly}(\gamma)$. From previous considerations, Eqn. (3.61), we know that the overlap of the initial state $|\psi(0)\rangle$ and the evolved state, the ground state of the adiabatically perturbed Hamiltonian, have an average overlap of no more than $\mathsf{tr}\,(P_0)\,(1 - \frac{3}{4}\sin^2(t\varepsilon/T))^N$. For large N and small ε, this means that the final overlap is of the order $\mathsf{tr}\,(P_0)\exp(-\frac{3\varepsilon^2 N}{4})$ if a phase of error correction is not involved.

When error correction is introduced to this scenario, this maps into the situation where our quantum memory is initially encoded in the perturbed subspace, but decoding is using the original, unperturbed, error correction strategy. In the specific instance of the perturbation $\mathcal{U}(T)$, we find that X rotations are applied probabilistically on each site, and hence our QECC must have a superior error threshold.

Hastings and Wen [57] reveal a similar interpretation holds for all possible perturbations since all local terms are converted into quasi-local rotations.

Rapidly oscillating perturbations

Another extreme scenario is when perturbations are allowed to oscillate with arbitrary frequencies. A simple construction shows that for stabilizer Hamiltonians, this allows the in-

troduction of arbitrary errors in constant time. We expect that optimal control theory may provide the tools to generalize such results to arbitrary Hamiltonians.

Consider a stabilizer Hamiltonian H_0 and a logical error to implement $L = P_M P_{M-1} \dots P_2 P_1$, which is decomposed into Pauli operators P_i on different sites. We then consider the time dependent Hamiltonian perturbation

$$V(t) = \varepsilon(t) \sum_i e^{-iH_0 t} P_i e^{iH_0 t}. \tag{3.43}$$

This perturbation is weak if $\varepsilon(t)$ is sufficiently small. Furthermore, given that H_0 is a stabilizer Hamiltonian, $V(t)$ may be written as a sum of local terms (at least as local as the stabilizer operators). Finally, the dependence of $\varepsilon(t)$ on time, is to allow for $\varepsilon(0) = 0$ which makes the initial encoding equivalent for both perturbed and unperturbed Hamiltonians.

The point of such a perturbation, is that it is possible to explicitly calculate the evolution of the system state in the interaction picture.

$$|\psi_I(t)\rangle = \Pi_i e^{-iP_i \int_0^t \varepsilon(t')dt'} |\psi_I(0)\rangle \tag{3.44}$$

This means that after a constant time t_f such that $\frac{\pi}{2} = \int_0^{t_f} \varepsilon(t')dt'$, the target operation L is perfectly implemented in the interaction picture. If $|\psi(0)\rangle$ is an eigenstate, then L is also implemented in the Schrödinger picture, modulo a global phase.

Taking L to be a logical operator of the stabilizer code used, this means that time dependent perturbations of sufficiently high frequency can destroy stored information in constant time. Here, sufficiently high frequency refers to having perturbation terms which oscillate with frequencies at least as high as those corresponding to localized excitations.

3.6.2 Stabilizer Hamiltonians and energetic environment

In what follows, we consider a model in which an environment starts out in an arbitrarily energetic state. However, the couplings between system and environment are required to remain small and local.

For simplicity, we assume that the system is defined by a stabilizer Hamiltonian H_S and that it starts out in an eigenstate $|\psi_0\rangle$ of all stabilizer operators. We will consider a sequence of M Pauli operators on different sites $L = P_M P_{M-1} \dots P_2 P_1$ compounding to a logical operation. In the case of translationally invariant stabilizer codes, explicit constructions

for these operators are given in [69]. Finally, we may assume a code state $|\psi_0\rangle$, such that $\langle\psi_0| L |\psi_0\rangle = 0$.

Motivated by the realization that, in order to introduce logical errors, we need to transfer some energy from the environment to the system, we choose a specific environment Hamiltonian $H_E = -H_S^*$ (at this point, the complex conjugate is unnecessary, but will become useful later). This means that all steps up in energy in the system correspond to an identical step down in energy in the environment. We start the environment state in $|\psi_0^*\rangle$.

In this scenario, the coupling

$$H_{SE} = \varepsilon \sum_{i=1}^{M} P_{S,i} \otimes P_{E,i}^* \tag{3.45}$$

is enough to produce the logical error L in constant time $\frac{\pi}{2\varepsilon}$. To see this, consider the two states $P_{S,\mathbf{i}} |\psi_0\rangle P_{E,\mathbf{i}}^* |\psi_0^*\rangle$ and $P_{S,\mathbf{i}} P_{S,i} |\psi_0\rangle P_{E,\mathbf{i}}^* P_{E,i}^* |\psi_0^*\rangle$. Here, the subindex $\mathbf{i}$ is an arbitrary binary vector indicating which values of j a product of $P_{S,j}$ (respectively $P_{E,j}^*$) should be taken over. First of all, since we have assumed H_S is a stabilizer, and the $P_{S,i}$ are Pauli operators, the aforementioned states are zero eigenstates of $H_S \otimes \mathbb{1}_E + \mathbb{1}_S \otimes H_E$. Furthermore, the effective Hamiltonian for the perturbation term $\varepsilon P_{S,i} \otimes P_{E,i}^*$ acting on the pair of states $P_{S,\mathbf{i}} |\psi_0\rangle P_{E,\mathbf{i}}^* |\psi_0^*\rangle$ and $P_{S,\mathbf{i}} P_{S,i} |\psi_0\rangle P_{E,\mathbf{i}}^* P_{E,i}^* |\psi_0^*\rangle$ is just a matrix

$$\varepsilon \begin{pmatrix} 0 & 1 \\ 1 & 0 \end{pmatrix},$$

independent of $\mathbf{i}$. This means that we can consider the action of the different $P_{S,i} \otimes P_{E,i}^*$ terms independently:

$$e^{-iH_{SE}t} |\psi_0\rangle = \left(\bigotimes_{i=1}^{M} e^{-i\varepsilon P_{S,i} \otimes P_{E,i}^* t} \right) |\psi_0\rangle .$$

Due to the effective Hamiltonian, $P_{S,\mathbf{i}} |\psi_0\rangle P_{E,\mathbf{i}}^* |\psi_0^*\rangle$ is mapped to $P_{S,\mathbf{i}} P_{S,i} |\psi_0\rangle P_{E,\mathbf{i}}^* P_{E,i}^* |\psi_0^*\rangle$ in a time $\pi/(2\varepsilon)$. Thus, the effect of the entire perturbation is to rotate, in a time $\pi/(2\varepsilon)$ from $|\psi_0\rangle$ to $L |\psi_0\rangle$.

Of course, this approach requires the environment state to have a very high initial energy, namely to start in one of its highest energy states. A refinement of this argument allows us to only change the sign of stabilizers in H_E which share support with L. For a local stabilizer code in d spatial dimensions consisting of N^d qubits, it was shown [69, 22] that there are logical operators L with support on $k \propto N^{d-1}$ sites. The initial state of the environment

$|\psi_E\rangle = |\psi_0^*\rangle$ is still an eigenvector of these stabilizers, with the same eigenvalues. Thus, coupling to an environment with an energy proportional to N^{d-1}, may also introduce logical errors in the same time. This means that the energy required from the environment per system qubit tends to 0 as $\frac{1}{N}$ (compare to perturbations, which introduce an energy ε per site). The catch however, is that the distribution of the energy in the initial environment is highly specific and is in general very different from distributions that may be provided by low temperature thermal states.

We conclude that no stabilizer Hamiltonian will be capable of providing a guarantee for the logical integrity of stored information under the presence of an adversarial, weakly coupled, local environment. Further statistical assumptions such as energy distribution associated to a low temperature environment state need to be included in addition to the weak local coupling assumptions.

3.6.3 Non-stabilizer Hamiltonians

Stabilizer Hamiltonians are not the only possible candidates for providing information protection, although they are particularly attractive because local errors remain as local errors (not propagating or multiplying in the absence of perturbations). Let us now consider the more general case of distance preserving Hamiltonians i.e. ones which might not leave local errors perfectly localized, but do not increase the distance of the error as defined by an error correcting code[4]. Using the same construction as in the previous section, we will show that weak coupling to an environment can also introduce the relevant logical error into a distance preserving Hamiltonian (i.e. a logical operation converting between the most distant code states) for classical memories, by which we mean that one set of local errors becomes irrelevant, say Z errors, and the presence of a logical error on the classical bit depends only on the local X errors present. The distance preserving assumption means that the number of X errors is preserved, $[H_S, \sum_i Z_i] = 0$. The maximum distance between any 2 states is for the eigenstates $\bigotimes_i |0\rangle_i$ and $\bigotimes_i |1\rangle_i$, suggesting we should use these states for encoding.

Similarly to the previous subsection, we introduce an environment, and a perturbative

[4] As an aside, note that the 3D XZ-compass code [11] is an example of a code where the errors do not remain in fixed positions, but preserve the values of the observables (since the observables commute with the Hamiltonian). This suggests that applying explicit error correction is already likely to become much more problematic for these codes.

coupling between system and environment,

$$H(\varepsilon) = H_S \otimes \mathbb{1}_E + \mathbb{1}_S \otimes H_E + \varepsilon \sum_i X_{i,S} \otimes X_{i,E}. \tag{3.46}$$

The system Hamiltonian is weakly coupled to a "mirror" system $H_E = -H_S^*$. This perturbative coupling is responsible for the evolution of a mirrored state $|0\rangle^{\otimes N} |0\rangle^{\otimes N}$, eigenstate of the unperturbed Hamiltonian $H(0)$.

To analyze the evolution, let us consider the action of the operators X_i in terms of the eigenstates of H_S. Due to the commutation relation, there must be $\binom{N}{m}$ eigenstates $\{|\psi_{m,j}\rangle\}$ of H_S which are simultaneous eigenvectors of $\sum_i Z_i$ with eigenvalue $2m - N$. We can thus express the eigenvectors $|\psi_{m,j}\rangle$ of H_S in terms of the canonical basis as

$$|\psi_{m,j}\rangle = \sum_{\mathbf{i}:w(\mathbf{i})=m} \alpha(m)_{\mathbf{i},j} X_{\mathbf{i}} |0\rangle^{\otimes N} = \sum_{\mathbf{i}:w(\mathbf{i})=m} \alpha(m)_{\mathbf{i},j} |\mathbf{i}\rangle , \tag{3.47}$$

where $\mathbf{i}$ are binary vectors with m non zero components and $|\mathbf{i}\rangle$ are the respective states from the canonical basis. The matrix $\alpha(m)$ is unitary as it relates two orthonormal bases of the same subspace. Define

$$\begin{aligned} |\overline{m}\rangle &= \frac{1}{\sqrt{\binom{N}{m}}} \sum_{\mathbf{i}:w(\mathbf{i})=m} |\mathbf{i}\rangle |\mathbf{i}\rangle \\ &= \frac{1}{\sqrt{\binom{N}{m}}} \sum_{j,k,(i):w(\mathbf{i})=m} \alpha(m)^*_{\mathbf{i},j} \alpha(m)_{\mathbf{i},k} |\psi_{m,j}\rangle \left|\psi^*_{m,k}\right\rangle \\ &= \frac{1}{\sqrt{\binom{N}{m}}} \sum_j |\psi_{m,j}\rangle \left|\psi^*_{m,j}\right\rangle . \end{aligned} \tag{3.48}$$

From this, one obtains that

$$(H_S \otimes \mathbb{1}_E - \mathbb{1}_S \otimes H_S^*) |\overline{m}\rangle = 0, \tag{3.49}$$

implying that any non trivial evolution of $|\overline{m}\rangle$ arises exclusively from the perturbative coupling and is given by

$$H(\varepsilon) |\overline{m}\rangle = \varepsilon J_m \left|\overline{m-1}\right\rangle + \varepsilon J_{m+1} \left|\overline{m+1}\right\rangle , \tag{3.50}$$

with $J_m = \sqrt{m(N+1-m)}$. These are precisely the coefficients performing perfect state transfer between $\left|\overline{0}\right\rangle = |0\rangle^{\otimes 2N}$ and $\left|\overline{N}\right\rangle = |1\rangle^{\otimes 2N}$ in a constant time $t = \frac{\pi}{2\varepsilon}$ [29, 68].

These results exclude the possibility of proving robustness against weak adversarial coupling to an arbitrarily initialized environment, even of many classical memories using the

repetition code (such as Ising models). We learn that if the environment can provide enough energy, then even weak local couplings may be sufficient to produce logical operations. This also motivates the desire to encode in the ground state space of the Hamiltonian since, were we to encode in a higher energy subspace, the environment needs less energy to cause destructive effects. Alternatively, the mechanism presented here could present a useful way to implement gates on a memory.

3.7 Further applications

Constructed perturbations and results presented in this chapter have focused on elucidating limitations of passive quantum memories. However, our results may be recast in the following other scenarios.

Adiabatic Quantum Computation- The standard approach to adiabatic quantum computation consists of implementing an adiabatic evolution

$$H(t) = f(t)H_i + (1 - f(t))H_f, \tag{3.51}$$

between Hamiltonians H_i and H_f, where $f(0) = 1$ and $f(T) = 0$. While the ground state of the initial Hamiltonian H_i is expected to be readily prepared, the ground state of the final Hamiltonian H_f encodes the result of the desired quantum computation. An energy gap no less than γ between ground state and excited states of $H(t)$ is required for the duration of the adiabatic evolution.

In this context, it is possible that Hamiltonian perturbations could change the initial or final ground state, and maybe even close the gap during the Hamiltonian trajectory. For example, a time dependent perturbation

$$V(t) = \mathcal{U}H(t)\mathcal{U}^\dagger - H(t), \tag{3.52}$$

with $\mathcal{U}$ defined as in Eq. (3.3), can make the perturbed initial and final ground states almost orthogonal to the unperturbed versions (see Eq. (3.8)), while keeping the same gap as $H(t)$. Even assuming the perturbed initial ground state is exactly prepared, only if the final state belongs to a code space with an error threshold, will it be possible to reliably recover the desired result, as in 3.6.1.

Connections between adiabatic quantum computation and passive quantum memories can be expected to continue into the regime where error correction is incorporated, and future studies may better elucidate the issues involved in developing a fault-tolerant theory of adiabatic quantum computation [82].

Topological Quantum Computation- Difficulties in implementing quantum memories can also be related to some of the difficulties in implementing a topological quantum computation. In particular, in section 3.4 we illustrated how constant Hamiltonian perturbations can create and propagate anyons in the 2D toric code. In the context of topological quantum computation, where gates are implemented through the braiding of anyons, the existence of perturbations capable of creating and propagating anyon pairs is at least equally disturbing as in the memory scenario.

Quantum Simulations- One of the most interesting uses of a quantum computer is likely to be the simulation of other quantum systems. While one could express these simulations in terms of the circuit model of quantum computation, and from there create a circuit-based theory of fault-tolerance for quantum simulation, it would be advantageous to understand how this could be implemented more directly, via the simulation of an encoded Hamiltonian.

A logical first step would be to encode the state of each subsystem to be simulated into a quantum memory. Thus, establishing when quantum memories exist, or when they fail, has implications in this case. One of the most commonly applied techniques in Hamiltonian simulation is that of the Trotter-Suzuki decomposition, where pulses of non-commuting Hamiltonians are combined into one effective Hamiltonian to some accuracy δ. This inaccuracy may be treated as a time dependent Hamiltonian perturbation. Given the power such perturbations were shown to have, it is with great care that one should consider the use of passive quantum memories as elements for such quantum simulators.

3.8 Conclusions

In this chapter, we have studied several constraints on the extent to which a many body Hamiltonian can be expected to protect quantum information against weak local coupling to an environment. First of all, we showed that gapped local Hamiltonians have eigenstates which are asymptotically unstable under local Hamiltonian perturbations. This result, commonly referred to as Anderson's orthogonality catastrophe [10] shows that a gap is not sufficient to

guarantee protection against errors [65, 53]. We proved that a weakly coupled cold environment can alter the evolution of any quantum state leading to an exponentially small overlap between initial and final states in constant time. Taking these results together, we conclude that quantum memory schemes must encode information into a logical subsystem instead of restricting to a particular subspace.

When applied to the 3D XZ-compass model [11], a self-correcting quantum memory proposal, we find that the standard QECC protocol is not capable of recovering the encoded information after a constant time. This means that the unperturbed order parameter is not preserved. Our results extend to other systems revealing that the code and error correcting process must possess an error threshold. Similar conclusions may be drawn in scenarios where information encoding and evolution follow a perturbed Hamiltonian but read-out and decoding do not.

Further explicit local Hamiltonian perturbation constructions illustrate that while adapting for known perturbations is theoretically possible, arbitrary unknown perturbations can destroy the storage properties of codes such as the 2D Toric code in a time $O(\log N)$. In this case, the proposed adversarial Hamiltonian perturbation heavily relies on the absence of a macroscopic energy barrier (it is possible to transform orthogonal encoded states via a sequence of local operations while keeping intermediate states in a low energy subspace). By considering the 2D Ising model, we have argued that, in and of itself, a macroscopic energy barrier is not sufficient to protect against perturbations. Let us stress once more, that the perturbations considered are highly atypical, and that furthermore, we expect that genuine dissipation mechanisms will play a key role in analyzing the robustness of such models.

Finally, we have considered strong noise models such as time varying Hamiltonian perturbations and weak coupling to an arbitrarily initialized environment. We showed that these noise models could apply logical transformations on information protected by stabilizer Hamiltonians or distance preserving classical memories in constant time. Although we consider such noise models to be too strong to be of practical relevance, we expect these result to provide insight into how one may prove properties of passive quantum memories and under which assumptions. For instance, since such time-varying Hamiltonian perturbations can destroy the 4D toric code, then when trying to prove robustness against static perturbations, Lieb-Robinson bounds are unlikely to be beneficial.

Having proven a variety of limitations for quantum memory models and elucidated some required conditions, the next step is to incorporate this deeper understanding into new designs for quantum memories. One major route is to establish a set of necessary and sufficient conditions under which a quantum memory is protected against unknown weak static perturbations. Under such a model, we may once again raise the question of whether good protecting Hamiltonians in two or three spatial dimensions exist. Furthermore, one would hope to find similar conditions under an extended perturbation model allowing a perturbatively coupled local environment. Here, a central problem is to determine which physically realistic assumption may be made on the environment such that positive results are still attainable (i.e. conditions on the initial state of the environment, such as it being prepared in its ground state). Finally, one may study the possibility of engineering an out of equilibrium environment to provide additional protection to quantum information.

3.A State evolution in perturbed gapped Hamiltonians

Energy gaps are considered as a positive feature for a protecting Hamiltonian, since they are expected to provide an energetic barrier which an error process is required to overcome. However, it will be shown that for sufficiently large N, the fidelity of the unperturbed eigenstates acquires an upper bound close to $1/2$ after being evolved under the effect of a perturbed Hamiltonian for a time inversely proportional to the gap energy γ.

If a system is perturbed, but we do not know the nature of the perturbation, the best strategy is, arguably, to continue using the unperturbed encoding (i.e. the eigenstates of the unperturbed Hamiltonian). The survival probability for an unperturbed eigenstate $|\psi_0\rangle$ of H after evolution under a perturbed Hamiltonian $\tilde{H}$ for a given time t (Eq. (3.3)) is, without error correction

$$S(t) = \left|\langle\psi_0| e^{-it\tilde{H}} |\psi_0\rangle\right|^2 = \left|\langle\psi_0|\mathcal{U}e^{-itH}\mathcal{U}^\dagger |\psi_0\rangle\right|^2, \tag{3.53}$$

i.e. we can express $S(t)$ as the overlap of $\mathcal{U}^\dagger |\psi_0\rangle$ with itself under the evolution of the unperturbed Hamiltonian H. Furthermore, in terms of the eigenstate decomposition

$$\mathcal{U}^\dagger |\psi_0\rangle = \sum_j \alpha_j |\psi_j\rangle \quad \text{where} \quad H|\psi_j\rangle = E_j |\psi_j\rangle, \tag{3.54}$$

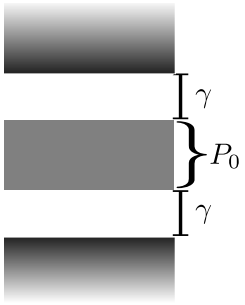

Figure 3.4: There is an energy gap γ separating the eigenenergies corresponding to an exponentially small subspace P_0 from the energies of the Hamiltonian eigenstates giving rise to the rest of the Hilbert space.

$S(t)$ may be expanded as

$$S(t) = \sum_{i,j} |\alpha_i|^2 |\alpha_j|^2 \cos[(E_i - E_j)t]. \tag{3.55}$$

Assume the initial state $|\psi_0\rangle$ belongs to an energy subspace P_0 of H (i.e. $\langle\psi_0| P_0 |\psi_0\rangle = 1$), and that H imposes an energetic gap γ between the subspace P_0 and its orthogonal subspace (see figure 3.4). This allows the sum in Eq. (3.55) to be split as

$$\begin{aligned} S(t) = &\sum_{|\psi_i\rangle,|\psi_j\rangle\in P_0} |\alpha_i|^2 |\alpha_j|^2 \cos((E_i - E_j)t) \\ &+ \sum_{|\psi_i\rangle,|\psi_j\rangle\notin P_0} |\alpha_i|^2 |\alpha_j|^2 \cos((E_i - E_j)t) \\ &+ 2 \sum_{|\psi_i\rangle\in P_0,|\psi_j\rangle\notin P_0} |\alpha_i|^2 |\alpha_j|^2 \cos((E_i - E_j)t) \end{aligned} \tag{3.56}$$

We then define R, the $\mathcal{U}P_0\mathcal{U}^\dagger$ subspace overlap of $|\psi_0\rangle$ as

$$R = \langle\psi_0| \mathcal{U}P_0\mathcal{U}^\dagger |\psi_0\rangle = \sum_{|\psi_i\rangle\in P_0} |\alpha_i|^2 . \tag{3.57}$$

Taking the time average $\langle S(t')\rangle_{t'\in[0,t]} = \frac{1}{t}\int_0^t S(t')dt'$, and noting that

$$|E_i - E_j| \geq \gamma \;\Rightarrow\; \left| \int_0^t \cos\left((E_i - E_j)t'\right) dt' \right| \leq \frac{1}{\gamma}, \tag{3.58}$$

Poincaré recurrences are averaged out, providing a bound

$$\langle S(t')\rangle_{t'\in[0,t]} \leq R^2 + (1-R)^2 + \frac{2}{\gamma t} R(1-R). \tag{3.59}$$

Although the bound in Eq. (3.59) is minimized for $R = 1/2$, this does not imply that the smallest values for $\langle S(t')\rangle_{t'\in[0,t]}$ are actually obtained for $R = 1/2$.

A sufficient condition for the existence of a weak perturbation yielding $R = \frac{1}{2}$ may now be obtained by means of continuity arguments. First, note that R depends continuously on the parameter ε appearing in the definition of the rotation $\mathcal{U}$, and $R = 1$ for $\varepsilon = 0$. This means that if, for some $\varepsilon_0 > 0$, we find that $R < 1/2$, then R must be equal to $1/2$ for some smaller positive value $0 < \varepsilon < \varepsilon_0$.

As in the previous subsection, we may take $\langle R\rangle_{\mathcal{U}}$ as an average of the overlap R over different directions of the rotation $\mathcal{U}$. An expression for $\langle R\rangle_{\mathcal{U}}$, in terms of the depolarizing channel is given by

$$\langle R\rangle_{\mathcal{U}} = \mathsf{tr}\left(P_0 \Delta_{\lambda(\varepsilon)}^{\otimes N}\left(|\psi_i\rangle\langle\psi_i|\right)\right). \tag{3.60}$$

Including the dimension of the subspace P_0, the same bound as in Eq. (3.8) may be used, leading to

$$\langle R\rangle_{\mathcal{U}} \leq \mathsf{tr}\left(P_0\right)\left(1 - \frac{3}{4}\sin^2(\varepsilon)\right)^N. \tag{3.61}$$

If the asymptotic growth of $\mathsf{tr}\left(P_0\right)$ is slower than $\left(1 - \frac{3}{4}\sin^2(\varepsilon)\right)^{-N}$, the bound (3.61) will be exponentially decreasing with N. This means that for sufficiently large N, and for most directions of rotation, there is some small rotation parameter ε yielding $R = 1/2$. For the important case of small ε and a constant dimension $\mathsf{tr}\left(P_0\right)$, large N refers to $N \sim O(\varepsilon^{-2})$.

For those $\mathcal{U}$ leading to $R = \frac{1}{2}$, the time averaged survival probability $\langle S(t')\rangle_{t'\in[0,t]}$ for the corresponding perturbation may be bounded as

$$\langle S(t')\rangle_{t'\in[0,t]} \leq \frac{1}{2} + \frac{1}{2\gamma t}. \tag{3.62}$$

We thus obtain that the overlap of initial encoded states and uncorrected evolved states will drop to values not much larger than $\frac{1}{2}$ in a time inversely proportional to the gap γ.

3.B The toric code

Kitaev introduced the toric code [74] with the intention of achieving reliable storage of quantum information at the physical level, as in classical stable storage, rather than by periodically performing explicit error correction procedures. He proposed that the Hamiltonian of the physical system being used to store the quantum information could, by its nature, make

the information stable. His proposal consisted of a 2D system with non trivial topology (such as the surface of a torus) with a stabilizer Hamiltonian composed of local terms. Qubits could then be stored in the ground subspace with a degeneracy of 4^g, with g being the genus of the surface on which the physical qubits are located.

In the toric code Hamiltonian, the physical qubits are located on the edges of a planar grid covering the 2D surface. For concreteness and simplicity, we shall restrict to the case were the surface is a torus and the grid is an $N \times N$ square lattice (i.e. $2N^2$ physical qubits). The Hamiltonian is composed of commuting terms which are products of Pauli operators on different sites (it is a stabilizer Hamiltonian). For each vertex s of the grid, there is a star (or vertex) term $A_s = \prod_{j \in \text{star}(s)} X_j$ which is the product of X operators over all the qubits of edges reaching s. Analogously, for each face p of the grid, there is a plaquette (or face) term $B_p = \prod_{j \in \text{boundary}(p)} Z_j$ which is the product of Z operators over all the qubits of edges surrounding the face p. Since each vertex and face have either 0 or 2 common edges, the terms A_s and B_p always commute. Hence all terms of the toric code Hamiltonian

$$H = -\sum_s A_s - \sum_p B_p \tag{3.63}$$

commute, and may be simultaneously diagonalized. Since $\prod_s A_s = I$ and $\prod_p B_p = I$, there are only $2N^2 - 2$ independent binary quantum numbers asociated to these terms (stabilizer operators) and each valid configuration determines a subspace of dimension 4. Due to this, violations of plaquette (vertex) conditions $A_s |\psi\rangle = |\psi\rangle$ ($B_p |\psi\rangle = |\psi\rangle$) always come in respective pairs. Following usual nomenclature, virtual particles called vertex (plaquette) anyons are respectively associated to these excitations. The set of stabilizers may be completed with a pair of logical observables consisting of the product of Z (X) operators along non contractible loops on the lattice (dual lattice), which may not be expressed as a product of plaquette (star) terms as illustrated in figure 3.5. Together with the set of Hamiltonian stabilizers any commuting pair of these four logical operators ($\bar{X}_1, \bar{X}_2, \bar{Z}_1$ and $\bar{Z}_2$) uniquely determine the state.

A stated prerequisite for using the toric code as a protecting Hamiltonian is that the energy splitting of the ground space due to Hamiltonian perturbations should be small. This is argued through the use of degenerate perturbation theory and the fact that it only gives non-zero splitting when the order taken is at least the lattice width/height, claiming an

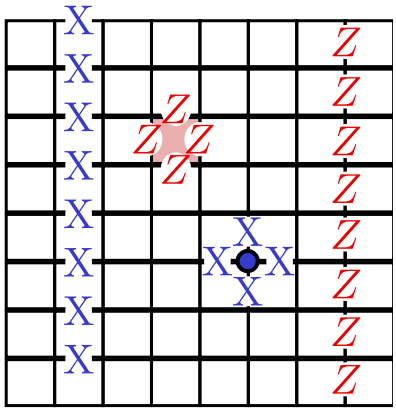

Figure 3.5: Each edge in the grid represents a physical qubit and opposite sides of the grid are identified by toric periodic boundary conditions. Typical plaquette and vertex operators are depicted near the center. Two vertical loop operators, $\bar{X}_1$ and $\bar{Z}_2$, which allow breaking the degeneracy are also presented. One can take these to be the X and Z operators for the first and second logically encoded qubits respectively. The complementary (anticommuting) operators are given by analogous horizontal loops.

exponential suppression of perturbations in the ground space.

The interaction terms in this Hamiltonian may be used as the syndrome measurements of an error correcting code with the desirable property that they are all geometrically local. Such codes provide a way of obtaining a fault tolerance threshold without requiring the use of concatenated quantum error correction. In this case, increasing the lattice size allows periodic measurements to suppress the effect of errors up to any desired accuracy [32] provided the accumulated error probability between measurements is below a certain threshold.

We will briefly review how error syndromes are interpreted and corrected, making the simplifying assumption that the error syndromes are measured perfectly. These syndromes, i.e. measurements of the stabilizers, reveal the presence of any anyons on the lattice, but do not distinguish between their origin, so it is up to us to determine how these anyons should be paired up in order to annihilate them. For each of the two kinds of anyon, the error correcting procedure will pair up the anyons and annihilate them by applying a connecting string of operators on them. If the connections performed and the actual origin of the anyons form topologically trivial loops (contractible loops), the error correction will have been successful. If however, the actual error pathways, together with the connections performed by the error

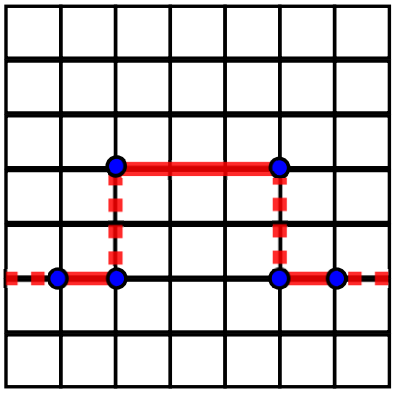

Figure 3.6: Illustration of a possible configuration of three vertex anyon pairs (small circles). Segments indicate possible qubits where Z rotations could be introduced in order to remove the anyons. Solid and dotted segments illustrate the anyon matching arising from l_1-EC and l_∞-EC respectively. Since together they complete a non-trivial loop, the matchings are logically inequivalent.

correction procedure complete one, or an odd number of, non-trivial loops, then a logical error will have been implemented.

Different criteria for pairing anyons may lead to logically different results. This is illustrated in figure 3.6, where two different criteria are used to pair up six anyons. In particular, if one of the criteria compensates the actual error path, allowing recovery of the initial state, the other will complete the error path into an undesired logical operation.

There are two correction protocols which we will consider, as they are expected to perform adequately when correcting a small proportion of randomly located errors. The first, which we refer to as l_1-EC, consists of minimizing the sum of distances among paired anyons, for which there is a polynomial time algorithm [122]. The second, l_∞-EC minimizes the furthest distance among paired anyons.

3.C Full Depolarization of the Toric Code's Protected Subspace

In the section 3.4.2, we gave a construction for a single logical error X_1, X_2, Z_1 or Z_2 to be applied with a probability exponentially close to 50%, independent of the model used

for error correction. This is not sufficient to show that we get full depolarization of the two-qubit subspace because it is not automatically clear that all 4 logical errors can be introduced simultaneously in the same model; the problem being that crossing paths for anti-commuting operations do not necessarily have a well-defined phase, and the perfect state transfer operations can fail. Indeed, if two non commuting anyon propagation paths of equal length cross at their midpoints, the amplitude corresponding to full propagation on both paths can be seen to be 0 at times! It is the aim of this section to extend the setting of (Sec. 3.4.2) to multiple logical errors while ensuring that the failure probability remain exponentially small with system size, thereby allowing a fully depolarizing map on the code-space with probability exponentially close to 1.

The basic idea behind this construction is that, for large systems, the propagation of the anyons is essentially ballistic. Hence, we can divide our lattice into sections, and ensure that the paths for anyons of different types only cross in regions where we can be (almost) guaranteed of the order in which the anyons pass through. It is then our task to bound the error probability.

Let us first consider the probability $p_s(t)$ of finding a propagated anyon at site s after a propagation time t which is given in [70] as

$$p_s(t) = f(s; D, \sin^2 t) = \sin^{2s} t \cos^{2(D-s)} t \binom{D}{s}, \tag{3.64}$$

where f is the binomial distribution function and D is the propagation length (i.e. there are $D+1$ possible anyon sites in the path). Here time has been normalized such that perfect transfer occurs at $t = \frac{\pi}{2}$. Correspondingly, if P is the perfect transfer Hamiltonian for vertex anyons and Π_0 is the projector onto the subspace with a unique anyon at the transfer start site, then

$$\begin{gathered} e^{-itP}\Pi_0 = \textstyle\sum_s \alpha_s(t) Z^{\otimes s}\Pi_0 \\ \text{where } |\alpha_s(t)| = \sqrt{p_s(t)} \end{gathered} \tag{3.65}$$

and $Z^{\otimes s}$ is the tensor product of s consecutive Z operators along the anyon propagation path.

We are now in condition to compare an the actual evolution imposed by two non commuting anyon propagations $|\psi(t)\rangle$ and an ordered idealization of it $|\psi_{b;a}(t)\rangle$

$$\begin{aligned} |\psi(t)\rangle &= \mathcal{U} e^{-it(P_a+P_b)} \mathcal{U}^\dagger |\psi_0\rangle \\ |\psi_{b;a}(t)\rangle &= \mathcal{U} e^{-itP_a} e^{-itP_b} \mathcal{U}^\dagger |\psi_0\rangle . \end{aligned} \tag{3.66}$$

We will assume that the physical qubit corresponding to the crossing of both paths is between anyon sites $s_a - 1$ and s_a of the anyon path associated to P_a and between anyon sites $s_b - 1$ and s_b of the anyon path associated to P_b. Furthermore, we will assume $s_a \gg s_b$, where what is meant by ($\gg$) will soon be made clear. Under these conditions, we will see that $|\psi(t)\rangle$ and $|\psi_{b;a}(t)\rangle$ are almost equal (at least during the time period corresponding to perfect state transfer).

By definition, we have that $\langle\psi(0)|\psi_{b;a}(0)\rangle = 1$. Let us now bound how fast this overlap can actually decay

$$\frac{d\ \langle\psi(t)|\psi_{b;a}(t)\rangle}{d\ t} = i\,\langle\psi(t)|\,[P_b, e^{-itP_a}]e^{-itP_b}\mathcal{U}^\dagger\,|\psi_0\rangle\,. \tag{3.67}$$

This allows bounding

$$\left|\frac{d\ \langle\psi(t)|\psi_{b;a}(t)\rangle}{d\ t}\right| \leq \left|[P_b, e^{-itP_a}]e^{-itP_b}\mathcal{U}^\dagger\,|\psi_0\rangle\right|. \tag{3.68}$$

Now let $\Pi_\emptyset^{(a)}$ and $\Pi_0^{(a)}$ be projectors onto the subspace with no anyons in the path of P_a and the subspace where a single anyon is located at the initial site and define $\Pi_\emptyset^{(b)}$ and $\Pi_0^{(b)}$ analogously. Recalling that $|\psi_0\rangle$ is a code state and our choice of rotation $\mathcal{U}$, we have

$$\begin{aligned}(\Pi_\emptyset^{(a)} + \Pi_0^{(a)})\mathcal{U}^\dagger\,|\psi_0\rangle &= \mathcal{U}^\dagger\,|\psi_0\rangle \\ (\Pi_\emptyset^{(b)} + \Pi_0^{(b)})\mathcal{U}^\dagger\,|\psi_0\rangle &= \mathcal{U}^\dagger\,|\psi_0\rangle\,.\end{aligned} \tag{3.69}$$

Commuting these projectors and using the expansion (3.65) of the perfect transfer we may express the RHS of equation (3.68) by

$$\left|[P_b, \sum_s \alpha_s(t) Z^{\otimes s}\Pi_0^{(a)}]\sum_r \alpha_r(t) X^{\otimes r}\Pi_0^{(b)}\mathcal{U}^\dagger\,|\psi_0\rangle\right| \tag{3.70}$$

There is only one possible non commuting term in P_b and this only for $s \geq s_a$. Furthermore, this term cancels for all but two terms in the sum over s'. We may then rewrite (3.70) as

$$\left|\begin{array}{l} 2J_{s_b}\ \sum_{s\geq s_a}\alpha_s(t)Z^{\otimes s}\Pi_0^{(a)}\times \\ \times\left(\alpha_{s_b}(t)X^{\otimes s_b - 1} + \alpha_{s_b-1}(t)X^{\otimes s_b}\right)\Pi_0^{(b)}\mathcal{U}^\dagger\,|\psi_0\rangle \end{array}\right| \tag{3.71}$$

Where J_{s_b} is the strength of the term performing an anyon swap between sites s_b and $s_b - 1$. Since each coefficient accompanies an orthogonal component of the state, we may recall the definition in (3.65) and rewrite (3.71) as

$$2J_{s_b}\sqrt{[p_{s_b-1}(t) + p_{s_b}(t)]\sum_{s\geq s_a} p_s(t)}\sin^2\varepsilon, \tag{3.72}$$

where $\sin^2\varepsilon$ is the amplitude of $\Pi_0^{(a)}\Pi_0^{(b)}\mathcal{U}^\dagger|\psi_0\rangle$. An exponentially small upper bound will now be given for the expression inside the square root .

$$\begin{aligned} & [p_{s_b-1}(t)+p_{s_b}(t)]\textstyle\sum_{s\geq s_a}p_s(t) \\ \leq\ & \textstyle\sum_{r\leq s_b}f(r,D,\sin^2 t)\sum_{s\geq s_a}f(s,D,\sin^2 t) \\ =\ & F(s_b,D,\sin^2 t)F(D-s_a,D,\cos^2 t), \end{aligned} \tag{3.73}$$

where $F(k,N,p)=\sum_{i=0}^{k}f(i,N,p)$ is the cumulative binomial distribution function. Assuming $\frac{s_b}{D}\leq\sin^2 t\leq\frac{s_a}{D}$ we may use Hoeffding's inequality [58] to bound (3.73) as

$$e^{-2\frac{(D\sin^2 t-s_b)^2}{D}}e^{-2\frac{(D\sin^2 t-s_a)^2}{D}}\leq e^{-\frac{(s_a-s_b)^2}{D}}, \tag{3.74}$$

with equality holding for $\sin^2 t=\frac{s_a+s_b}{2D}$. In turn, a tighter bound can be obtained by using Hoeffding's inequality on a single factor of (3.73) when $\sin^2 t\geq\frac{s_a}{D}$ or $\frac{s_b}{D}\geq\sin^2 t$.

Taking $D=N/2-1$ as in Sec. 3.4.2 and $s-r\geq s_a-s_b\geq D/6$ for instance, the obtained upper bound becomes exponentially small in N. In turn, the derivative (3.68) is exponentially small, meaning that the actual evolution is approximated by the ordered evolution with exponentially good precision in N.

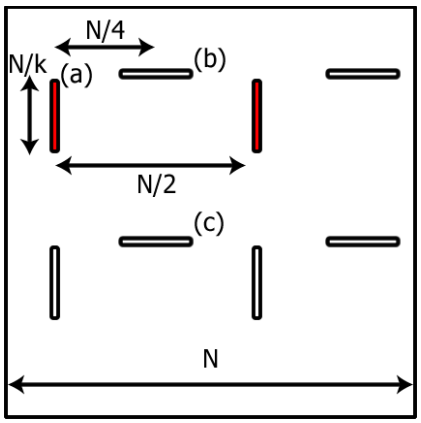

Figure 3.7: In an $N\times N$ lattice, there are two sets of N/k rows ($k\sim O(1)$) and two sets of columns and rows, each of which corresponds to the construction of (Sec. 3.4.2) for a different error type ($\bar{X}_1$, $\bar{Z}_2$ are introduced by columns starting at horizontal stripes and $\bar{Z}_1$ and $\bar{X}_2$ are introduced by rows starting from vertical stripes).

We have formally proven that for two non commuting anyon propagation paths which intersect with a sufficiently large offset (i.e. $\geq D/6$) the evolution can be accurately approximated by ordered anyon propagation. There is no obstacle in generalizing this result to many

such anyon paths, as required to introduce logical errors with high probability. Some leading factors of order N^2 appear but crucial factors remain exponentially decreasing in N.

In Fig. 3.7, we illustrate a configuration allowing the simultaneous introduction of all possible logical errors by anyon propagation within the lattice. The marked stripes of width N/k indicate locations where perpendicular anyon propagations begin or end. The perturbation to be introduced is chosen randomly as in Sec. 3.4.2, such that each propagation row/column starts with equal probability in either of each pair of opposing stripes. Taking k fixed allows sufficiently many repetitions of the single row/column construction that the probability of introducing each type of logical error approaches $\frac{1}{2}$ exponentially fast with N. Thus, after a perturbed evolution for time $t_f = O(N)$, and a final application of an arbitrary error correcting protocol based on unperturbed syndrome measurement, the resulting state is exponentially close to the maximally mixed state $\mathbb{1}/4$ of the code-space.

Chapter 4

Quantum memories based on engineered dissipation

Storing quantum information for long times without disruptions is a major requirement for most quantum information technologies. A very appealing approach is to use *self-correcting* Hamiltonians, i.e. tailoring local interactions among the qubits such that when the system is weakly coupled to a cold bath the thermalization process takes a long time. Here we propose an alternative but more powerful approach in which the coupling to a bath is engineered, so that dissipation protects the encoded qubit against more general kinds of errors. We show that the method can be implemented locally in four dimensional lattice geometries by means of a toric code, and propose a simple 2D set-up for proof of principle experiments.

4.1 Introduction

There are two existing approaches to providing coherent quantum storage on many-body systems. The first one corresponds to *fault tolerant quantum circuits*[113, 47]. If one can perform quantum gates and provide fresh initialized qubits with a sufficiently high accuracy and frequency, then quantum computing and in particular, quantum memory is possible for a time exponential in the dedicated resources.

More recently, Kitaev [32, 74] proposed that it might be possible to protect quantum

information passively by engineering of suitable Hamiltonian systems, in analogy to magnetic domains for classical memories. While an energetically degenerate code subspace insensitive to Hamiltonian perturbations is a necessary condition, it has become clear that there are additional requirements for this approach to quantum memories to work. Possibly the most important requirement is to cope with the undesired coupling between the storage system and its environment. In this direction, the approach that has benefited from the most theoretical progress goes by the moniker of *self–correcting* Hamiltonians, [11, 9, 53, 27].

For *self–correcting* Hamiltonians, a weak local coupling to a thermal bath is assumed. Making a Born-Markov approximation, the evolution of the system can be described by a thermalizing master equation. While for general local couplings, any initial state will decay to the unique Gibbs state, it is still possible for the decay rate of specific observables to become smaller as the number N of subsystems increases. This leads to the possibility of storing quantum information by encoding it on a pair of slowly decaying anticommuting many-body observables. A Hamiltonian will thus be called *self–correcting* provided that below a certain finite bath temperature the dissipative dynamics leads to information lifetimes growing with the system size (typically following an exponential increase). Alicky et al. [9] rigorously proved an exponentially long relaxation time for protected observables in the 4D toric code. Chesi et al. [26] generalized this result deriving a criteria for quantum memory based on *self–correcting* Hamiltonians and lower bounds on the storage times. However, it is in general not known how non thermal noise or even thermalization under a perturbed Hamiltonian [104] affects this lifetime. In particular, this may be the case whenever the qubits are weakly coupled to an additional bath which induces a small rate of depolarization[103].

Building on previous results, we propose and analyze an alternative way of protecting quantum states. The method is similar to that of protecting Hamiltonians, but now the main idea is to tailor the coupling of the qubits to a bath, so that the engineered dissipation extends the life-time of the encoded qubit. Apart from being passive (i.e. not requiring the burden of interrogating the quantum memory at intermediate times), the main advantage of this scheme is that it can potentially correct for other kinds of errors beyond those generated by thermalization, including depolarizing noise. In particular, we propose a specific method in 4 spatial dimensions inspired by toric codes and obtain evidence of its performance with the help of numerical simulations. We also investigate a simplified 2-dimensional model protecting

only from phase errors which could be a good candidate for proof of principle experiments.

Many-body classical memories based on dissipation (often under the name of *asynchronous celular automata*) have naturally appeared in the context of classical fault tolerant computation. For example, using a simple local update rule on a 2D lattice, Toom [119, 50] showed that classical information can be protected against weak local noise. A more elaborate update rule by Gács [41] provide protection even on a 1D lattice. These results already suggest that dissipation may offer a powerful alternative to the existing methods for constructing many-body quantum memories, as investigated in the present work. In fact, several authors have already proposed the use of continuous quantum error correcting codes [105, 5, 109, 101, 87]. However previous works concentrate on a single level of error correction and do not address the large N many-body scenario. A notable exception is the work of Dennis et al. [32] introducing a *heat bath algorithm* (thermal dissipation for the 4D toric code) in order to simplify the efficacy analysis of a local many body quantum error correction algorithm. At the crux of this approach is that thermal dissipation can be interpreted not only as introducing decoherence (errors), but also as performing a form of error correction, with the balance between the two effects roughly given by the bath temperature. Indeed, this heat bath algorithm can already be seen as a dissipative quantum memory lending itself to more natural engineering. In fact, engineered dissipation is more general in that it need not satisfy detailed balance conditions and thus its power extends that of cooling a *self–correcting* Hamiltonian. In other words, the steady state need not be an equilibrium state and its dynamics may show a net flow (imagine a funnel receiving water from a hose). As the classical results show, this more general kind of dissipation may be crucial in order to correct general kind of errors.

Our proposal can be viewed as another example where engineered dissipation may become a useful and alternative tool in the context of quantum information processing, beyond quantum computation [125], state engineering [125, 34], or entanglement creation [76]. In all those cases, it is desirable to be able to couple small subsets of qubits to Markovian environments so that their evolution equation follows a prescribed master equation. As exposed in [125], dissipative gadgets provide a direct way of implementing this is in terms of damped qubits; that is, a set of qubits which themselves follow a damping master equation due to their coupling to an environment. Those qubits can be directly coupled to the physical qubits of the quantum memory or computer to provide the desired dissipation, and thus appear as

an important resource in dissipative quantum information processing.

This chapter is organized as follows. In section 4.2 we briefly present the general idea of engineered dissipative quantum memories. In section 4.3 we display two different but rather obvious approaches to dissipative quantum memories and discuss why they are not entirely satisfactory. In section 4.4 we present a specific method in 4 spatial dimensions as well as the results of numerical simulations which validate the performance of the scheme. section 4.5 contains a simplified version in 2 spatial dimensions which corrects against phase errors and that could be tested experimentally in the near future. In section 4.6 we show how one can use dissipative qubits to engineer the dissipation and analyze under which condition one can use them in this context. All previous section contain the main statements of our work. The detailed proofs of our results and more thorough explanations are given in the appendices.

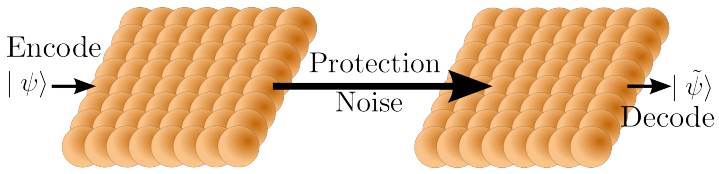

Figure 4.1: We assume that a piece of quantum information is encoded into a many body system. The engineered dissipation, is then responsible for making the degrees of freedom which carry the encoded quantum information resilient against the uncontrolled noise processes taking place. Finally, the decoding process extracts the quantum information from the collective degrees of freedom.

4.2 Statement of the problem

We consider a logical qubit encoded in N physical qubits, which are appropriately coupled to an environment providing dissipation. We describe the action of the engineered environment, as well as of the other sources of decoherence through a master equation

$$\dot{\rho} = \mathcal{L}_{\text{diss}}(\rho) + \mathcal{L}_{\text{noise}}(\rho) \tag{4.1}$$

Here, ρ is the density operator for the qubits, $\mathcal{L}_{\text{diss}}$ the Liouvillian describing the engineered dissipation, and $\mathcal{L}_{\text{noise}}$ will denote a noise term contribution to the master equation. This

could be local depolarizing noise for instance

$$\mathcal{L}_{\text{noise}}(\rho) = \Gamma_\varepsilon \mathcal{L}_{\text{dep}}(\rho) = \Gamma_\varepsilon \sum_{n=1}^{N} \frac{\mathbb{1}_n}{2} \otimes \text{tr}_n(\rho) - \rho, \tag{4.2}$$

or any other weak local noise term. Our goal is to show that for appropriate choices of $\mathcal{L}_{\text{diss}}$ we can extract the encoded qubit reliably after a time which substantially increases with N.

In general, any trace preserving dissipative master equation as $\mathcal{L}_{\text{diss}}$ may be write in Lindblad form [84]

$$\dot{\rho} = \mathcal{L}(\rho) = -i[H, \rho] + \sum_k 2L_k \rho_0 L_k^\dagger - \{L_k^\dagger L_k \rho\}_+, \tag{4.3}$$

consisting of a Hamiltonian term describing the unitary evolution, and a dissipative part which may be written in terms of Lindblad or jump operators L_k. Furthermore, the models of engineered dissipation we propose can be seen to adhere to a more benign form

$$\dot{\rho} = \sum_l \Gamma_l \left[T_l(\rho) - \rho\right], \tag{4.4}$$

where T_l are positive trace preserving channels. For these particular cases, the time dependent density matrix may be given an explicit stochastic expansion in the form of

$$\rho(t) = e^{-\Gamma t} \sum_{n=0}^{\infty} \frac{T^n \rho(0)}{n!}, \tag{4.5}$$

where $\Gamma = \sum_l \Gamma_l$ and $T(\rho) = \sum_l \Gamma_l T_l(\rho)$. This stochastic expansion will be useful for both proofs and Monte Carlo simulations.

4.3 Straightforward QECC encoding

Here we introduce and analyze two straightforward methods of encoding a QECC in the dissipation. The first one consist of coupling all the qubits with a reservoir in such a way that each application of a jump operator a whole error correction procedure takes place. In the second, we encode the QECC in several Lindblad terms, so that each jump correspond to an execution of a part of the QEC. The main purpose of this section is to show that those simple approaches do not work as one could imagine, and thus it illustrates why the design of engineered quantum memories is not a trivial task. Both approaches require multibody coupling to a single environment, where the number of system qubits coupled to the same

damped qubit grows with N, the size of the memory. In principle perturbation theory gadgets allow the engineering of such terms, provided their respective intensity decay exponentially with the number of subsystems involved. Not withstanding, a strength increasing with N would be required to make the first approach work, while in the second approach only a polynomial decrease with the number of subsystems involved would preserve functionality. In the next section we will present a scheme which circumvents these problems, although still with the caveat that it requires non-local couplings (as it works in 4 spatial dimensions).

4.3.1 Single Jump Operator

One major obstacle to traducing the usual error correction strategies to a dissipative scenario is due to the random times at which dissipative terms enact the recovery operations. We illustrate this problem in the case of a straightforward approach to dissipative protection. One can always implement in the dissipative Liouvillian a standard quantum error correction procedure which preserves the logical qubit: $\mathcal{L}_{\text{diss}}(\rho) = \Gamma[\mathcal{R}(\rho) - \rho]$, where $\mathcal{R}$ is a full recovery operation and Γ adjusts the rate at which the recovery operation is applied (imagine full correction of an N qubit QECC). Apart from the unrealistic nature of highly many–body dissipation terms required in this construction, it is easy to see that it does not serve our purposes. The reason can be seen by unraveling the quantum jump operators [25], there is a finite N independent probability for more than $\frac{1}{\Gamma_\varepsilon}$ time to elapse until the next recovery operation. Such long times allow too many errors to accumulate for any QECC to recover with high fidelity.

The alternative is to have dissipation implement many independent processes instead of a single monolithic error correction procedure. Ideally, having independent processes take care of removing independent error sets can make the accumulation of a critical fraction of errors exponentially unlikely. The difficulty of having independent dissipation processes is that contrary to the circuit model the order of their application is not enforced in any way. Thus, directly encoding each gate of a QECC recovery circuit into a dissipation term generally leads to a meaningless evolution. However, we will show that in specific cases where dissipation terms commute or show some order property lending itself to rigorous analysis, the asynchronous nature is not an obstacle.

4.3.2 Concatenated QECC Dissipation

It is indeed possible to design a many-body dissipative quantum memory. The strategy is to take the dissipation term as a sum of recovery operations occurring on different groups of qubits. Those operations correspond to recovery of the different logical qubits at each level of a simple concatenated QECC [75]. Intuitively, one may argue that the difficulty of implementing a given dissipation term increases with the number of qubits involved. We attempt to compensate for this difficulty by imposing that the operator norm required for such Lindblad terms decays with a power law respect to the number of physical qubits involved. More specifically, we take

$$\mathcal{L}_{\text{diss}}(\rho) = \Gamma \sum_{l,n} \delta^{M-l} [\mathcal{R}_{l,n}(\rho) - \rho]. \tag{4.6}$$

Here, $l = 0, 1, \ldots, M-1$ denotes the level of concatenation, and n further specifies on which set of qubits the recovery operations $\mathcal{R}_{l,n}$ are applied. In appendix 4.C, we show that if the local noise rate Γ_ε is sufficiently small then initially encoded information is lost at a rate which is exponentially small with respect to the number of qubits used (i.e. double exponentially small with the level of concatenation M). The weakness condition on the noise can be made precise by

$$\Gamma_\varepsilon < \Gamma_\varepsilon^\star = \frac{\delta^2 \Gamma}{k^2}, \tag{4.7}$$

where k is the number of physical qubits in the code to be concatenated. Assuming the perfect 5 qubit QECC and taking the strength of many body terms inversely proportional to the number of bodies ($\delta = 1/5$), a threshold of $\Gamma_\varepsilon^\star = 1.6 \times 10^{-3} \Gamma$ is obtained for the noise rate. When the error rate is below the error threshold, the relaxation rate for the encoded information has an exponentially small upper bound given by

$$\tau^{-1} \leq \Gamma_\varepsilon \delta^M \left(\frac{\Gamma_\varepsilon}{\Gamma_\varepsilon^\star} \right)^{2^M - 1} \tag{4.8}$$

The above scheme is mainly of formal interest, since the non local recovery operations encoded in the dissipative master equation require many qubits at different locations to interact with the same environment. While the necessary scaling of such terms needs to be polynomial for our proof to go through, the derivation of such terms based on effective many-body Hamiltonians and the dissipative gadgets we propose is expected to decay exponentially with the number of bodies involved. Even more realistically, one would expect many-body

dissipation terms to cope with many body error terms arising from imperfect implementation. In practice, it would be desirable to find a set up where the dissipation terms are spatially localized by considering the qubits arranged in a lattice.

4.4 Local dissipative protection in 4D

In classical systems Toom's rule [119] has been proven to be a simple translationally invariant update rule in a 2D Periodic Boundary Condition (PBC) lattice which is capable of preserving classical information, provided that the noise contribution to the dynamic is sufficiently weak. While we have not been able to extend this rule for quantum protection in 2D, we will consider a quantum analog of Toom's rule for 4D. The underlying QECC used is the 4D toric code, a stabilizer quantum error correcting code with 6 body stabilizer generators which can be made spatially local in a 4D PBC lattice. Dennis et al.[32] proposed it as a local QECC, and the corresponding stabilizer Hamiltonian was recently rigorously proven to be *self–correcting* by Alicki et al. [9]. We derive a local master equation for protecting information encoded into the 4D toric code based on a Toom like rule introduced by Ahn [6] and study its efficiency for protecting encoded observables. We then consider the protection process and numerically study the lifetime of information when depolarization errors are introduced extensively at a small yet constant rate.

A fully rigorous description of the QECC and the local update rule used is provided in the appendix 4.B. For the moment it is sufficient to specify that the master equation has the form of eq. (4.1) where the specific $\mathcal{L}_{\text{diss}}$ used associated to the 4D toric code will be called $\mathcal{L}_{\text{4D-TCToom}}$ and $\mathcal{L}_{\text{noise}}$ is weak extensive depolarizing noise as in eq. (4.2). The numerical results (Fig. 4.2) strongly support the existence of a critical error rate $\Gamma_{\varepsilon}^{\star} \approx 0.004 \times \Gamma$ (where Γ is the correction rate to be specified) below which, the lifetime of the encoded information increases exponentially with the lattice size.

Although the results above have no obvious practical implication, they suggest that local models may exist in spatial dimensions lower than 4 (for the search of quantum memories based on protecting Hamiltonians in lower dimension see [11, 27, 53]). The hope, is that even if self-correcting quantum memories fail to exist in lower dimensions, the use of engineered dissipation may still provide a solution.

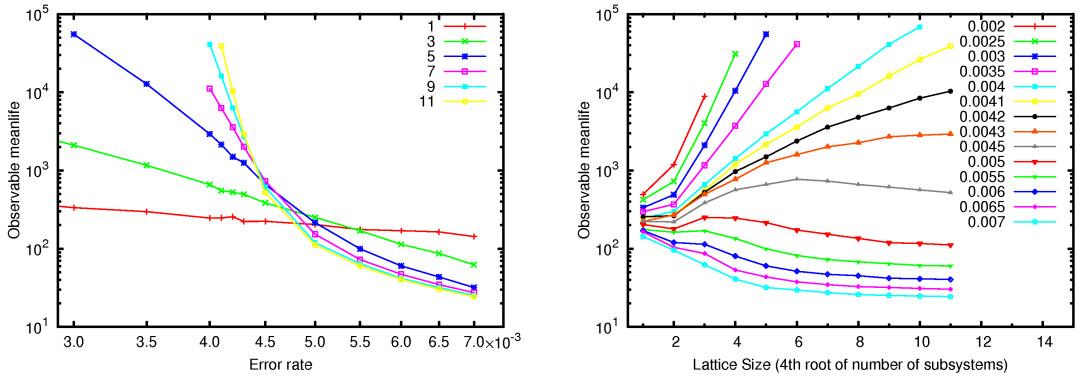

(a) Lifetime Vs. error rate

(b) Lifetime Vs. lattice size

Figure 4.2: The mean time to error for a logical observable is plotted in log scale units of $\frac{1}{\Gamma}$. Error rates Γ_ε are provided in units of Γ. The plots further suggests the existence of a critical value for error rates $\Gamma_\varepsilon^\star \approx 0.004$. (a) Each curve corresponds to a fixed odd value of the lattice size N. The independent axis $\Gamma_\varepsilon/\Gamma$ is also in log scale suggesting that for each fixed N the information lifetime show an asymptotic (small Γ_ε) power law dependence with $1/\Gamma_\varepsilon$ with the exponent increasing for larger N. (b) Each curve corresponds to a fixed value of the error rate Γ_ε. For low error rates $\Gamma_\varepsilon < \Gamma_\varepsilon^\star$, lifetime is seen to improve exponentially with N.

4.4.1 Numerical simulations

The key feature that allows us to perform efficient simulations of the relaxation times for logical observables, is that the terms in $\mathcal{L}_{\text{4D-TCToom}}$ may be naturally split in two subsets, where terms in one subset commute with terms in the other. Thus, efficient classical Monte Carlo simulations provide unbiased estimates for expectation values and correlations for half of the stabilizers and half of the logical observables. Throughout each simulation the relevant error corrected logical observable was measured on a copy of the system state after every unit of simulated time. Simulation were interrupted when a measurement outcome differing from the initial value was obtained. For each parameter, lattice size N and the depolarization rate Γ_ε, a total of 1000 such runs were performed and the simulated times were averaged to obtain the relaxation time presented. These simulations where performed on 62 AMD Opteron processors taking a total of five days to obtain the data presented (Fig. 4.2).

4.5 Accessible toy model

As a a proof of principle, we now present an engineered dissipation toy model providing protection for quantum information. One can implement the underlying ideas of dissipative quantum memories with 2D lattices at the expense of being able to correct only for dephasing noise

$$\mathcal{L}_{\text{phase}}(\rho) = \Gamma_{\varepsilon}^{z} \sum_{n=1}^{N} \sigma_n^z(\rho)\sigma_n^z - \rho. \tag{4.9}$$

Given a noise model including only one type of error (such as σ^z phase errors) we will be able to cast a classical memory prescription into a quantum scenario. A first step, is to define two logical observables

$$Z^{EC} \equiv \bigotimes_s \sigma_s^z \qquad X^{EC} \equiv \theta\left(\sum_s \sigma_s^x\right) \tag{4.10}$$

where θ is the Heaviside step function. The first observable Z^{EC} commutes with the noise $\mathcal{L}_{\text{phase}}$ and is thus completely immune to it. The noise can only change the value of X^{EC}, for the part of ρ which is in the ± 1 eigenspace of $\sum_s \sigma_s^x$ (i.e. states for which the absolute magnetization in the X direction is minimal). Dissipation will protect the X^{EC} observable by keeping most of ρ in a high X magnetization subspace. The master equation $\dot{\rho} = \mathcal{L}_{\text{NN}}(\rho)$ for nearest neighbor majority voting is written as a Liouvillian in Lindblad form [84] as

$$\mathcal{L}_{\text{NN}}(\rho) = \Gamma \sum_{<s,r,t>} L_{s,r,t}\rho L_{s,r,t}^{\dagger} - \frac{1}{2}\{L_{s,r,t}^{\dagger}L_{s,r,t}, \rho\}_{+}, \tag{4.11}$$

where the index s runs over all sites, $r \neq t$ are nearest neighbors of s and the Lindblad operators are given by

$$L_{s,r,t} \equiv \sigma_s^z \frac{1 - \sigma_s^x \otimes \sigma_r^x}{2} \frac{1 - \sigma_s^x \otimes \sigma_t^x}{2}. \tag{4.12}$$

This is, the first factor performs a phase flip when the second and third factors (projectors) are non zero (i.e. when site s points differently than its two neighbors r and t). The Lindblad operators are designed such that they also commute with Z^{EC} and can only change X^{EC} in the portion of ρ with minimal X magnetization.

The stability of the X^{EC} observable in such an evolution can be mapped to magnetization metastability in classical studies [18, 30]. Restricting r and t to be north and east neighbors in an $N \times N$ PBC lattice, one recovers Toom's rule [119, 50] which is proven to provide an exponential survival time, even in the presence of biased errors. However, the PBC requirement is experimentally unrealistic.

We numerically consider an experimentally accessible setup which does not require periodic boundary conditions. Physical qubits will be located on an $N \times N$ 2D square lattice sites. The sites r and t are taken among all possible nearest neighbors of s. The number of valid neighbor combinations are $\binom{4}{2} = 6$ for inner sites s, $\binom{3}{2} = 3$ for lattice border sites s and only one combination for corner sites. In the following plot (Fig. 4.3), we show how having a protective dissipation term $\mathcal{L}_{NN}$ can increase the relaxation time of X^{EC}, a many-body encoded observable (red). This is in contrast to the complementary observable which does not benefit from dissipative protection. On the contrary, given any depolarization rate, the relaxation time of Z^L decreases with the inverse of the number of physical qubits involved (blue).

4.6 Dissipative gadgets

As we have shown, the possibility of controlled quantum dissipation opens a host of new possibilities for QIP [34, 125, 76]. However, while some naturally occurring forms of dissipation may be readily exploited, it is crucial to have a systematic way of engineering arbitrary dissipative dynamics. A way of achieving complete control over the dissipation is to be capable of engineering independent Lindblad jump operators while keeping their interference with each other weak. For this we must assume availability of many body Hamiltonians, achievable through perturbation theory gadgets [64, 19] and of some naturally occurring dissipation, namely in the form of *damped qubits*. We apply the *approximation of independent rates of variation* [31] pg. 356 on the damped qubits which requires the bath correlation time for the damping process to be much shorter than the inverse of any coupling constant in the system. Coupling to these *damped qubits* can thus be seen as a resource in the design of quantum dynamics, analogous to freshly initializing qubits in quantum circuits.

Coupling the system to a *damped qubit* ancillary degree of freedom was proposed as a possible path to engineer arbitrary effective dissipative dynamics [125]. More specifically, the Hamiltonian coupling $H = \omega(L \otimes \sigma^+ + L^\dagger \otimes \sigma^-)$ to an ancilla with damping rate γ leads to an effective dissipative dynamics of the system corresponding to the Lindblad operator $\omega\sqrt{2/\gamma}L$. Here $\sigma^- = |0\rangle\langle 1|$ and $\sigma^+ = |1\rangle\langle 0|$.

In order to use these dissipation gadgets as basic building blocks in more complex scenarios, it is essential to make explicit possible limitations and restrictions of the implemented

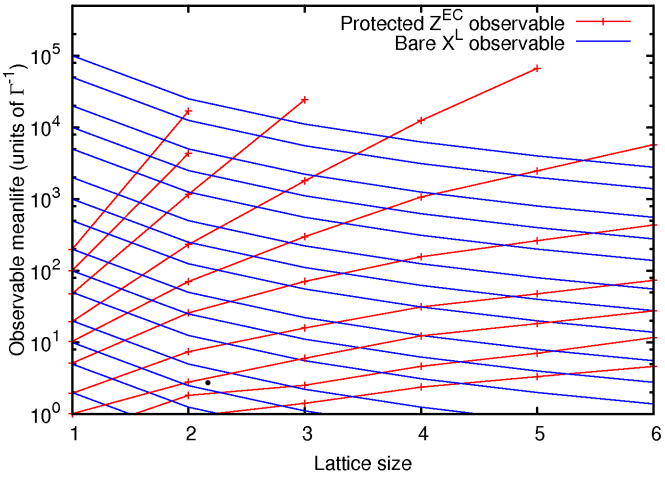

Figure 4.3: Relaxation time for Z^{EC} (red curves) and X^L (blue curves) in units of Γ^{-1}. Each red curve presents the relaxation time τ_Z (numerically obtained) corresponding to one value of the relative dephasing rate Γ/Γ_{phase} given by the intercept at $N = 1$. Blue curve have the functional form $\tau_X = \Gamma_{dep}^{-1} * N^{-2}$ and each corresponds to one value of Γ/Γ_{dep} also given by the intercept at $N = 1$. The lifetime τ of the encoded logical qubit can be seen to be estimated by $\tau \approx min\{\tau_X, \tau_Z\}$. Given Γ/Γ_{dep} and Γ/Γ_{phase}, one may intersect the corresponding curves to obtain the value of N leading to the optimal qubit lifetime τ. For example, if $\Gamma_{dep} = 5 \times 10^{-5}\Gamma$ and $\Gamma_{phase} = 0.1\Gamma$ the optimal lattice size of 4×4 allows a $\times 100$ increase in the quantum information relaxation time τ. A more extreme case may be seen when $\Gamma_{phase} = 0.01\Gamma$ and $\Gamma_{dep} \leq 5 \times 10^{-5}\Gamma$ where a factor $\times 50$ is gained by simply using a 2×2 lattice.

dissipation. In appendix 4.A we provide a detailed derivation of the effective system dynamics which makes three main contributions to our understanding of dissipative gadgets. Firstly, while the usual approach of adiabatic elimination obtains an effective dynamics in terms of a coarse grained time, our derivation shows that excluding a short initial transient period, this temporal coarse graining is not necessary. Secondly, we provide explicit bounds on the deviation from the desired state and instantaneous dynamics which are accompanied by a smallness prefactor $(\omega/\gamma)^2$. Finally, we include an independent internal dynamic for the system, and show, that the resulting effective dissipation carries through essentially unaffected provided the strength of the internal dynamics is sufficiently weak. While the last

point already suggests that the extensive application of local dissipation gadgets should be well behaved, a fully rigorous analysis is beyond the scope of this thesis.

4.7 Conclusions and perspectives

We have introduced engineered dissipation as a tool to protect against general quantum noise and proposed examples providing protection from local noise. In the case of concatenated code dissipation, we prove that information can be made resilient against any strictly local noise. Numerical simulations with depolarizing noise strongly suggest dissipative protection may be made spatially local in 4D. For purely dephasing noise we propose a dissipative protection scheme local in 2D. Proof of principle experiments could be realized with trapped ions, or atoms in optical lattices.

A self-correcting thermalization scheme associated to the 4D toric code Hamiltonian can provide encoded quantum information similar protection against depolarizing noise. In this sense, we have not illustrated the advantage of engineered dissipation. While the approach we have taken with the 4D TC is analogous to Toom's 2D update rule for classical information the thermalization of the 4D toric code can be seen as analogous to thermalization of the 2D Ising model respect to unbiased noise. However, stretching such parallelism with the classical problem suggests that engineered dissipation may be strictly more powerful and that it may be possible to engineer a 2D local dissipation mechanism capable of protecting quantum information. Indeed, while in 1D there can not be a self-correcting classical memory, a 1D local dissipative master equation due to Gács [41] is proven to provide increased classical information lifetime with the chain size. Inspired by Gács' construction, Harrington [55] has proposed a local quantum error correction scheme in 2D capable of protecting against quantum errors. To make this into a dissipative scheme, the requirements of a) a global synchronization clock, b) logarithmically increasing local storage space c) error free evolution of classical information, all need to be relaxed. Whether these assumptions can be relaxed, or other schemes in 2D or 3D exist are important questions that may dictate the fate of the practical applications for dissipative quantum memories.

4.A Adiabatic elimination of ancilla

In this section, we prove that Master equations with arbitrary Lindblad operators may be engineered to high accuracy by coupling the system to ancillary resource qubits which are themselves being cooled. The basic idea is to extend the system with an additional binary degree (spin 1/2) of freedom per Lindblad operator L to be implemented. These degrees of freedom are further assumed to be strongly dissipatively driven with a rate γ into a $|0\rangle\langle 0|$ ground state. We will show that a target dissipative evolution composed of a single Lindblad jump operator

$$\mathcal{L}_{\text{target}}(\rho) = L\rho L^\dagger - \frac{1}{2}\left\{L^\dagger L, \rho\right\}_+, \tag{4.13}$$

may be implemented within a small error margin. The technique used for the proof follows the adiabatic elimination of the excited ancilla subspace in spirit, but takes into account corrections in order to provide rigorous bounds on the deviations from the intended evolution.

Our derivation starts by assuming that the full dynamics of the system can be written as

$$\dot{\rho} = -i[H, \rho] + 2\gamma\sigma^-\rho\sigma^+ - \gamma\left\{\sigma^+\sigma^-, \rho\right\}_+ + \gamma\mathcal{L}_{\text{sys}}(\rho) \tag{4.14}$$

where $\sigma^+ = |1\rangle\langle 0|_A$ and $\sigma^+ = |1\rangle\langle 0|_A$ are raising and lowering operators on the ancilla qubit and the Hamiltonian H couples the system to the ancilla

$$H = \omega(L \otimes \sigma^+ + L^\dagger \otimes \sigma^-) \tag{4.15}$$

and $\mathcal{L}_{\text{sys}}$ is an additional evolution term with no effect on the ancillas. Here, the assumption that is implicitly being made, is that we may independently sum the interaction Hamiltonian H to the dissipative dynamics on both the system and the ancilla. In the case of the ancilla decay this is the *approximation of independent rates of variation* [31] pg. 356, which assumes correlation times for the reservoir responsible for spontaneous decay to be much shorter than any other relevant time in the system. An important example where this approximation holds to a great degree of accuracy is for two level atoms at optical frequencies, where the autocorrelation time of the coupled vacuum fluctuations can be as much as ten orders of magnitude shorter than the inverse of any of the other coupling constants. Since our derivation for the weak system Liouvillian does not require temporal coarse graining, the successively incorporation of Hamiltonian interactions rigorously leads to the additive appearance of the desired Liouville terms up to leading order. Assuming $\varepsilon = \omega/\gamma \ll 1$ we can rescale to a

unitless time by incorporating a factor γ leading to the following differential equations for the reduced density matrices.

$$\dot{\rho}_{00} := \langle 0|\,\dot{\rho}\,|0\rangle = 2\rho_{11} - i\varepsilon L^\dagger \rho_{10} + i\varepsilon \rho_{01} L + \mathcal{L}_{\text{sys}}(\rho_{00}) \tag{4.16}$$

$$\dot{\rho}_{01} := \langle 0|\,\dot{\rho}\,|1\rangle = -\rho_{01} + i\varepsilon \rho_{00} L^\dagger - i\varepsilon L^\dagger \rho_{11} + \mathcal{L}_{\text{sys}}(\rho_{01}) \tag{4.17}$$

$$\dot{\rho}_{11} := \langle 1|\,\dot{\rho}\,|1\rangle = -2\rho_{11} - i\varepsilon L \rho_{01} + i\varepsilon \rho_{10} L^\dagger + \mathcal{L}_{\text{sys}}(\rho_{11}) \tag{4.18}$$

From here, we may obtain the integral forms

$$\begin{aligned}\rho_{01}(\tau) =& e^{-\tau}\rho_{01}(0) + \int_0^\tau e^{-t'}\mathcal{L}_{\text{sys}}[\rho_{01}(\tau - t')]dt' \\ &+ i\varepsilon \int_0^\tau e^{-t'}[\rho_{00}(\tau - t')L^\dagger - L^\dagger \rho_{11}(\tau - t')]dt'\end{aligned} \tag{4.19}$$

$$\begin{aligned}\rho_{11}(\tau) =& e^{-2\tau}\rho_{11}(0) + \int_0^\tau e^{-2t'}\mathcal{L}_{\text{sys}}[\rho_{11}(\tau - t')]dt' \\ &- i\varepsilon \int_0^\tau e^{-2t'}[L\rho_{01}(\tau - t') - \rho_{10}(\tau - t')L^\dagger]dt'\end{aligned} \tag{4.20}$$

Assuming the initial conditions $\rho_{01}(0) = \rho_{11}(0) = 0$, that $\|L\| \leq 1$ and $\|\mathcal{L}_{\text{sys}}\| \leq E\varepsilon^2$, and using that $\|\rho_{00}\| + \|\rho_{11}\| \leq 1$ we may bound

$$\|\rho_{01}(\tau)\| \leq \tilde{\varepsilon} \quad \text{and} \quad \|\rho_{11}(\tau)\| \leq \tilde{\varepsilon}^2, \tag{4.21}$$

with $\tilde{\varepsilon} = \frac{\varepsilon}{1 - E\varepsilon^2}$. It is now straightforward to bound $\|\dot{\rho}_{00}(\tau)\| \leq (4 + E)\tilde{\varepsilon}^2$. We may now concentrate on tighter bounds composed of higher order terms in ε but also, of exponentially decaying terms. A first step to do this is to perform integraton by parts; on eq. (4.19) one obtains

$$\begin{aligned}\rho_{01}(\tau) =& i\varepsilon \rho_{00}(\tau)L^\dagger - i\varepsilon e^{-\tau}\rho_{00}(0)L^\dagger \\ &- i\varepsilon \int_0^\tau e^{-t'}\left[\dot{\rho}_{00}(\tau - t')L^\dagger + L^\dagger \rho_{11}(\tau - t')\right]dt' \\ &+ \int_0^\tau e^{-t'}\mathcal{L}_{\text{sys}}[\rho_{01}(\tau - t')]dt'.\end{aligned} \tag{4.22}$$

In the case of ρ_{11} we straightforwardly obtain

$$\begin{aligned}\rho_{11}(\tau) =& -\frac{i\varepsilon}{2}L\rho_{01}(\tau) \\ &+ \frac{i\varepsilon}{2}\int_0^\tau e^{-2t'}L\dot{\rho}_{01}(\tau - t')dt' + h.c. \\ &+ \int_0^\tau e^{-2t'}\mathcal{L}_{\text{sys}}[\rho_{11}(\tau - t')]dt'\end{aligned} \tag{4.23}$$

This expression may be massaged into a form which may be more readily bounded. The steps involved include, expanding $\dot{\rho}_{01}$ according to eq. (4.17), then expanding appearances of ρ_{01} according to eq. (4.22) and finally integrating numerical factors and grouping terms. After such manipulation, one reaches the expression

$$\begin{aligned}\rho_{11}(\tau) =&\frac{\varepsilon^2}{2}\Bigg[L\rho_{00}(\tau)L^\dagger - e^{-\tau}(2-e^{-\tau})L\rho_{00}(0)L^\dagger \\ &-\int_0^\tau e^{-t'}(2-e^{-t'})L\dot{\rho}_{00}(\tau-t')L^\dagger dt' \\ &-\int_0^\tau e^{-t'}(2-2e^{-t'})LL^\dagger\rho_{11}(\tau-t')dt'\Bigg] + h.c. \\ &+\frac{i\varepsilon}{2}\int_0^\tau e^{-2t'}L\mathcal{L}_{\text{sys}}[\rho_{01}(\tau-t')]dt' + h.c. \\ &+\int_0^\tau e^{-2t'}\mathcal{L}_{\text{sys}}[\rho_{11}(\tau-t')]dt'\end{aligned} \tag{4.24}$$

Using eqs. (4.22) and (4.24), one may prove the following higher order bounds

$$\|\rho_{01} - i\varepsilon\rho_{00}L^\dagger\| \leq (2E+5)\tilde{\varepsilon}^3 + \varepsilon e^{-\tau} \tag{4.25}$$

$$\|\rho_{11} - \varepsilon^2 L\rho_{00}L^\dagger\| \leq (3E+7)\tilde{\varepsilon}^4 + 2\varepsilon^2 e^{-\tau}, \tag{4.26}$$

Inserting these bounds into the definition of $\dot{\rho}_{00}$ we may bound deviation from the target evolution by

$$\|\dot{\rho}_{00} - 2\varepsilon^2\mathcal{L}_{\text{target}}(\rho_{00}) - \mathcal{L}_{\text{sys}}(\rho_{00})\| \leq (10E+24)\tilde{\varepsilon}^4 + 4\varepsilon^2 e^{-\tau} \tag{4.27}$$

After a short transient time of the order $\frac{1}{\gamma}\log\frac{1}{\varepsilon}$, the exponential term can be neglected. Furthermore, note that the internal system dynamics $\mathcal{L}_{\text{sys}}$ may be time dependent and thus encode correlations of different components of the system in its time dependence.

4.B 4D Toric code

4.B.1 The 4D Toric code as a stabilizer code

We will now provide an informal description of the 4D toric code. For every vertex of an $N \times N \times N \times N$ lattice, there are 6 orientations of faces on which physical qubits are located. Thus, the $6 \times N^4$ physical qubits are arranged on the 2D faces of a 4D PBC lattice. We can now introduce an over-complete set of local stabilizer generators for the code, half of which correspond to 1D edges, the other half corresponding to 3D cubes. For each 1D edge, there

is a tensor product operator $Z^{\otimes 6}$, the product of Z operators acting on the six 2D faces to which this edge belongs. Dual to this, for each 3D cube, there is a tensor product operator $X^{\otimes 6}$, the product of X Pauli operators over the six 2D faces of the cube. Two edge and cube stabilizers overlap iff the edge is an edge of the cube, and then their overlap will be in exactly two faces. Thus all stabilizer generators are seen to commute.

4.B.2 Logical degrees of freedom

Counting of the remaining degrees of freedom additional to the stabilizer syndrome obtained is not as straightforward as for the 2D toric code, where every syndrome with an even number of anyons was possible. In the 4D case, the required condition is that the set of unsatisfied stabilizers is only allowed to be a combination of closed loops (in the lattice and dual lattice respectively). However, one can explicitly construct six pairs of anticommuting logical operators which commute with all stabilizer terms, one pair for each of the six possible plane orientations. From each pair, one operator is a full plane of X rotations along a full plane wrapping around the grid in one of the six possible orientations. The second operator from each pair consists of a dual plane of Z operators arranged along the perpendicular plane orientation. Although analogous to the logical operators on the 2D toric code, this image probably stretches our 2D or at most 3D imagination. Thus, to obtain an intuition about this construction it is convenient to provide formal expressions which one may operate with.

4.B.3 4D PBC lattice notation

Each vertex of the 4D periodic lattice can be identified by a four component vector $\vec{v} = v_0, v_1, v_2, v_3 \in \mathbb{Z}_N^4$. For each vertex $\vec{v}$, there are four edges $\hat{e}$, six faces $\hat{p}$ and four cubes $\hat{c}$ having the vertex as a lower corner. These orientations may be described by four component binary vectors

$$\hat{e}, \hat{p}, \hat{c} \in \{(v_0, v_1, v_2, v_3) \quad | \quad v_i \in \{0, 1\}\}, \tag{4.28}$$

with edge $\hat{e}$, face $\hat{p}$, or cube $\hat{c}$ orientations satisfying the additional condition $\sum_{i=0}^{3} v_i$ equal to 1, 2 or 3 respectively. Each physical qubit can be identified with a tuple $\vec{v}, \hat{p}$, where $\hat{p}$ identifies the plane orientation and $\vec{v}$ its lower side corner. The Z type edge stabilizers $E_{\vec{v},\hat{e}}$

are given by

$$E_{\vec{v},\hat{e}} = \bigotimes_{\hat{e}\subset\hat{p}} Z_{\vec{v},\hat{p}} \otimes Z_{\vec{v}-\hat{p}+\hat{e},\hat{p}}, \tag{4.29}$$

with six participating physical qubits. Finally, the X type cube stabilizer $C_{\vec{v},\hat{c}}$ are given by

$$C_{\vec{v},\hat{c}} = \bigotimes_{\hat{p}\subset\hat{c}} X_{\vec{v},\hat{p}} \otimes X_{\vec{v}+\hat{c}-\hat{p},\hat{p}}, \tag{4.30}$$

also with six participating physical qubits.

We will now describe a set of logical operators commuting with all stabilizers which will be used to encode information in absence of errors. There is one pair of such anticommuting logical operators for each plane orientation $\hat{p}$ and they are given by

$$X^L_{\hat{p}} = \bigotimes_{n,m=1}^{N} X_{n\hat{e}_1+m\hat{e}_2,\hat{p}} \qquad Z^L_{\hat{p}} = \bigotimes_{n,m=1}^{N} Z_{n\hat{e}_3+m\hat{e}_4,\hat{p}}, \tag{4.31}$$

with $\hat{e}_1 + \hat{e}_2 \equiv \hat{p}$ and $\hat{e}_3 + \hat{e}_4 \equiv \hat{p}^\perp$. It is easy to see that according to this definition, the two logical operator $X^L_{\hat{p}}$ and $Z^L_{\hat{p}}$ anticommute, as they coincide only at qubit $(\vec{0},\hat{p})$. One can further verify that such operators commute with the complete set of stabilizers. Finally, it is not hard to see, that if one assumes the state to be in the code subspace (i.e. $+1$ eigenstate to all stabilizers), then any homologically equivalent surfaces results in equivalent definition for the operators.

4.B.4 4D Quantum Toom's rule

We now define a local update rule which will later be used in two ways, first as a dissipation mechanism capable of keeping errors from accumulating too badly, second as the basic component of an information recovery procedure permitting removal of all errors to allow information read-out. The update rule is analogous to Toom's rule for classical information stored in a 2D lattice. While the prescription of Toom's rule is to flip a bit if it is different to both its two lower side neighbors, the prescription in 4D will be to X "flip" a qubit if both its neighboring lower side Z edge stabilizers are not satisfied, but also to Z "flip" a qubit if both its lower side X cube stabilizers are not satisfied. This is, a local rotation may be performed depending on neighboring stabilizer state. This is in complete analogy to an interpretation of Toom's rule in terms of local stabilizers. One property that permits analytic and numerical analysis of such a scheme is the decoupling of recovery for X and Z logical operators.

For each qubit $(\vec{v}, \hat{p})$, we can write the super-operator describing the quantum jump implementing the update rule as

$$\mathcal{R}^Z_{\vec{v},\hat{p}}(\rho) = Z_{\vec{v},\hat{p}} P^X_{\vec{v},\hat{p}} \rho P^X_{\vec{v},\hat{p}} Z_{\vec{v},\hat{p}} + P^{X\perp}_{\vec{v},\hat{p}} \rho P^{X\perp}_{\vec{v},\hat{p}} \tag{4.32}$$

where $P^X_{\vec{v},\hat{p}}$ is the projector onto the subspace where a Z flip should be performed on qubit $(\vec{v}, \hat{p})$ and $P^{X\perp}_{\vec{v},\hat{p}}$ the orthogonal subspace. Assuming $\hat{p} = \hat{e}_1 + \hat{e}_2$ the projector may be defined as

$$P^X_{\vec{v},\hat{p}} = \frac{1}{4}(1 - E_{\vec{v},\hat{e}_1})(1 - E_{\vec{v},\hat{e}_2}). \tag{4.33}$$

Analogously, one may define an update rule $\mathcal{R}^X_{\vec{v},\hat{p}}$ which in a similar way, introduces an X "flip" depending on the corresponding projectors $P^Z_{\vec{v},\hat{p}}$ in terms of Z type stabilizers.

4.B.5 Full recovery and error corrected operators

The superoperators $\mathcal{R}^Z_{\vec{v},\hat{p}}$ and $\mathcal{R}^X_{\vec{v}',\hat{p}'}$ always commute. Only recovery operators of the same kind may lack commutation when considering neighboring plaquetes. In particular, to define a full recovery operation $\mathcal{R}$ in terms of these local recovery update rules, it is necessary to unambiguously specify an order of application. Indeed, in our simulation code, a sweep through the lattice is taken as this order and we observe a good performance in recovering the originally encoded observables (Fig. 4.4). Once the recovery operation $\mathcal{R}$ is unambiguously specified, it is possible to define robust logical observables $X^{EC}_{\hat{p}}$ and $Z^{EC}_{\hat{p}}$ such that

$$\mathrm{tr}(Z^{EC}_{\hat{p}}\rho) = \mathrm{tr}(Z^L_{\hat{p}}\mathcal{R}\rho) \qquad \mathrm{tr}(X^{EC}_{\hat{p}}\rho) = \mathrm{tr}(X^L_{\hat{p}}\mathcal{R}\rho). \tag{4.34}$$

Or more compactly

$$Z^{EC}_{\hat{p}} = \bar{\mathcal{R}}\left(Z^L_{\hat{p}}\right) \text{ and } X^{EC}_{\hat{p}} = \bar{\mathcal{R}}\left(X^L_{\hat{p}}\right). \tag{4.35}$$

Thus, error corrected logical observables (super-index EC), provide a robust result when evaluated on a state with sufficiently few errors and coincide with logical operators on the error-free subspace.

4.B.6 Master equation

We study a master equation including a locally depolarizing noise term of strength Γ_ε, and the proposed Lindblad terms intended to avoid error clusters from growing. The simulated

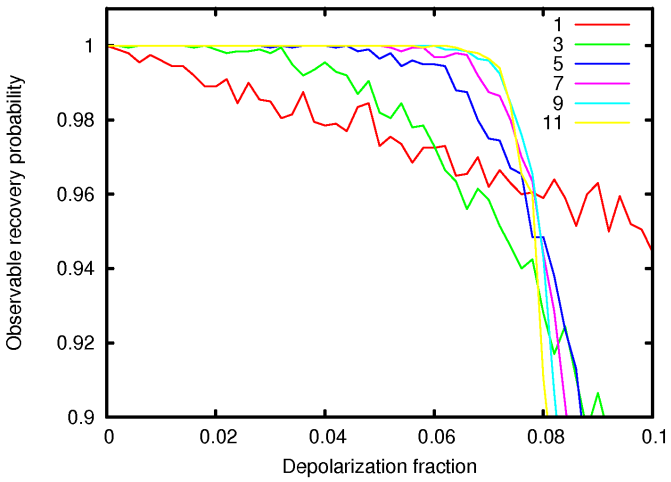

Figure 4.4: Recovery probability of an encoded observable in the 4D toric code is plotted as a function of depolarization probability per qubit. Odd lattices sizes from 1 to 11 are represented in the different curves and suggest a critical depolarization probability of approximately 7.5%.

master equation may be written as

$$\dot{\rho} = \mathcal{L}\rho = \Gamma \mathcal{L}_{4DToom}\rho + \Gamma_{\varepsilon}\mathcal{L}_{dep}\rho \tag{4.36}$$

where the dissipative protection $\mathcal{L}_{4DToom}$ is given by

$$\begin{aligned}\mathcal{L}_{4DToom}\rho = \sum_{\vec{v},\hat{p}} & L^{X}_{\vec{v},\hat{p}}\rho L^{X\dagger}_{\vec{v},\hat{p}} - \frac{1}{2}\left\{L^{X\dagger}_{\vec{v},\hat{p}}L^{X}_{\vec{v},\hat{p}},\rho\right\}_{+} \\ & + L^{Z}_{\vec{v},\hat{p}}\rho L^{Z\dagger}_{\vec{v},\hat{p}} - \frac{1}{2}\left\{L^{Z\dagger}_{\vec{v},\hat{p}}L^{Z}_{\vec{v},\hat{p}},\rho\right\}_{+}.\end{aligned} \tag{4.37}$$

The protecting Lindblad operators are

$$L^{Z}_{\vec{v},\hat{p}} = Z_{\vec{v},\hat{p}}P^{X}_{\vec{v},\hat{p}} \quad L^{X}_{\vec{v},\hat{p}} = X_{\vec{v},\hat{p}}P^{Z}_{\vec{v},\hat{p}}, \tag{4.38}$$

corresponding to the Toom like quantum jump superoperators $\mathcal{R}^{\{X,Z\}}_{\vec{v},\hat{p}}$ introduced in Eq. 4.32. We perform numerical experiments to determine the relaxation time for logical observables (i.e. $\mathrm{tr}[X^{EC}\rho(t)] \equiv \mathrm{tr}[X^{L}\mathcal{R}\rho(t)]$.) Evolutions are taken to start in a code state with an unambiguous X^L or Z^L logical value and consistency of the error corrected logical observables are checked regularly in time. The mean time to the first change in the value observed for X^{EC} or Z^{EC} is taken as an estimator of the relaxation time.

4.B.7 Numerical considerations

Evolution under this master equation can be numerically simulated efficiently for a commuting set of observables such as the edge stabilizers and a commuting set of logical observables. This means that a classical Monte Carlo simulation is enough to study the probability of obtaining the correct outcome when measuring distinct logical observables which were initially well defined. The results of such simulations are presented in (Fig. 4.2) for different sizes of the lattice grid up to 11 and different values for Γ_ε. These suggest a critical value for the noise rate $\Gamma_\varepsilon^\star \approx 0.004$, below which arbitrarily long relaxation times may be achieved by increasing the lattice size. Given that below threshold error rates, the information lifetime seems to grow exponentially with the lattice size, and that the simulation time per unit time is also proportional to the fourth power of the lattice size, it is numerically costly to extend our evidence to larger lattices.

4.B.8 Definition of efficient recovery $\mathcal{R}$

To check whether the encoded observable is still recoverable at time t, we apply a correction super-operator $\mathcal{R}$ on $\rho(t)$. The definition of $\mathcal{R}$ consists of sequentially applying the local jump superoperators $\mathcal{R}_{\vec{v},\hat{p}}^{\{X,Z\}}$ in a sweeping order. This shows a high performance for removing all error domains (i.e. it presents a numerical threshold to depolarizing noise on up to $\approx 7.5\%$ of the qubits as shown in (Fig. 4.4) .) Furthermore, computer simulations of $\mathcal{R}$ are efficient, requiring a minimal amount of $O(N^4)$ operations. This is important since the $\mathcal{R}\rho(t)$ must be checked every unit time to obtain an estimate of the relaxation times of error corrected logical observables.

4.C Concatenated-code dissipation

Paz and Zurek [105] presented the first studies of protecting quantum information through the use of a continuous dissipative process. They introduce a general master equation form for the class of stabilizer QECC and analyze their performance in some simple cases. In this section, we will adapt their construction and propose master equations for concatenated QECC which are provably robust against sufficiently weak local noise.

For stabilizer QECC, the recovery super-operator $\mathcal{R}$ can be written in Kraus form as

$$\mathcal{R}(\rho) = \sum_{(m)} R^{(m)} P^{(m)} \rho P^{(m)\dagger} R^{(m)\dagger}, \tag{4.39}$$

where $P^{(m)}$ are projectors onto orthogonal syndrome subspaces with $\sum_{(m)} P^{(m)} = \mathbb{1}$ and $R^{(m)}$ are unitary recovery operators of tensor product Pauli form. The operators $L^{(m)} = R^{(m)} P^{(m)}$ can be interpreted as Lindblad operators to give way to a protecting master equation. However, this approach can not provide more than a constant improvement in the relaxation time for logical observables. It can be seen that given an error rate and a correction rate, there is an upper bound on the relaxation time of the logical encoded bit which is independent of the code and the number of physical subsystems it uses.

We propose extending this master equation model to one which allows performing many such recovery operations in parallel. In the case of concatenated QECC these will correspond to error correction at the different levels of concatenation. Recovery operations at the same level of concatenation act independently of each other as they involve disjoint subsets of physical qubits. Most of the work goes into designing recovery operations at different levels of concatenation which do not interfere undesirably (i.e. commute) and proving that they provide a similar protection from local errors to the one achieved by concatenated QECC in the circuit model.

We will define a dissipative concatenated quantum memory based on a $[[k, 3, 1]]$ QECC. An M-level encoding will thus make use of k^M physical qubits. A labeling for each physical qubit may be given in terms of an M component vector $\vec{v} \in \mathbb{Z}_k^M$ (i.e. with each component going from 1 to k. Partial vectors $\vec{v}$ with $M - l$ components will identify mutually disjoint blocks of k^l physical qubits. Thus if $\vec{v}$ denotes a particular set of k^l physical qubit, then the vector $v_0 : \vec{v}$, with one additional component v_0 and identifies a sub-block of k^{l-1} physical qubits. The number of components of a vector $\vec{v}$ will be denoted by $\mid \vec{v} \mid$, with $\emptyset$ being the unique zero component vector.

A stabilizer QECC on k qubits can be characterized by the definition of the Stabilizers $S^{(j)}$, the projectors onto syndrome subspaces $P^{(j)}$ and the corresponding error recovery operators $R^{(j)}$, the logical operators X^L, Y^L, Z^L, the recovery super-operator $\mathcal{R}$ and the error corrected Pauli observables X^{EC}, Y^{EC}, Z^{EC}. It is instructive to present the definition of these objects for a simple QECC making it easier to latter provide the recursive definitions required for the

concatenated QECCs. These definitions are given by

$$\begin{aligned} S^{(j)} &= s1^{(j)} \otimes s2^{(j)} \otimes \ldots \otimes sk^{(j)} \\ P^{(j)} &= \sum \alpha_{i,j} S^{(i)} \\ R^{(j)} &= r1^{(j)} \otimes r2^{(j)} \otimes \ldots \otimes rk^{(j)} \\ \mathcal{R}(\rho) &= \sum R^{(k)} P^{(k)} \rho P^{(k)} R^{(k)} \\ \sigma^{L} &= \sigma 1 \otimes \sigma 2 \otimes \ldots \otimes \sigma k \\ \sigma^{EC} &= \overline{\mathcal{R}}(\sigma^{L}). \end{aligned} \tag{4.40}$$

The $\alpha_{i,j}$ are coefficients relating stabilizer operators with specific projectors. Lowercase Latin letters as well as σ, stand for one of the four single qubit Pauli operators $\{1, X, Y, Z\}$. Thus σ^L, is a logical operator on the code and as a stabilizer code can be expressed as a tensor product of single qubit operators. Finally $\overline{\Lambda}$ denotes the super-operator dual to Λ (i.e. if $\Lambda(\rho) = \sum_k A_k \rho A_k^\dagger$, then $\overline{\Lambda}(O) = \sum_k A_k^\dagger O A_k$).

We may now give the analogous definitions for the case of an M level concatenated code. Here, objects must be further specified by a vector $\vec{v}$ of at most M components indicating the physical qubit or group of qubits they act on. Some of these objects require a base case definition for $\mid \vec{v} \mid = M$,

$$\begin{aligned} \sigma_{\vec{v}}^{L} &= \sigma_{\vec{v}} \\ \sigma_{\vec{v}}^{EC} &= \sigma_{\vec{v}} \\ \mathcal{F}_{\vec{v}} &= \mathbb{1}. \end{aligned} \tag{4.41}$$

In this case, $\vec{v}$ identifies on which physical qubit(s) the operators act on. The super-operator $\mathcal{F}$ represents the full recovery operation which is trivial in the case of physical qubits. For the rest of the objects, definitions are only required for $\mid \vec{v} \mid < M$.

$$\begin{aligned} S_{\vec{v}}^{(j)} &= (s1^{(j)})_{1:\vec{v}}^{EC} \otimes \ldots \otimes (sk^{(j)})_{k:\vec{v}}^{EC} \\ P_{\vec{v}}^{(j)} &= \sum \alpha_{i,j} S_{\vec{v}}^{(i)} \\ R_{\vec{v}}^{(j)} &= (r1^{(j)})_{1:\vec{v}}^{L} \otimes \ldots \otimes (rk^{(j)})_{k:\vec{v}}^{L} \\ \mathcal{R}_{\vec{v}}(\rho) &= \sum R_{\vec{v}}^{(k)} P_{\vec{v}}^{(k)} \rho P_{\vec{v}}^{(k)} R_{\vec{v}}^{(k)} \\ \sigma_{\vec{v}}^{L} &= (\sigma 1)_{1:\vec{v}}^{L} \otimes \ldots \otimes (\sigma k)_{1:\vec{v}}^{L} \\ \sigma_{\vec{v}}^{EC} &= \overline{\mathcal{F}}_{\vec{v}}(\sigma_{\vec{v}}^{L}) \\ \mathcal{F}_{\vec{v}} &= \mathcal{R}_{\vec{v}} \circ (\mathcal{F}_{1:\vec{v}} \otimes \ldots \otimes \mathcal{F}_{k:\vec{v}}) \,. \end{aligned} \tag{4.42}$$

The main distinction from non-concatenated definitions is that the subindex $\vec{v}$ has been incorporated everywhere. In addition, tensor product decomposition of operators now runs either in terms of logical operators (super-index L) or error corrected observables (super-index EC). Finally, a distinction is made between $\mathcal{F}_{\vec{v}}$, which corrects all errors in a given block of qubits denoted by $\vec{v}$ and $\mathcal{R}_{\vec{v}}$ which corrects for only the highest level errors within that block. This distinction may seem artificial since for a simple code (i.e. $\mid \vec{v} \mid = M-1$) a full correction corresponds to correcting the highest level error blocks possible.

We will now concentrate on some of the properties these recursive definitions carry that will later allow us to define the dissipative concatenated QECC and prove robustness results. The main property relating logical and error corrected operators verified by definition is

$$\mathrm{tr}[\sigma_{\vec{v}}^{EC}\rho] = \mathrm{tr}[\sigma_{\vec{v}}^{L}\mathcal{F}_{\vec{v}}(\rho)]. \tag{4.43}$$

The meaningfulness of error corrected operators thus stems from the fact that if relatively few errors are applied to an encoded state, the error corrected operator provides the same expectation value as the logical operator on the unerred state

$$\mathrm{tr}[O_{\vec{v}}^{EC}\mathcal{E}(\rho)] = \mathrm{tr}[O_{\vec{v}}^{L}\rho] \quad \forall\rho \in \mathrm{codespace}_{\vec{v}}, \tag{4.44}$$

provided that the error super-operator $\mathcal{E}$ contains only "few error" Kraus operators. More precisely, the expectation values are equal provided that the Kraus operators for $\mathcal{E}$ contain less than $\lfloor\frac{d+1}{2}\rfloor^{M-|\vec{v}|}$ errors. More can be said in terms of the structure of correctable errors. Namely, there is a constant error threshold provided a random distribution of uncorrelated errors is assumed.

Another key property which can be guaranteed inductively is that the commutation/anticommutation relation between logical operators and error corrected observables should be the same as between bare operators.

$$[\sigma 1_{\vec{v}}^{EC}, \sigma 2_{\vec{v}}^{L}]_{\pm} = 0 \quad \Leftrightarrow \quad [\sigma 1, \sigma 2]_{\pm} = 0 \tag{4.45}$$

An even stronger statement can be made about products of logical operators (error corrected observables)

$$\sigma 1\sigma 2 = \theta\sigma 3 \Rightarrow \begin{cases} \sigma 1_{\vec{v}}^{L}\sigma 2_{\vec{v}}^{L} = \theta\sigma 3_{\vec{v}}^{L} \text{ and} \\ \sigma 1_{\vec{v}}^{EC}\sigma 2_{\vec{v}}^{EC} = \theta\sigma 3_{\vec{v}}^{EC} \end{cases}, \tag{4.46}$$

where θ is a phase in $\{1, -1, i, -i\}$.

The projector operators at each level are related to the presence of logical errors at the immediately preceding level. This can be seen through the identity

$$P_{\vec{v}}^{(j)} = R_{\vec{v}}^{(j)} P_{\vec{v}}^{(0)} R_{\vec{v}}^{(j)} \qquad R_{\vec{v}}^{(0)} = \mathbb{1}, \tag{4.47}$$

which relates $P_{\vec{v}}^{(0)}$, the trivial syndrome projector to other syndrome projectors. The relation of this projector with the recovery operations is captured by

$$P_{\vec{v}}^{(0)} \mathcal{R}_{\vec{v}}(\rho) P_{\vec{v}}^{(0)} = \mathcal{R}_{\vec{v}}(\rho). \tag{4.48}$$

The master equation.- considered for a dissipative protection on a concatenated QECC will contain error terms $\mathcal{D}_{noise,\vec{v}}$ on single physical qubits $\vec{v}$ as well as correction terms corresponding to each of the blocks. The full master equation reads

$$\dot{\rho} = \sum_{|\vec{v}|=M} \mathcal{D}_{noise,\vec{v}}(\rho) + \sum_{|\vec{v}|<M} \mathcal{D}_{correct,\vec{v}}(\rho). \tag{4.49}$$

Error terms $\mathcal{D}_{noise,\vec{v}}$ are single qubit superoperators with norm bounded by $\left\|\mathcal{D}_{noise,\vec{v}}\right\| \leq \Gamma_{noise}$. The protective dissipation $\mathcal{D}_{correct,\vec{v}}$ is defined by

$$\mathcal{D}_{correct,\vec{v}}(\rho) = \Gamma_{correct,\vec{v}}[\mathcal{R}_{\vec{v}}(\rho) - \rho] \tag{4.50}$$

which can be written in Lindblad form as

$$\mathcal{D}_{correct,\vec{v}}(\rho) = \sum_{(j)} L_{\vec{v}}^{(j)} \rho L_{\vec{v}}^{(j)\dagger} - \frac{1}{2} \left\{ L_{\vec{v}}^{(j)\dagger} L_{\vec{v}}^{(j)}, \rho \right\}_{+} \tag{4.51}$$

with Lindblad operators

$$L_{\vec{v}}^{(j)} = \sqrt{\Gamma_{correct,\vec{v}}} R_{\vec{v}}^{(j)} P_{\vec{v}}^{(j)}. \tag{4.52}$$

We will prove the robustness of the highest level observables $X_{\emptyset}^{EC}, Y_{\emptyset}^{EC}, Z_{\emptyset}^{EC}$ under the combination of weak local noise and this dissipative protection. To do this, we focus on the observables $\{P_{\vec{v}}^{(j)} : |\vec{v}| < M\}$. Together with an arbitrary error corrected observable at the highest level, these constitute a complete set of quantum numbers. The most attractive features of these observables is that both single qubit Pauli errors and the recovery operations may be described by classical deterministic transition rules in terms of this specific set of quantum numbers. Furthermore, the events influencing each of these quantum numbers may be simply characterized. Namely, only recovery or physical error events located at $\vec{u} \succcurlyeq \vec{v}$ can

influence the validity of $P_{\vec{v}}^{(j)}$. This will allow us to provide upper bounds for the probability of introducing logical errors.

It is useful to define certain additional projectors in terms of the set of commuting projectors $\{P_{\vec{v}}^{(j)} : M > |\vec{v}|\}$

$$\begin{aligned} \text{HasError}(\vec{v}) &= \mathbb{1} - P_{\vec{v}}^{(0)} \\ \text{IsError}(j:\vec{v}) &= P_{\vec{v}}^{(X_j)} + P_{\vec{v}}^{(Y_j)} + P_{\vec{v}}^{(Z_j)} \\ \text{Enabled}(j:\vec{v}) &= \mathbb{1} - P_{\vec{v}}^{(0)} - P_{\vec{v}}^{(X_j)} - P_{\vec{v}}^{(Y_j)} - P_{\vec{v}}^{(Z_j)} \end{aligned} \tag{4.53}$$

The recovery operation $\mathcal{R}_{\vec{v}}$ has a non trivial effect only for the subspace "HasError($\vec{v}$)". Furthermore, in the subspace "IsError($j:\vec{v}$)", the effect of applying the recovery operation $\mathcal{R}_{\vec{v}}$ is to apply a logical operation on $j:\vec{v}$. Finally, the projector "Enabled($j:\vec{v}$)" the difference between the two and indicates that there is already a logical error among the immediate components of $\vec{v}$, but that it is not at $j:\vec{v}$. This last projector will be instrumental in bounding the probability for physical errors to be raised as logical errors. In the case of the perfect five qubit code, it is a necessary and sufficient condition for a logical operation at $j:\vec{v}$ be seen (in terms of the stabilizers) as raising a logical operation at $\vec{v}$. The following short hand notation will be used to express the probability of satisfying these predicates (projectors)

$$\langle P\rangle_t = \text{tr}[P\rho(t)]. \tag{4.54}$$

4.C.1 Bounding error probabilities

of constitute the core of proving the robustness of error corrected observables under such a dissipative dynamics as Eq. (4.49). In particular, we wish to prove inductively that

$$\forall t \quad \langle \text{HasError}(\vec{v})\rangle_t \leq p_n \quad \text{where}\, n = M - |\vec{v}|. \tag{4.55}$$

Since the initial state $\rho(0)$ is by Hypothesis a code state at all levels, we have that

$$\forall \vec{v}: \quad \langle \text{HasError}(\vec{v})\rangle_{t=0} = 0. \tag{4.56}$$

The trick now is to obtain an upper bound on the rate at which these probabilities may increase and upper-bound the actual probability by a fixed-point value. Let us first illustrate

this method by considering a simple example provided by $|\vec{v}| = M - 1$.

$$\begin{aligned} &\frac{d\langle \text{HasError}(\vec{v})\rangle_t}{dt} \leq \\ &k\Gamma_{\text{noise}} - \Gamma_{\text{correct},\vec{v}}\langle \text{HasError}(\vec{v})\rangle_t \end{aligned} \tag{4.57}$$

Note that we have excluded processes by which a physical error cancels a preexisting error.

From the rate bound, we may extract a fixed-point upper-bound and use it to bound the actual probability

$$\langle \text{HasError}(\vec{v})\rangle_t \leq \frac{k\Gamma_{\text{noise}}}{k\Gamma_{\text{noise}} + \Gamma_{\text{correct},\vec{v}}}. \tag{4.58}$$

Assuming $\Gamma_{\text{correct},\vec{v}} \geq \Gamma_{\text{correct},M-|\vec{v}|}$, we may further simplify the bound to

$$\langle \text{HasError}(\vec{v})\rangle_t \leq \frac{k\Gamma_{\text{noise}}}{\Gamma_{\text{correct},1}} =: p_1. \tag{4.59}$$

We may take a similar approach to bound the rate at which errors accumulate at higher levels (i.e. $M - |\vec{v}| = n + 1$). However, the expressions required here are a bit more complicated.

$$\frac{d\langle \text{HasError}(\vec{v})\rangle_t}{dt} \tag{4.60}$$

$$\leq \sum_{\substack{\vec{u}\succ\vec{v} \\ |\vec{u}|=M}} \Gamma_{\text{noise},\vec{u}} \left\langle \prod_{\vec{u}\succcurlyeq\vec{w}\succ\vec{v}} \text{Enabled}(\vec{w}) \right\rangle_t \tag{4.61}$$

$$-\Gamma_{\text{correct},\vec{v}}\langle \text{HasError}(\vec{v})\rangle_t$$

$$\leq \Gamma_{\text{noise}} \sum_{\substack{\vec{u}\succ\vec{v} \\ |\vec{u}|=M}} \prod_{\vec{u}\succcurlyeq\vec{w}\succ\vec{v}} \langle \text{Enabled}(\vec{w})\rangle_t \tag{4.62}$$

$$-\Gamma_{\text{correct},\vec{v}}\langle \text{HasError}(\vec{v})\rangle_t$$

$$\leq \Gamma_{\text{noise}} \sum_{\substack{\vec{u}\succ\vec{v} \\ |\vec{u}|=M}} \prod_{\vec{u}\succ\vec{w}\succ\vec{v}} \langle \text{HasError}(\vec{w})\rangle_t \tag{4.63}$$

$$-\Gamma_{\text{correct},\vec{v}}\langle \text{HasError}(\vec{v})\rangle_t$$

$$\leq k^{n+1}\Gamma_{\text{noise}} \prod_{j=1}^{n} p_j \tag{4.64}$$

$$-\Gamma_{\text{correct},n+1}\langle \text{HasError}(\vec{v})\rangle$$

A non trivial step is taken in going from [4.61] to [4.62], where the probability of a conjunction is taken to be a product of probabilities (i.e. independent probabilities). This property will be proven in appendix 4.D.

In turn, this leads to the fixed point bound

$$\langle \text{HasError}(\vec{v})\rangle_t \leq \frac{k^{n+1}\Gamma_{\text{noise}} \prod_{j=1}^{n} p_j}{\Gamma_{\text{correct},n+1}} =: p_{n+1}. \tag{4.65}$$

From here, we inductively derive the expression

$$p_n = \frac{\Gamma_{\text{noise}}^{2^{n-1}} k^{2^n-1}}{\Gamma_{\text{correct},n} \prod_{j=1}^{n-1} \Gamma_{\text{correct},j}^{2^{n-1-j}}}. \tag{4.66}$$

Making the additional assumption $\Gamma_{\text{correct},j} = \Gamma_{\text{correct}} \delta^j$ we may simplify this expression to obtain

$$p_n = \left(\frac{\Gamma_{\text{noise}} k^2}{\Gamma_{\text{correct}} \delta^2} \right)^{2^{n-1}} \frac{\delta}{k}. \tag{4.67}$$

In turn, this tells us that if $\Gamma_{\text{noise}} < (\delta/k)^2 \Gamma_{\text{correct}}$, then the probability of having non trivial syndrome decreases double exponentially with the level of the syndrome.

Our final goal is to obtain an expression bounding the rate at which logical errors are introduced. One possibility, is to study the decay rate for any of the three highest level logical Pauli observables. Since these three constitute a full set of observables for the logical subsystem, their preservation implies high fidelity storage of quantum information [7].

A logical error or flip of the highest level logical observables, can be introduced whenever a physical error occurs at a site which is enabled to raise the error at all levels. Employing bounds similar to those in Eqs. (4.61)-(4.64) one arrives at

$$\frac{d\langle X_{\emptyset}^{\text{EC}} \rho(t) \rangle_t}{dt} \tag{4.68}$$

$$\leq \sum_{|\vec{u}|=M} \Gamma_{\text{noise},\vec{u}} \left\langle \prod_{\vec{u} \succcurlyeq \vec{w} \succ \emptyset} \text{Enabled}(\vec{w}) \right\rangle_t \tag{4.69}$$

$$\leq \Gamma_{\text{noise}} \delta^M \left(\frac{\Gamma_{\text{noise}} k^2}{\Gamma_{\text{correct}} \delta^2} \right)^{2^M - 1}, \tag{4.70}$$

indicating that for a sufficiently low physical error rate, the logical error rate is suppressed double exponentially in terms of M, similar to results for concatenated QECC in a quantum circuit model.

4.D Proof of independence for the Enabled property

In this section we assume a Pauli noise model and prove that the Enabled property along the different truncations of the same physical address are statistically independent. More specifically, the factorization

$$\left\langle \prod_{\vec{u} \succcurlyeq \vec{w} \succ \vec{v}} \text{Enabled}(\vec{w}) \right\rangle_t = \prod_{\vec{u} \succcurlyeq \vec{w} \succ \vec{v}} \langle \text{Enabled}(\vec{w}) \rangle_t \tag{4.71}$$

holds for a noise process of Pauli form

$$\mathcal{D}_{noise,\vec{v}}(\rho) = \sum_{\sigma\in\{X,Y,Z\}} \Gamma_\sigma \left(\sigma_{\vec{v}}\rho\sigma_{\vec{v}} - \rho\right). \tag{4.72}$$

The restriction of the noise process to Pauli form Eq. (4.72) is clearly undesired. However, it provides a sufficient condition to prove Eq. (4.71), which does not hold for general noise. We expect the need for this assumption to be an artifact of our proof technique and that our main result, i.e. Eq. (4.68), will essentially hold for any independent noise model.

The proof relies on the independence of the different processes which introduce physical errors and perform recovery operations. An event $\mathrm{Ev}_{\vec{w}}$ will be associated to each vector $\vec{w}$, with $|\vec{w}| = M$ corresponding to the introduction of physical errors at $\vec{w}$ and $|\vec{w}| < M$ corresponding to recovery operation $\mathcal{R}_{\vec{w}}$. Each event $\mathrm{Ev}_{\vec{w}}$ can be seen as the state dependent application of a tensor product Pauli operator. Furthermore, for $|\vec{w}| < M$ the operator only depends on the quantum numbers $P^{(j)}_{\vec{w}}$ and must be a logical Pauli operators at some $w_0 : \vec{w}$. The correction operators satisfy this property by design. In turn, for $|\vec{w}| = M$, $\mathrm{Ev}_{\vec{w}}$ applies a randomly chosen physical Pauli operator at $\vec{w}$ according to the Pauli form noise model Eq. (4.72). It can be seen that under these conditions, only events $\mathrm{Ev}_{\vec{w}}$ such that $\vec{w} \succ \vec{v}$ can directly affect the quantum numbers $P^{(j)}_{\vec{v}}$. Thus, given a history L of events $\mathrm{Ev}_{\vec{w}}$ applied to an initially encoded state, the quantum numbers $P^{(j)}_{\vec{v}}$ are well defined and depend only on the sub-history of events L' containing the events $\mathrm{Ev}_{\vec{w}}$ with $\vec{w} \succcurlyeq \vec{v}$.

Since $\mathrm{Enabled}(v_0 : \vec{v})$ can be defined in terms of the $P^{(j)}_{\vec{v}}$ it may only depend on the sub-history of events $\mathrm{Ev}_{\vec{w}}$ with $\vec{w} \succcurlyeq \vec{c}$. Furthermore, $\mathrm{Enabled}(v_0 : \vec{v})$ will be shown not to depend direct or indirectly on events $\mathrm{Ev}_{\vec{u}}$ with $\vec{u} \succcurlyeq v_0 : \vec{v}$. This can be seen as a consequence of $\mathrm{Enabled}(v_0 : \vec{v})$ commuting with any Pauli operator acting on qubits $\vec{w}$ with $\vec{w} \succcurlyeq v_0 : \vec{v}$.

Proving Eq. (4.71) may be split in the following steps

$$\left\langle \prod_{\vec{u}\succcurlyeq\vec{w}\succ\vec{v}} \text{Enabled}(\vec{w}) \right\rangle_t \tag{4.73}$$

$$= \sum_L p_L(t)\, \text{tr}[\prod_{\vec{u}\succcurlyeq\vec{w}\succ\vec{v}} \text{Enabled}(\vec{w}) L\rho_0] \tag{4.74}$$

$$= \sum_L p_L(t) \prod_{\vec{u}\succcurlyeq\vec{w}\succ\vec{v}} \text{tr}[\text{Enabled}(\vec{w}) L\rho_0] \tag{4.75}$$

$$= \sum_L p_L(t) \prod_{\vec{u}\succcurlyeq\vec{w}\succ\vec{v}} \text{tr}[\text{Enabled}(\vec{w}) L_{\vec{w}}\rho_0] \tag{4.76}$$

$$= \prod_{\vec{u}\succcurlyeq\vec{w}\succ\vec{v}} \sum_{L_{\vec{w}}} p_{L_{\vec{w}}}(t)\, \text{tr}[\text{Enabled}(\vec{w}) L_{\vec{w}}\rho_0] \tag{4.77}$$

$$= \prod_{\vec{u}\succcurlyeq\vec{w}\succ\vec{v}} \langle \text{Enabled}(\vec{w})\rangle_t, \tag{4.78}$$

which will be subsequently explained and justified. As a first step, the master equation defining $\rho(t)$ is unraveled [25] into event histories L to obtain Exp. (4.74). Given that every event history L implements a Pauli operator which produces eigenstates to all the projectors $\text{Enabled}(\vec{w})$, the $0,1$ expectation values may be factorized to obtain Exp. (4.75). Expectation values depend only on disjoint sub-histories $L_{w_0:\vec{w}}$ (a history of events uniquely determined by filtering events $\text{Ev}_{\vec{u}}$ such that $\vec{u} \succ \vec{w}$ but not $\vec{u} \succ w_0 : \vec{w}$ from L), leading to Exp. (4.76). Furthermore, the sum of p_L consistent with given sub-histories $L_{\vec{w}}$ may be written as a product of the independent probabilities $p_{L_{\vec{w}}}$ of such sub-histories, thus leading to Exp. (4.77). Finally, each factors in Exp. (4.76) may be seen to be the history unraveling of each of the factors in Exp. (4.78), which is what we set out to prove.

Chapter 5

Record qubit storage time using NV-center proximal ^{13}C

In this chapter we introduce Nitrogen-Vacancy (NV) centers in diamond, a physical system which has demonstrated outstanding qualities for quantum information applications. Using this system, joint effort with the group of Mikhail Lukin at Harvard have lead to the experimental realization of record coherent storage times for room temperature solids. The emphasis of this chapter is theoretical, providing special attention to the authors contribution, namely, the design and identification of decoupling techniques to extend the coherence time of a ^{13}C nuclear spin. As a complement, a copy of the original published article, Science 336 (2012) 1283-1286, is appended to the printed version of this thesis with permission of AAAS.

5.1 Introduction

Stable quantum bits, capable of both storing quantum information for prolonged times and with the potential of being integrated into small portable devices can constitute a building block for quantum information applications. In this chapter, we focus on a very specific physical system with the goal of furthering the current record for room-temperature coherent storage. Nitrogen-Vacancy center are a natural candidate for this endeavour since they have been shown to permit coherent storage even at room temperature. The contribution of

this work is to provide models for the dominant decoherence mechanisms and provide an enhancement of coherence times via a combination of techniques such as material engineering, dissipative environment engineering and dynamical decoupling.

5.1.1 Outline

First the physical system of the NV-center is described taking care to enumerate the relevant degrees of freedom at different energy scales: a) the orbital electronic levels which allow for optical pumping and fluorescence detection, b) the electronic spin degrees of freedom which can be optically detected and initialized, c) the nuclear spin degrees of freedom which couple coherently to the electronic spin and are otherwise well isolated. We then proceed to explain how the coherent coupling between a neighbouring ^{13}C nuclear spin and the electronic spin of the NV center can be used to achieve single shot readout and initialization with fidelities as high as 97%. At this point, we reach the main contribution of this work, which is the modelling of ^{13}C nuclear spin decoherence and depolarization in tandem with the design and implementation of techniques to prevent it. These techniques are of two kinds: a) dissipative driving of the environment (electronic spin) to achieve a motional narrowing regime b) coherent driving of the ^{13}C memory spin to dynamically decouple it from nuclear spins in its vicinity. Following the main theme of this thesis, we describe how to use available controls to initialize, store and read out a qubit. Finally, perspectives on how to further increase coherent storage times and applications are discussed.

5.2 An introduction to NV centers

Nitrogen-vacancy centers are deep center defects in the diamond crystal structure consisting of a substitutional nitrogen impurity and a nearest neighbour vacant cite in the diamond lattice (see figure 5.1(a)). These centers are extremely stable, even under continuous irradiation and ambient conditions. Like atoms, NV centers respond to optical transitions and have electronic and spin degrees of freedom. The host lattice, provides the advantage that the center will be pined in space. This in turn, allows measuring the fluorescence of a single center, optically addressing it and to some extent, characterizing its local environment. The ab-initio calculation of the electronic structure continues to be a subject of research and is

beyond the scope of this thesis [43, 42]. The widely accepted energy structure for these centers is presented here in a phenomenological way.

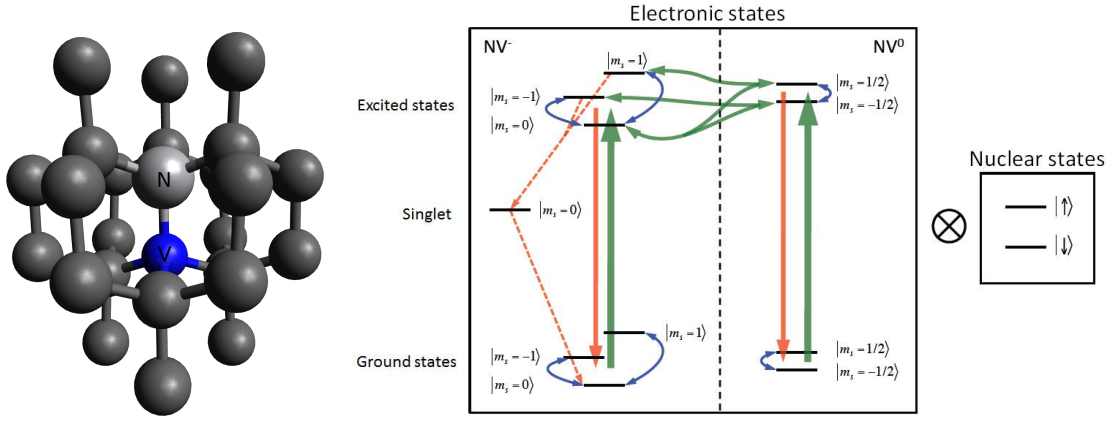

(a) NV-center real-space layout

(b) NV-center energy levels

Figure 5.1: a) An NV-center is obtained by removing two nearest neighbour carbons in the diamond lattice and replacing one of them by a nitrogen atom (light grey) while keeping the lattice location vacant (blue). In practice, a way to fabricate these centers is via high temperature annealing of natural or implanted nitrogen impurities until they become attached to a vacancy. b) Schematic level diagram for an NV center (left box) and a ^{13}C nuclear spin (right box) under illumination with green laser light. The green arrows indicate optical transitions addressed by our green laser pulse, red arrows show electronic decay and blue arrows indicate depolarization of the electronic spin. The transition rates for NV are taken from [88] with the decay rate from the electronic excited state to the ground state $\tilde{\gamma} = \frac{1}{13ns}$, the decay rate from the singlet to $m_s = 0$ of the electronic ground state $\Gamma = \frac{1}{300ns}$ and the decay rate from the electronic excited states with $m_s = \pm 1$ to the singlet $\tilde{\gamma}_b = 0.3\tilde{\gamma}$. Moreover we assumed the decay rate of the excited state of NV^0 to be on the same order as for NV. The deionization rate from NV to NV^0 is taken to be $\gamma_1 = \frac{I/I_{sat}}{70ns}$ and the ionization rate $\gamma_2 = 2\gamma_1$ [126]. The depolarization time for the electronic spin for NV is taken to be $T_{1e}^{NV^-} = 8ms$ and for the case of NV^0, $T_{1e}^{NV^0} = 6\mu s$ [126]. All the remaining rates are taken to be zero. Reprinted from Science **336** (2012) 1283-1286 with permission from AAAS.

5.2.1 Electronic energy levels

Two possible charge states have been found to be long lived for NV centers, a neutral state NV^0 and a singly charged state NV^-. Each of these charge states can be electronically excited with respective zero-phonon lines of 2.16eV (575nm) for NV^0 and 1.945eV (637nm) for NV^-. Compare this to a band gap of 5.5eV for diamond. There are 6 electrons contributing to the electronic structure of the NV^-, one valence electron for each of the nearest neighbour carbons of the vacancy, two from the substitutional nitrogen and an extra negative charge. The nitrogen and the vacancy partially break the symmetries of the diamond lattice leaving only a C_{3V} symmetry around the axis they define (see figure 5.1(a)). The NV^- is most abundant in nautral diamond, and will also play a dominant role in this work. However, the NV^- can become deionized by optical irradiation so NV^0 should not be dismissed completely.

The orbital ground state of NV^- transforms as A_1 (i.e. is invariant) under C_{3V} symmetry transformations. There are two dipole allowed excited states at 1.945eV with E character which can be optically excited and fluoresce. By employing a Hanbury Brown and Twiss type setup to collect NV-center fluorescence, it is possible to ascertain that a single center is being detected[78]. Typically, excitation and fluorescence processes occur primarily through the phonon sidebands (630–800nm), with the excited states showing a radiative lifetime of ≈13ns. However, there is also a slower non radiative decay channel for the excited states via a shelf state which is responsible for polarizing the electronic spin.

While the NV^- energy structure is relatively well understood, knowledge of NV^0 states and dynamics have not reached the same degree of maturity and consensus. In our study, we consider a simple model for the NV^0 in which only a doublet ground state and exited state are involved [126]. However, there are a few reasons why our results do not show a strong dependence on the detailed description of NV^0. The main one, is that all of the coherent manipulation of our system occurs exclusively in the NV^- states. Furthermore, it is expected that at the relevant filling conditions, the NV centers spend more than twice as much time in NV^- states than in NV^0 states, even during optical irradiation. Finally, the electronic spin depolarization is more than 1000 times faster for NV^0 state than for NV^- and experiments suggest that NV^0 states have no orbital angular momentum. This leads us to expect that the weak hyperfine interaction with distant ^{13}C can be neglected due to motional averaging.

5.2.2 Electronic spin sublevels

Both the ground orbital state and the discussed excited states of NV^- have an additional triplet spin structure which is mainly preserved by optical transitions. Electronic spin-spin interactions provide a zero-field splitting (ZFS) described by $\Delta_{gs/es}S_z^2$. In the long lived electronic ground state $\Delta_{gs} \approx 2.87$GHz allows microwave (MW) driving of electronic transitions. For the excited states, the ZFS is approximately half as strong $\Delta_{es} \approx 1.43$GHz [96]. However, due to the short lifetime of excited orbital states coherent control is more reliable in the ground state. Additionally, the energy levels of electronic spin states are shifted by an external magnetic field B which in our setup will be fixed along the NV symmetry axis. Microwave pulses can coherently drive transitions among these electronic states. The feature which makes NV center electronic spins most attractive, is their optical polarizability (into $m_s = 0$ state) and the possibility of optical measurement via spin dependent fluorescence.

5.2.3 Nuclear spin environment

At longer time scales, nuclear spins, which interact with the electronic spin degree of freedom via hyperfine interaction begin to play a relevant role in NV-center dynamics. The Nitrogen atom of the NV-center provides a nuclear spin which is universally present, either the naturally occurring ^{14}N with $(I = 1)$ or its less likely (0.4%) stable isotope ^{15}N with $(I = 1/2)$ which may also be selectively implanted. Due to its universality, many proposals have been made involving the nitrogen nuclear spin[116], however, its strong coupling with the NV electronic spin rule out prolonged coherent storage. Due to the strong electronic ZFS, and the symmetric placement of the nitrogen the $A_{zz}^N I_z^N S_z$ is the only remaining term of the hyperfine interaction in the electronic ground space, with $A_{zz}^N \approx -2.16$MHz. The nitrogen nuclear spin also present a zero field splitting given by $P(I_z^N)^2$, with $P \approx -5$MHz.

While most carbon atoms (^{12}C) in the diamond lattice have no nuclear spins the remaining ^{13}C nuclear spins $(I = 1/2)$ provide a bath with which the electronic NV-spin may interact. In particular, the hyperfine interaction of the electronic spin with nearest neighbour ^{13}C, is even greater than with the ^{14}N nuclear spin. From first principles, the hyperfine interaction

of the electronic spin with a ^{13}C nuclear spins is given by

$$\begin{aligned} H_{hf} = &- \gamma_e \gamma_{^{13}C} \frac{2\mu_0 \pi \hbar^2 |\psi_e(\mathbf{r}=\mathbf{0})|^2}{3} \mathbf{S} \cdot \mathbf{I}^{^{13}C} \\ &+ \frac{\hbar^2 \mu_0 \gamma_e \gamma_{^{13}C}}{4\pi} \left\langle \frac{1}{r^3} \left(\mathbf{S} \cdot \mathbf{I}^{^{13}C} - 3(\mathbf{n} \cdot \mathbf{S})(\mathbf{n} \cdot \mathbf{I}^{^{13}C}) \right) \right\rangle , \end{aligned} \tag{5.1}$$

where γ_e and $\gamma_{^{13}C}$ are the gyromagnetic moments of the electron and the ^{13}C nuclear spin respectively, r and $\mathbf{n}$ are the magnitude and direction of the position $\mathbf{r}$ of the electron respect to the nuclear spin and the brackets denote expectation value with respect to the electronic wave function $\psi_e(\mathbf{r})$ (taking coordinate origin at the nuclear spin). The first term corresponds to a Fermi contact interaction whereas the second corresponds to the usual magnetic dipole-dipole interaction. In the case of the NV-center, the electronic wave function actually corresponds to six valence electrons. In practice, the hyperfine interaction can be represented by an orbital state dependent hyperfine tensor

$$H_{hf} = \sum_{\mu,\nu \in \{x,y,z\}} S_\mu A^{\mu,\nu} I_\nu . \tag{5.2}$$

For proximal nuclear spins, this tensor can be obtained experimentally and/or from first principle electronic wave function calculations. For distant nuclear spins, the contact interaction decays exponentially and can be discarded, and a point-dipole approximation which places all electronic density at the NV is justified for estimating the hyperfine tensor[97].

In addition to the interaction with the electronic spin, each nuclear spin interacts directly with the external magnetic field $H_b = \gamma_{^{13}C} \hbar \mathbf{B} \cdot \mathbf{I}$. Finally, relatively weak magnetic dipole-dipole interactions exists among the nuclear spins

$$H_{dd} = \sum_{j<k} -\frac{\mu_0}{4\pi} \frac{\gamma_j \gamma_k \hbar^2}{{r_{jk}}^3} \left(3(\mathbf{I}_j \cdot \mathbf{n}_{jk})(\mathbf{I}_k \cdot \mathbf{n}_{jk}) - \mathbf{I}_j \cdot \mathbf{I}_k \right) , \tag{5.3}$$

where j, k index over the different nuclear spins and the vector $\mathbf{r}_{jk}$ with length r_{jk} and orientation $\mathbf{n}_{jk}$ is the relative position of the two nuclear spins.

The stable ^{13}C isotope occurs with a natural abundance of 1.1%, whereas material engineering may reduce this ratio to as low as 0.01%. This reduction is a key ingredient to our approach of using ^{13}C nuclear spins as memories since it effectively reduces the dipole-dipole coupling among neighbouring ^{13}C and the typical hyperfine interaction with the NV electronic spin. This second effect allows reaching the motional narrowing regime in which the electronic spin is driven faster than the hyperfine interaction time.

The effective surrounding ^{13}C concentration determines the coherence time of the electronic spin as having a time scale similar to the hyperfine coupling[14]. Thus, in order to have some degree of coherent coupling between the NV electronic spin and a ^{13}C, the closest nuclear spin should be significantly closer than the others. In the case of the experiment conducted the nearest ^{13}C spin addressed was at a distance of 1.7nm. Given the sample ^{13}C to ^{12}C concentration of 10^{-4}, approximately 7% of the NV-centers have such a proximal ^{13}C. Thus, significant search needs to be conducted in order to locate an NV presenting a single ^{13}C with such a strong hyperfine interaction which can be clearly singled out from the rest of the nuclear spin environment. Alternatively it may be possible to improve on existing techniques to place single ^{13}C nuclear spins close to an NV-center [115] such that sample quality is not compromised.

5.3 Qubit initialization and readout

Relatively long coherence times have been demonstrated in bulk electron spin resonance (ESR) and nuclear magnetic resonance (NMR) experiments [79, 13, 121]. A shortfall of theses systems is that single spin initialization and readout are quite challenging and only global addressing can be used. In contrast, one of the attractive qualities of NV-centers is the possibility of optically inducing spin polarization and optically detected magnetic resonance. Due to diffraction limits, the optically achievable spatial resolution ≈200nm is orders of magnitude higher than what is achievable with microwave or radio-frequency allowing to resolve single NV centers at sufficiently low density. A second advantage is the large optically achievable spin polarizations (90% for the electronic spin [36] or even 98% for isotopic ^{15}N nuclear spins [62]) which are unachievable by thermal equilibration in standard NMR or ESR experiments. Furthermore, the single spin repetitive readout techniques that will be discussed allow achieving an even higher degree of polarization on neighbouring ^{13}C nuclear spins.

In this section we will describe ^{13}C initialization and single shot readout following the work by Neumann et al. [95] (see figure 5.3). The main ingredients of this approach are a) optical readout and initialization of electronic spin b) $C_n\mathrm{NOT}_e$ logic gate which flips the electronic spin conditioned on the ^{13}C nuclear spin c) arbitrary gates acting on the ^{13}C nuclear spin. Finally, we may infer the nuclear state and our uncertainty of it from the photon counting statistics which is obtained. We will describe these steps one by one in what follow and finally

combine them to provide high fidelity initialization and readout.

5.3.1 Electronic spin initialization and readout

The NV^- center undergoes mostly spin preserving cycling transitions into its excited state when driven by laser light at (λ =532nm). It quickly (≈13ns) fluoresces from the electronic excited state emitting into the phonon sideband (630–800nm). Depending on factors such as strain and magnetic field misalignment with the NV axis, the electronic spin preservation may be imperfect. Additionally, the $|m_s = \pm 1\rangle$ orbitally excited states decay non-radiatively into an orbital singlet state which eventually decays mainly into the $m_s = 0$ spin state of the ground state space. The shelving of the $|m_s = \pm 1\rangle$ states into a metastable states leads to a differential fluorescence count with the $m_s = 0$ state initially showing more counts (see figure 5.2). Repolarization of the electronic spin into the $m_s = 0$ state occurs on the time scale of ≈150ns so the electronic spin can be expected to be completely repolarized after $\approx 1\mu s$. Regretfully, due to relatively low collection efficiencies the probability of not collecting any fluorescence photons during such a time is higher than 98% for both electronic spin states.

5.3.2 C_nNOT_e

For distant ^{13}C nuclear spins the dominant energy scale is due to the external magnetic field $B = (244.42 \pm 0.02)$Gauss which leads to a precession frequency of $\omega_{^{13}C} \approx 261.5$kHz. Second in strength comes the hyperfine interaction of the electronic spin with the closest ^{13}C nuclear spin was $A_{\|} = (2\pi)(2.66 \pm 0.08)$kHz (approximately 1% of the Zeeman splitting due to the external magnetic field). Taking the RWA with respect to the energy levels of the electronic spin ground space the hyperfine interaction terms not commuting with S_z may be discarded due to the huge zero field splitting $\Delta_{gs} \approx 2.87$GHz. Furthermore, estimating $A_{\|} \sim A_{\perp}$ we may conclude that $A_{\perp}$ will have no first order contribution to the energy levels and can contribute only a small $O(A_{\perp}/\omega_{^{13}C})$ modification to the magnetic ^{13}C nuclear spins quantization axis.

In order to define a C_nNOT_e gate which flips the electronic qubit depending on the state projection of the nuclear ^{13}C qubit we first restrict ourselves to a two level subspace for the electronic spin spanned by $|m_s = 0\rangle$ and $|m_s = 1\rangle$. First, a resonant microwave $\pi/2$ pulse prepares the state $(|m_s = 0\rangle + |m_s = 1\rangle)/\sqrt{2}$. This is followed by a free precession period of $\tau = \pi/A_{\|}$ which is at the heart of the C_nNOT_e gate. Finally, a second $\pi/2$ microwave pulse is

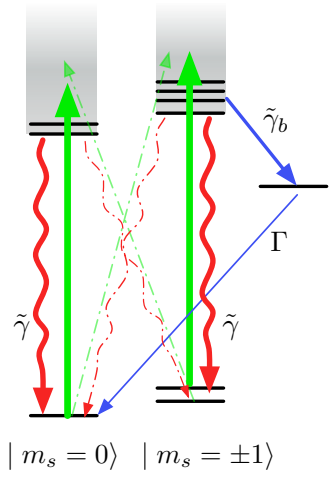

Figure 5.2: The $|m_s = \pm 1\rangle$ excited states decay into the singlet shelve state with a rate $\tilde{\gamma}_b \approx 0.3\tilde{\gamma}$ which in turn decays mainly into the $|m_s = 0\rangle$ ground state at a slower rate $\Gamma \approx \frac{1}{300ns}$. No photons are emitted during the time spent in the shelf state leading to a lower initial fluorescence intensity for the $|m_s = \pm 1\rangle$ states. Eventually, the electronic spin becomes polarized into the $|m_s = 0\rangle$ independent of the initial state. Such a $1/e$ decay occurs on a time scale of the order of $150ns$ and steady state polarization can be assumed after 1μs (these rates depend on the strength of the optical driving).

applied, taking care to use the opposite phase as for the first one. This sequence implements the

$$C_nNOT_e = \begin{pmatrix} 1 & 0 & 0 & 0 \\ 0 & 1 & 0 & 0 \\ 0 & 0 & 0 & i \\ 0 & 0 & i & 0 \end{pmatrix} \tag{5.4}$$

which is the desired transformation (up to phases in the computational basis). Note that if the relative phase of the $\pi/2$ microwave pulses is the opposite of the one expected, the implemented gate will be

$$C_{\bar{n}}NOT_e = \begin{pmatrix} 0 & 1 & 0 & 0 \\ -1 & 0 & 0 & 0 \\ 0 & 0 & -i & 0 \\ 0 & 0 & 0 & +i \end{pmatrix}, \tag{5.5}$$

which is also acceptable up to phases in the computational basis and a swap in the definition of the computational basis states for the ^{13}C nuclear spin. It is experimentally challenging to control the MW frequency such that it does not drift from the electronic resonance frequency over a period τ. A frequency mismatch δ such that $\delta\tau = \pm\pi/2$ would already erase all measurable contrast. This requires the resonance frequency to be matched within 1kHz. Such drifts may be induced by temperature since the ZFS Δ_{gs} has been reported to show a temperature dependence of around $(2\pi)74\frac{kHz}{K}$ imposing a thermal stability of 0.02K. This is experimentally challenging, and is avoided by defining the nuclear states $|\uparrow\rangle$, $(|\downarrow\rangle)$ as corresponding to high (low) fluorescence. In the experimental setup considered, such frequency drifts do occur on the time scale of 30 minutes changing this definition.

The MW pulses manipulating the electronic spin were performed with a Rabi frequency on the order of (2π)40MHz which is more than 10000 times faster than the hyperfine splitting and provides pulses which are approximately instantaneous with respect to it. Additionally the ^{14}N nuclear spin can be assumed to be dynamically polarized to 71% by the optical driving due to an anti-crossing in the electronic excited state [62].

5.3.3 Nuclear spin gates and preparation of arbitrary states

By repetitively mapping the state of the nuclear spin onto the electronic spin and performing fluorescence detection, it is possible to determine the state (either $|\uparrow\rangle$ or $|\downarrow\rangle$) to a very high precision (purity). A full set of single qubit gates allows us to prepare any known state from such a known initial state. Using radio-frequency driving with well controlled phases and in resonance with the $\omega_{^{13}C}$ magnetic Zeeman splitting, (261kHz) it is possible to drive coherent transitions on the ^{13}C nuclear spins. In the considered experimental setup, these transitions could be driven with Rabi frequencies of $\approx (2\pi)$100kHz.

5.3.4 Repetitive readout and initialization

As mentioned earlier, each time the nuclear spin state is mapped into the electronic spin, fluorescence counts provide an average of no more than 0.02 photon detections. In addition to the low photon collection efficiency and imperfect contrast between $|m_s = 0\rangle$ and $|m_s = 1\rangle$ states, there are other factors which lead to low contrast such as: imperfect initialization of $m_s = 0$, imperfect $C_n NOT_e$ gate implementation due to electronic dephasing and unpolarized

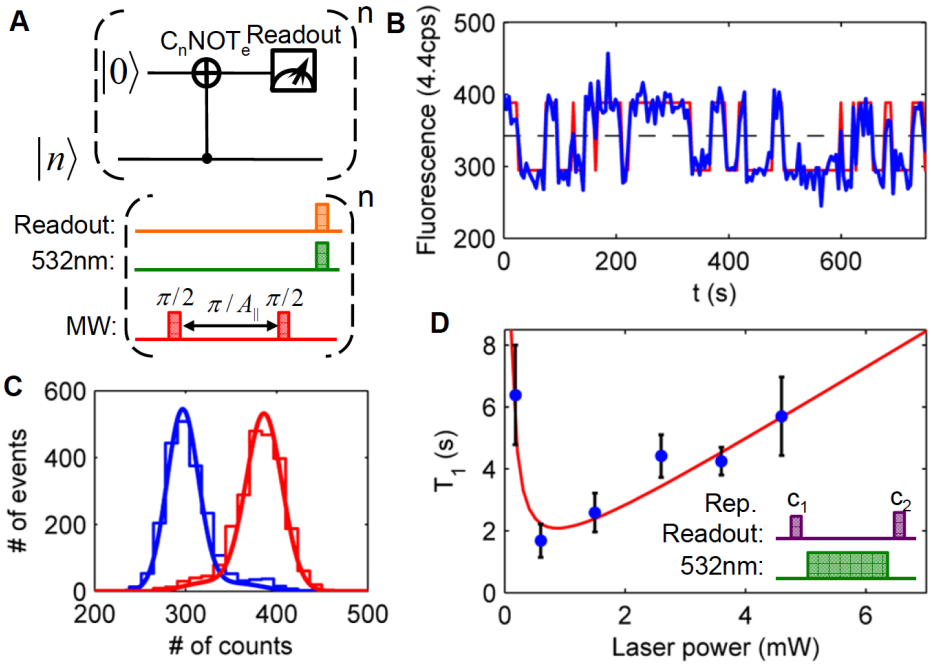

Figure 5.3: Nuclear ^{13}C qubit readout. a) Circuit diagram of repetitive readout of the nuclear spin $|n\rangle$. The readout uses a C_nNOT_e gate consisting of multiple repetitions of an electronic spin Ramsey sequence and subsequent repolarization. Many repetitions are needed to accumulate the small amounts of information provided by each measurement attempt. b) Fluorescence time trace showing single shot readout of the nuclear spin and corresponding quantum jumps. The integration time for a single point is 4.4 s. c) Histogram of continuous repetitive readouts (20000 in 4.4 s) showing two overlapping distributions of fluorescence photon counts corresponding to nuclear spin states: $|\downarrow\rangle$ (blue) and $|\uparrow\rangle$ (red). d) Nuclear spin orientation lifetime, T_{1n} as a function of 532 nm laser power. As shown in the inset, each data point is extracted from a series of two repetitive readout sequences, the first one corresponding to initialization and the second to measurement. The solid red curve represents the theoretical prediction from the simple model of nuclear depolarization induced by the off-axis dipolar hyperfine field. Reprinted from Science **336** (2012) 1283-1286 with permission from AAAS.

component of ^{14}N, complete failure due to (de)ionization of the NV-center. These are the reasons why the measurement is repeated 20000 times taking 4.4s in order to achieve a reasonable contrast between nuclear spin states (see figure 5.4). However, due to the nuclear

spin depolarization ($T_{1n} \approx 25s$ during repetitive readout), further increase in the repetition number provides little improvement for the readout fidelity.

In order to prepare definite nuclear spin states, it is possible to post select measurements for which the number of photons counts is above/below predefined thresholds. In the case of the experiment realized these were taken to be 147(195) photon counts during the last 10000 repetitions (2.2s) which leads to an initialization fidelity of $\approx 97\%$. In the case of measurement, readout fidelity can be estimated at $(91.9 \pm 2.5)\%$ from the overlap between the count distributions associated to the two possible initial states.

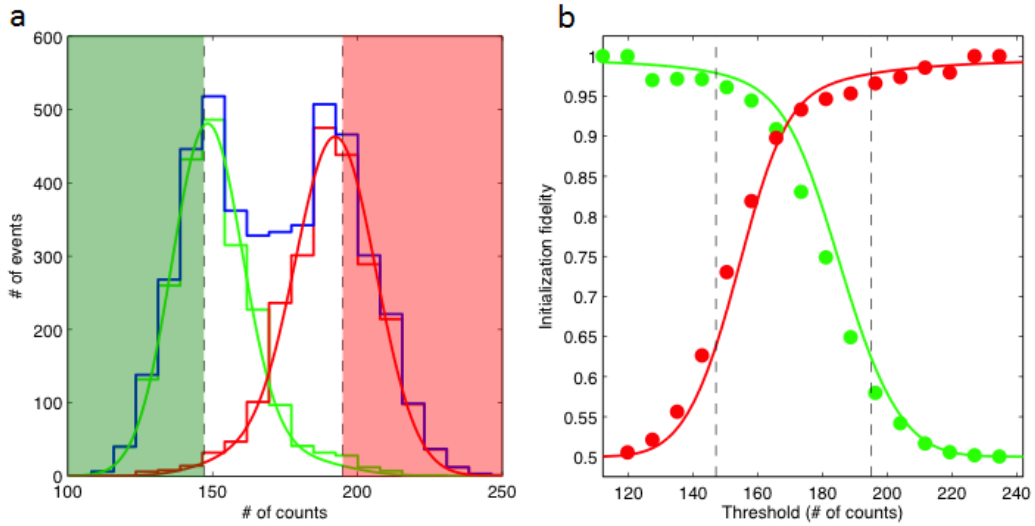

Figure 5.4: Photon count statistics and initialization fidelity a) The number of events associated to a given number of detected photons is plotted in a histogram (blue) after initialization of the nuclear spin in $|\downarrow\rangle$ (green) and $|\uparrow\rangle$ (red) and 10000 repetitive readouts (2.2s). The solid curves correspond to a theoretical fit accounting for the effect of a possible nuclear spin flips on the ideally Gaussian distributions. The green and red regions indicate photon count numbers for which initialization is assumed in the $|\downarrow\rangle$ respectively $|\uparrow\rangle$ nuclear states. b) The green and red curves indicate the initialization fidelity of $|\downarrow\rangle$ respectively $|\uparrow\rangle$ nuclear states as a function of the count threshold taken. Stricter count thresholds lead to higher fidelity but to discarding a larger fraction of initializations with the net effect of prolonging the effective initialization time required. Reprinted from Science **336** (2012) 1283-1286 with permission from AAAS.

5.4 Nuclear spin coherence and depolarization

One of the main achievements of this work is to demonstrate a prolonged coherent storage time afforded by the ^{13}C nuclear spin. In order to do this, we must first understand the processes that lead to nuclear spin depolarization and dephasing. In the dark (laser turned off), no decay of the ^{13}C nuclear spin was detected in a time of 200s, so we may assume that under these conditions, spin flip processes are suppressed on this time scale.

In order to measure the coherence time of the ^{13}C nuclear spin, an NMR Ramsey experiment is performed. After a measurement based initialization, a $\pi/2$ RF pulse puts the ^{13}C nuclear spin in a superposition $|\uparrow + \downarrow\rangle/\sqrt{2}$. Then it is left to freely precess for a variable time t. A second $\pi/2$ RF pulse is applied before a final repetitive readout of the ^{13}C spin. Each measurement must be repeated many times in order to get to estimate the expectation value of $|\uparrow\rangle\langle\uparrow|$. The detected oscillation of $|\uparrow\rangle\langle\uparrow|$ decay on a time scale of $T_{2n}^{\star} = (8.2 \pm 1.3)$ms. The origin of this relatively fast dephasing are electronic spin flips which occur on a longer time scale than the hyperfine coupling $T_{1e} > A_{\parallel}^{-1}$. Indeed, experimental measurements yield $T_{1e} = (7.5 \pm 0.8)$ms confirming $T_{1e} \approx T_{2n}^{\star}$. The reason for this is that a single flip of the electronic spin timed at random during a period $\pi/A_{\parallel}$ imprints a completely random phase on the ^{13}C nuclear spin.

5.4.1 Spin fluctuator model and motional narrowing

The approach we take to reduce dephasing is to continuously drive the electronic spin from the magnetic states $|m_s = \pm 1\rangle$ into non magnetic $|m_s = 0\rangle$ state. By doing this with a green laser beam, electronic (de)ionization transitions are also driven at rates $\gamma_{(2)1}$ as well as increasing the effective depolarization time of the electronic spin. A regime analogous to motional averaging [63] can be achieved when the mixing time of the defined process is faster than the hyperfine coupling. In this regime, both T_{1n} and T_{2n} increase linearly with the laser intensity.

In order to qualitatively understand the process of motional narrowing, let us consider an illustrative simplified scenario with only two possible NV eigenstates $\left|m_s = \pm\frac{1}{2}\right\rangle$, each having its own hyperfine interaction with the proximal ^{13}C nuclear spin. We assume that the NV state is driven incoherently as is the case for the laser driving. Finally, we assume that transitions among electronic states occur at a rate γ. The nuclear spin Hamiltonian is then

given by

$$H_n = (\omega_{^{13}C})BI_z + f(t)\sum_{\beta=x,y,z} A_{z,\beta}I_\beta \tag{5.6}$$

where the RWA has been taken respect to the electronic spin and the operator S_z has been replaced by the time-dependent stochastic variable $f(t) = \{\pm\frac{1}{2}\}$ described by a telegraph process with a single forward/backward transition rate γ (we assume $\langle f(t)\rangle = 0$). The two time correlation function for this process is given by

$$\langle f(t)f(0)\rangle = \langle f^2(0)\rangle e^{-2\gamma|t|} = \frac{1}{4}e^{-2\gamma|t|}. \tag{5.7}$$

In the actual experimental scenario, a good fraction of the transition rates are proportional to the laser intensity.

The nuclear spin Hamiltonian can be rewritten as

$$H_n = (\omega_{^{13}C})BI_z + f(t)\left(A_\parallel I_z + A_{z,+}I_+ + A_{z,-}I_-\right) \tag{5.8}$$

where $A_\parallel = A_{z,z}$, $I_\pm = (I_x \pm iI_y)$ and $A_{z,\pm} = A^\star_{z,\mp} = (A_{z,x} \mp iA_{z,y})/2$. Note that $|A_{z,\pm}| = \sqrt{A^2_{z,x} + A^2_{z,y}}/2 \equiv: A_{z,\perp}/2$.

We can now provide an estimate for the nuclear spin dephasing time T_{2n} induced by the term $A_{z,z}(t)I_z$. The phase contribution to the nuclear spin at time T is given by $\Phi_{FID} = \int_0^T A_{z,z}(t)dt$. Assuming $\gamma \gg 1/T, A_{z,z}$, the accumulated phase Φ_{FID} will follow an approximately normal distribution and we may compute the expectation value for the nuclear coherence

$$\langle e^{i\Phi_{FID}}\rangle \approx e^{-\frac{1}{2}\langle\Phi^2_{FID}\rangle} \approx e^{-T/T_{2n}}. \tag{5.9}$$

Where we may calculate $T_{2n} = \frac{8\gamma}{A^2_\parallel}$ from

$$\frac{1}{2}\langle\Phi^2_{FID}\rangle = \frac{1}{2}\int_0^T dt\int_0^T dt' A^2_\parallel\langle f(t)f(t')\rangle \approx \frac{1}{2}\int_0^T dt\int_{-\infty}^{\infty} dt' A^2_\parallel\langle f(t)f(t')\rangle = \frac{A^2_\parallel}{8\gamma}T. \tag{5.10}$$

Thus, for transition rates increasing linearly with the laser intensity, the coherence time T_{2n} also increases proportionally. Indeed, applying this approach, it was possible to increase the nuclear spin coherence time by two orders of magnitude $T^\star_{2n} = (0.53 \pm 0.14)s$ by simply applying green laser light (10mW).

Let us now consider a simple estimate for the T_{1n} or nuclear spin flipping process due to the telegraph type switching of the hyperfine interaction. First order time-dependent

perturbation theory provides an estimate for the transition rates in both directions (lowering and raising), given by

$$\Gamma_{\uparrow} = \left(\frac{A_{\perp}}{2}\right)^2 S_q(-\gamma_{^{13}C}B) \text{ and } \Gamma_{\downarrow} = \left(\frac{A_{\perp}}{2}\right)^2 S_q(\gamma_{^{13}C}B). \tag{5.11}$$

where $S_q(\omega)$ is defined as

$$S_q(\omega) = \int_{-\infty}^{\infty} d\tau e^{i\omega\tau} \langle f(\tau) f(0) \rangle \tag{5.12}$$

and according to eq. (5.7) can be calculated to be $S_q(\gamma_{^{13}C}B) = \frac{\gamma}{4\gamma^2 + (\gamma_{^{13}C}B)^2}$. This leads to the transition rates,

$$1/T_{1n,opt} = \Gamma_{\downarrow} + \Gamma_{\uparrow} = \frac{A_{\perp}^2}{8} \frac{\gamma}{\gamma^2 + (\omega_{^{13}C}B/2)^2} \tag{5.13}$$

In the dark, the nuclear spin lifetime is no longer limited by the optically induced depolarization (note that the numerator in eq. (5.13) vanishes but the denominator does not). In this context resonant dipole-dipole interactions among ^{13}C nuclear spins may provide a significant contribution. The dipole-dipole interactions take the form

$$H_{dd} = D_{dd} \left[3(\mathbf{I} \cdot \mathbf{n})(\mathbf{I}' \cdot \mathbf{n}) - \mathbf{I} \cdot \mathbf{I}'\right], \tag{5.14}$$

where $\mathbf{I}$ is the memory spin operator and $\mathbf{I}'$ is the spin operator for a neighbouring ^{13}C nuclear spin and $\mathbf{n}$ is a unit vector oriented in the direction connecting the two nuclei. At the present ^{13}C concentration, the D_{dd} can be expected to be of the order of $1Hz$. Since we do not know the precise direction of $\mathbf{n}$ with respect to the static magnetic field we shall assume an intensity of approximately D_{dd} for each of the components. This is much smaller than the Zeeman splitting of the nuclear spins due to the external magnetic field B and even smaller than the dephasing rate at experimentally addressed laser intensity. Consider a simplified model in which there is a single neighbouring ^{13}C nuclear spin. The electronic spin spends approximately 1/3 of the time in the $|m_s = 0\rangle$ state, the only state which is expected to allow resonant $I_- I'_+ + I_+ I'_-$ transitions from the dipole-dipole interaction. The permanence time of the electronic spin in the $|m_s = 0\rangle$ state is exponentially distributed with parameter $1/T_{1e}$. The flip-flop probability per visit to $|m_s = 0\rangle$ may be estimated by

$$\frac{1}{T_{1e}} \int_0^{\infty} e^{-t/T_{1e}} \sin^2(D_{dd}t) dt = \frac{D_{dd}^2}{2T_{1e}^{-2} + 2D_{dd}^2}, \tag{5.15}$$

whereas the rate of visits to the $|m_s = 0\rangle$ state is half the depolarization rate $\frac{1}{2T_{1e}}$. For $T_{1e}A_{\parallel} \gg 1$, the phase of the memory spin is lost on each $|m_s = \pm 1\rangle$ visit and thus, spin flips

accumulate incoherently with

$$T_{1n,dd} \approx 2\frac{T_{1e}^{-1} + D_{dd}^2 T_{1e}}{D_{dd}^2} \approx \frac{2}{D_{dd}^2 T_{1_e}}. \tag{5.16}$$

In practice, no significant depolarization was measured for the nuclear spin in a time scale of 200s, which is consistent with the long $T_{1n,dd}$ predicted by this last equation.

We may also analyse the dipole-dipole contribution to the memory flip rate in the motional narrowing regime of $T_{1e}A_{\parallel} \ll 1$. In this regime, we may start from a coarse grained time dynamics with respect to T_{1e} for the ^{13}C memory spin where the effect of the electronic spin are already included as a dissipative dephasing of rate T_{2n}^{-1}. This is valid since the time scale of the perturbation considered, nuclear dipole-dipole coupling, is expected to be of the order of 1 second and hence much longer than the necessary time coarse graining. We now consider the flip-flop between the memory spin and a neighbouring nuclear spin $D_{dd}(I_+I'_- + I_-I'_+)$. We may now take a time dependent perturbative expansion (now of a Liouvillian) in order to extract the effective flip-flop rates, which we identify with $T_{1n,dd}^{-1}$. We expand

$$\Gamma_{\uparrow\downarrow\to\downarrow\uparrow} t \approx \langle\downarrow\uparrow| e^{(\mathcal{L}_0+\mathcal{H}_{dd})t}(|\uparrow\downarrow\rangle\langle\uparrow\downarrow|)|\downarrow\uparrow\rangle \tag{5.17}$$

to first non vanishing (second) order in D_{dd}, where $\mathcal{L}_0$ includes the possibly different Zeeman splitting of the two nuclear spins and the dephasing of the memory spin whereas $\mathcal{H}_{dd}(\rho) = [D_{dd}(I_+I'_+I_-I'_+), \rho]$. After some relatively straightforward calculations and standard approximations we arrive at

$$T_{1n,dd}^{-1} \approx \Gamma_{\uparrow\downarrow\to\downarrow\uparrow} \approx 2\frac{D_{dd}^2 T_{2n}^{-1}}{T_{2n}^{-2} + \Delta_\omega^2} \tag{5.18}$$

where T_{2n} is the effective dephasing time of the memory spin and Δ_ω is the effective energy detuning between the two nuclear spins (i.e. the difference between individual effective Zeeman splitting possibly due to the presence of an effective field from the electronic spin or magnetic field gradient). Note that homogeneous variations in the external magnetic field do not contribute to the dephasing or energy detuning Δ_ω, since they would act equally on both nuclear spins.

This term may be ineffective on the memory spin due to a possibly large Δ_ω or effective dephasing rate T_{2n}^{-1}. However, this same analysis applies for any pair of ^{13}C spins in the neighbourhood of memory nucleus. In turn, flipping of neighbouring ^{13}C nuclear spins can

produce dephasing of the memory spin due to a change in the effective magnetic field they produce.

As evinced by the term Δ_ω^2 in the denominator of eq. (5.18), it is possible that the nuclear spin flip-flop processes to be frozen by energy detuning. However, the nuclear $I_z I'_z$ term of the nuclear dipole-dipole interactions will imprint a phase on the memory spin which is dependent on the environment state. Note that during coherence measurement experiments, the $\pi/2$ initialization RF pulse (as all RF pulses) acts globally on the ^{13}C nuclear spins and removes any hope of having a preferred basis for the states. The accumulated phase may not be reverted by applying a radio-frequency echo π pulses since these pulses flip both the memory spin and the environment leading to a continued accumulation of phase instead of a cancellation. This leads to the need of decoupling homo-nuclear dipole-dipole interactions.

5.4.2 Decoupling of homo-nuclear dipole-dipole interactions

As mentioned, the dipole-dipole interaction among ^{13}C nuclear spins starts playing a relevant role once one attempts to reach coherence times of the order of 1s. It is here that RF decoupling pulse sequences can be of use. Decoupling pulse sequences have been extensively studied in NMR where most of them have been introduced in order to study different aspect of nuclear spin dynamics [123]. The pulse sequence that was experimentally used was derived from MREV-8, which in turn is derived from a four pulse sequence named WaHuHa, after Waungh, Huber and Haberlen designed to decouple homonuclear dipole-dipole interaction[91].

One of the fruitful approaches to analyse these sequences is to use the average Hamiltonian theory. Here, the effect of the pulses are studied by moving into an interaction picture, a toggling frame with respect to the applied RF pulses. Provided that the characteristic frequencies ω of the natural Hamiltonian H satisfy $\omega t \ll 1$, where t is the time during which the Hamiltonian evolves between pulses and that the pulse time τ_p is negligible, a Magnus expansion may be performed to describe the effective Hamiltonian H_{eff}. The effective H_{eff} is defined such that the effective evolution of the system at times nt is given by $U(nt) = \exp(-intH_{eff})$ for integer values of n. The Magnus expansion gives a systematic series development of H_{eff} as

$$H_{\text{eff}} = H^{(0)} + H^{(1)} + H^{(2)} + \dots. \tag{5.19}$$

Assuming the piecewise constant interaction Hamiltonians $H_j = \prod_{l=1}^{j} U_l^{-1} H \prod_{l=j}^{1} U_l$ corre-

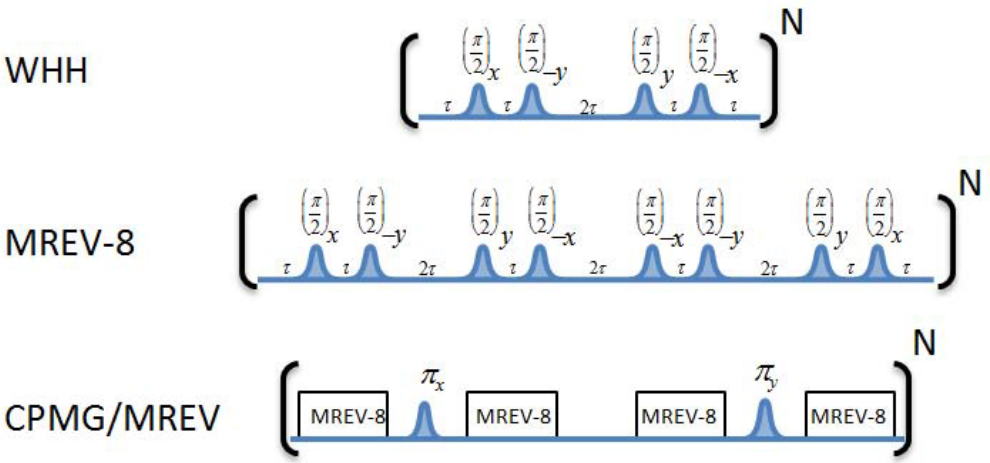

Figure 5.5: **Decoupling pulse sequences** The WHH sequence is capable of achieving dipole dipole decoupling with only 4 $\pi/2$ pulses each applied around the indicated axis. The MREV-8 has the same averaging effect as WHH for the dipole dipole coupling but shows a higher robustness to RF pulse errors. Finally, CPMG/MREV sequence includes additional π pulses to compensate external magnetic fields. Reprinted from Science **336** (2012) 1283-1286 with permission from AAAS.

sponding equal time intervals $\tau = t/M$ the the first two terms of the Magnus expansion can be reduced to

$$\begin{aligned} H^{(0)} =& \frac{1}{M}\sum_{j=1}^{M} H_j \\ H^{(1)} =& \frac{-i\tau}{2M}\sum_{j=1}^{M}\sum_{k>j}^{M}[H_k, H_j]. \end{aligned} \tag{5.20}$$

Subsequent terms sum higher order nested commutators, with n-th order commutators corresponding to $H^{(n)}$ which are expected to vanish due to a quickly decreasing prefactor.

The secular approximation for equal spin dipole-dipole interactions under an external magnetic field B in the z direction can be written as:

$$H_{dd} = \sum_{j>k} D_{jk}(3I_j^z I_k^z - \mathbf{I}_j \cdot \mathbf{I}_k) \tag{5.21}$$

where the coupling frequency is given by $D_{jk} = \hbar^2\gamma_{^{13}C}^2\mu_0/4\pi$. We find that already the WaHuHa pulse sequence cancels the effective dipolar interaction $H_{dd}^{(0)} = 0$. Moreover, due

to the symmetry of the pulse sequence, $U_{k+1} = U^{\dagger}_{M-k}$, all odd order terms of the Magnus expansion cancel $H^{(2n+1)}_{dd} = 0$. This leaves the second order term $H^{(2)}_{dd}$ as the first potentially non trivial correction. Assuming $\tau \approx 0.04$s for four repetitions of the CPMG/MREV-8 pulse sequence, in a 2s coherence measurement, and a typical dipole-dipole interaction of $D_{dd} \approx 1$Hz the prefactor for the leading correction is $(D_{dd}\tau)^2 D_{dd} \approx 10^{-3}$Hz which would not be detectable in coherence measures of a few seconds.

Combined detuning and dipolar

At high laser power, the ionization induced decoherence is suppressed by motional averaging. As discussed, the CPMG/MREV-8 RF pulse sequence can suppress the dipole-dipole interaction among nuclear spins up to second order in $D_{dd}\tau$. Furthermore, the sequence can also suppress, to all orders, the effect of finite detuning δI_z of the RF driving with respect to the actual Zeeman splitting of the nuclear spins which can be of the order of $(2\pi)10Hz$. However, the pulse sequence is not designed to suppress the combined effect of dephasing and dipolar interactions. Accordingly, the Magnus expansion can no longer be truncated to low order. In particular, terms of the form $(\delta\tau)^n D$ contribute to the expansion and the effective decoherence time is set by the value of τ for which $\delta\tau \approx 1$. This time can be estimated numerically yielding $T_2 \approx 2s$ (see figure 5.6),in good agreement with experiments. Thus, the dominant source of decoherence becomes the imperfect tuning of the RF driving used for the pulse sequence.

5.5 Conclusions and perspective

In this chapter we have presented a physical model for readout, initialization and storage of a ^{13}C spin proximal to an NV-center. The main contribution of the work comes in the form of characterization of decoherence and demonstration of decoherence avoiding mechanisms for a proximal ^{13}C nuclear spin. For (de)ionization rates γ much larger than the hyperfine interaction, the dephasing rate depends on the parallel component of the dipole field, $^1/_{T^*_{2n}} = \Gamma_{opt} + \Gamma_{dd}$, where Γ_{dd} is the spin-bath induced dephasing rate and $\Gamma_{opt} \sim \frac{A^2_{\parallel}}{\gamma}$ is the optically induced decoherence. The dashed red line in figure 5.7(b) demonstrates that this model is in good agreement with our data. Application of our decoupling sequence CPMG/MREV-8 (see

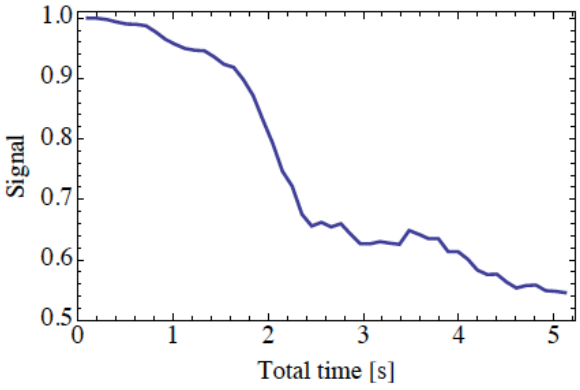

Figure 5.6: **Combined dephasing from detuning and dipole-dipole interactions** The unitary evolution of a system consisting of a memory ^{13}C nuclear spin and 5 bath spins was numerically calculated following a CPMG/MREV-8 (with $\delta = (2\pi)10$Hz driving detuning. The bath nuclear spins were randomly distributed according to a 0.01% ^{13}C concentration in the diamond lattice and averaged over 50 realizations. The average predicted coherence shows a significant decay after 2s. Reprinted from Science **336** (2012) 1283-1286 with permission from AAAS.

figure 5.7(a)) also allows us to suppress nuclear-nuclear dephasing. We find that the main imperfection in this decoupling procedure originates from a finite RF detuning. Accounting for this imperfection, we find excellent agreement with our data, as shown by the dashed blue line in figure 5.7(b). Moreover, this model indicates that the coherence time increases almost linearly as a function of applied laser intensity, suggesting a large potential for improvement.

The use of even higher laser intensities is limited by heating of the diamond sample, which causes drifts in the ESR transition [2]. However, this can be overcome via a combination of temperature control and careful transition-frequency tracking, yielding an order of magnitude improvement in the coherence time to approximately one minute. Further improvement can be achieved by decreasing the hyperfine and the dipole-dipole interaction strength through a reduction of the ^{13}C concentration, potentially resulting in hour-long storage times. Finally, it is possible to use coherent decoupling sequences and techniques based upon optimal control theory [71], which scale more favorably than our current dissipation-based method. With such techniques, we estimate that the memory lifetime can approach the timescale of phonon-induced nuclear depolarization, measured to exceed $T_{1n}^{max} \sim 36$ h [117].

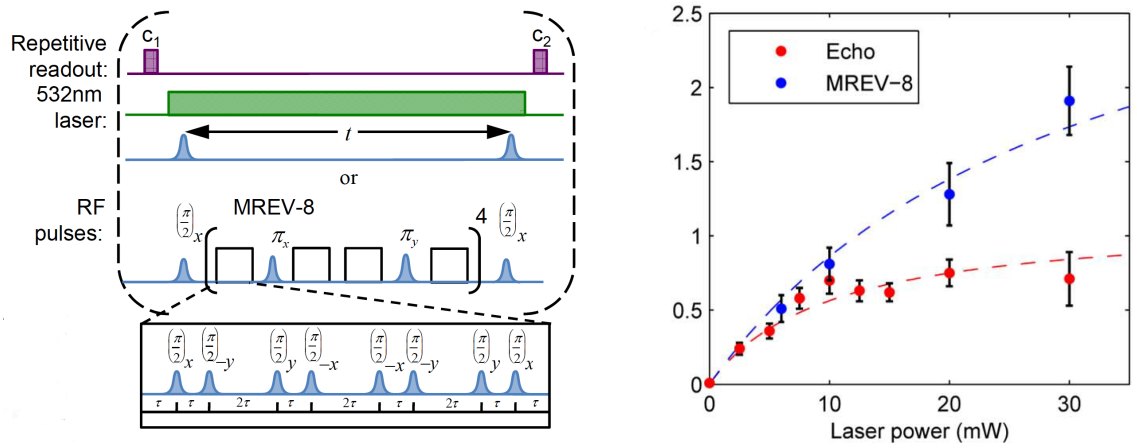

(a) Decoupling pulse sequence

(b) Intensity dependent coherence time

Figure 5.7: Experimental coherence extension a) Experimental sequence used to measure the nuclear coherence time. A modified Mansfield Rhim Elleman Vaughan (MREV) decoupling sequence [79] is utilized. It consists of 16 MREV-8 pulse trains interwoven with 8 phase-refocusing π-pulses. Each MREV-8 pulse sequence can be achieved through $\pi/2$ rotations around four different axes. b) Nuclear coherence as a function of green laser power. Red data constitute a measurement of T_{2n} using a nuclear spin echo; blue data T_{2n} contain the additional MREV sequence. The dashed fits are calculated from the spin-fluctuator model. Reprinted from Science **336** (2012) 1283-1286 with permission from AAAS.

Advanced material engineering could lead to the possibility of generating an array with a vast number of NV center, each with an associated proximal ^{13}C nuclear spin. Further progress needs to be demonstrated in order to be able to initialize and measure such an ensemble qubits independently. In the following chapter 6 we consider the potential applications of such an array for the realization of fraud resistant quantum tokens in the spirit of [129]. Furthermore, NV-based quantum registers can take advantage of the nuclear spin for storage, while utilizing the electronic spin for quantum gates and readout [36, 108]. In particular, recent progress in the deterministic creation of arrays of NV centers [120] and NV-C pairs‘[115], enables the exploration of scalable architectures [97, 131]. Finally, recent experiments have also demonstrated the entanglement of a photon with the electronic spin-state of an NV center [118]. Combining the advantages of an ultra-long nuclear quantum memory with the possibility of photonic entanglement opens up novel routes to long-distance

quantum communication and solid state quantum repeaters [35].

Chapter 6

Unforgeable noise-tolerant quantum tokens

The realization of devices which harness the laws of quantum mechanics represents an exciting challenge at the interface of modern technology and fundamental science. An exemplary paragon of the power of such quantum primitives is the concept of "quantum money" [129]. A dishonest holder of a quantum bank-note will invariably fail in any counterfeiting attempts; indeed, under assumptions of ideal measurements and decoherence-free memories such security is guaranteed by the no-cloning theorem. In any practical situation, however, noise, decoherence and operational imperfections abound. Thus, the development of secure "quantum money"-type primitives capable of tolerating realistic infidelities is of both practical and fundamental importance. Here, we propose a novel class of such protocols and demonstrate their tolerance to noise; moreover, we prove their rigorous security by determining tight fidelity thresholds. Our proposed protocols require only the ability to prepare, store and measure single qubit quantum memories, making their experimental realization accessible with current technologies.

6.1 Introduction

Recent extensions to Wiesner's original "quantum money" protocol [129] have garnered significant interest [1, 86, 94, 38, 39, 85]. One particular extension enables the authentication of quantum tokens via classical public communication with a trusted verifier [44]. However, to tolerate noise, the verification process must condone a certain finite fraction of qubit failures; naturally, such a relaxation of the verification process enhances the ability for a dishonest user to forge quantum tokens. It is exactly this interplay which we, here, seek to address, by focusing on a class of "quantum token"-protocols which involve either direct physical or classical communication verification of qubit memories.

6.2 Qticket

Our approach to quantum tokens extends the original quantum money primitive[129] by ensuring tolerance to finite errors associated with encoding, storage and decoding of individual qubits. We denote the tokens within our first primitive as quantum tickets (qtickets); each qticket is issued by the mint and consists of a unique serial number and N component quantum states, $\rho = \bigotimes_i \rho_i$, where each ρ_i is drawn uniformly at random from the set, $\tilde{Q} = \{|+\rangle, |-\rangle, |+i\rangle, |-i\rangle, |0\rangle, |1\rangle\}$, of polarization eigenstates of the Pauli spin operators. The mint secretly stores a classical description of ρ, distributed only among trusted verifiers. In order to redeem a qticket, the holder physically deposits it with a trusted verifier, who measures the qubits in the relevant basis. This verifier then requires a minimum fraction, F_{tol}, of correct outcomes in order to authenticate the qticket; following validation, the only information returned by the verifier is whether the qticket has been accepted or rejected.

The soundness of a qticket, e.g. the probability that an honest user is successfully verified, depends crucially on the experimental fidelities associated with single qubit encoding, storage and decoding. Thus, for a given qubit ρ_i, we define the map, M_i, which characterizes the overall fidelity, beginning with the mint's encoding and ending with the verifier's validation; the average channel fidelity[98] is then given by, $F_i = 1/|\tilde{Q}| \sum_{\rho_i} \mathsf{tr}[\rho_i M_i(\rho_i)]$. With this definition, the verification probability of an honest user is,

$$p_{\text{h}} = \frac{1}{|Q|} \sum_{\rho \in Q} \mathsf{tr}[P_{\text{acc}} M(\rho)] \geq 1 - e^{-ND(F_{\text{exp}} \| F_{\text{tol}})}, \tag{6.1}$$

where $Q = \tilde{Q}^{\otimes N}$, P_{acc} represents the projector onto the subspace of valid qtickets, $M = \bigotimes_i M_i$, $F_{\text{exp}} = 1/N \sum_i F_i$ is the per qubit average experimental fidelity, and the relative entropy D is a measure of distinguishability between two binary probability distributions. Crucially, so long as the average experimental fidelity associated with single qubit processes is greater than the tolerance fidelity, an honest user is exponentially likely to be verified.

To determine a tight security threshold, we consider the counterfeiting of a single qticket. For a given tolerance fidelity (F_{tol}) set by the verifiers, a qticket is only accepted if at least $F_{\text{tol}}N$ qubits are validated. In the event that a dishonest user attempts to generate two qtickets from a single valid original, *each* must contain a minimum of $F_{\text{tol}}N$ valid qubits to be authenticated. As depicted in Fig. 1a., in order for each counterfeit qticket to contain $F_{\text{tol}}N$ valid qubits, a *minimum* of $(2F_{\text{tol}}-1)N$ qubits must have been perfectly cloned. Thus, for a set tolerance fidelity, in order for a dishonest user to succeed, he or she must be able to emulate a qubit cloning fidelity of at least $2F_{\text{tol}} - 1$. Crucially, so long as this fidelity is above that achievable for optimal qubit cloning (2/3) [128], a dishonest user is exponentially unlikely to succeed,

$$p_{\text{d}} = \frac{1}{|Q|} \sum_{\rho \in Q} \mathsf{tr}\left[P_{\text{acc}}^{\otimes 2} T(\rho)\right] \leq e^{-ND(2F_{\text{tol}}-1\|2/3)}, \tag{6.2}$$

where T represents any completely positive trace preserving (CPTP) qticket counterfeiting map. To ensure $2F_{\text{tol}} - 1 > 2/3$, the tolerance fidelity must be greater than 5/6, which is precisely the average fidelity of copies produced by an optimal qubit cloning map [128]. In certain cases, an adversary may be able to sequentially engage in multiple verification rounds; however, the probability of successfully validating counterfeited qtickets grows at most quadratically in the number of such rounds, and hence, the likelihood of successful counterfeiting can remain exponentially small even for polynomially large numbers of verifications. Rigorous statement and proofs of these claims are published as supporting information available online.

6.3 Cv-qticket

Our previous discussion of qtickets assumed that such tokens are physically transferable to trusted verifiers (e.g. concert tickets); however, in many situations, this assumption of physical deposition, may either be impossible or undesirable. Recently, it has been shown [44] that it

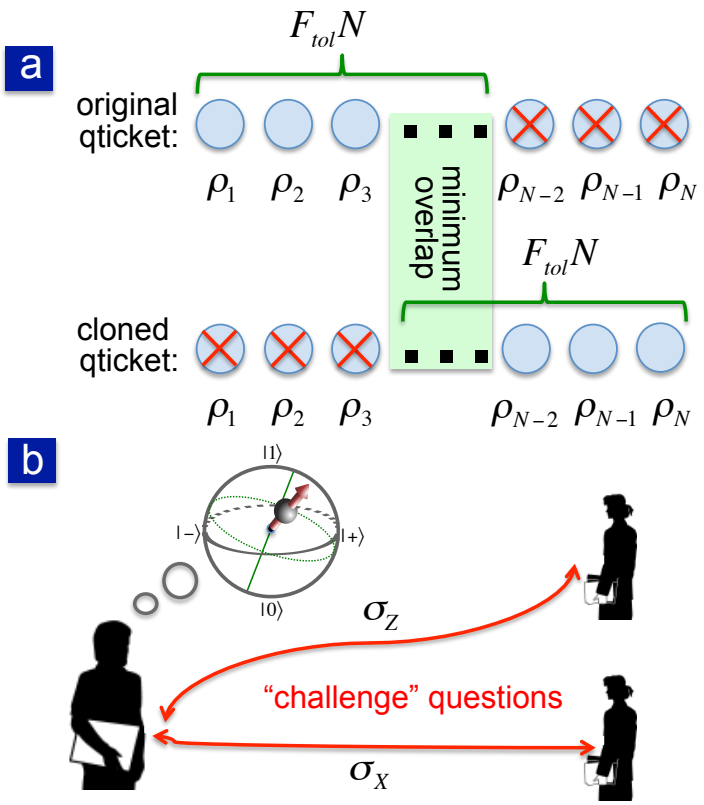

Figure 6.1: a) Depicts the pigeonhole type argument which is utilized in the proof of qticket soundness. For a tolerance fidelity F_{tol}, a qticket is only successfully authenticated if it contains at least $F_{\text{tol}}N$ valid qubits. However, for two counterfeit qtickets, not all valid qubits must coincide. The minimum number of perfectly cloned qubits enabling both qtickets to be accepted is, $(2F_{\text{tol}} - 1)N$. b) Depicts the quantum retrieval type situation envisioned for cv-qtickets. For two verifiers asking complementary "challenge" questions, the optimal strategy is for the user to measure in an intermediate basis. Such a strategy saturates the tolerance threshold, $F_{\text{tol}}^{\text{cv}} = \frac{1+1/\sqrt{2}}{2}$.

remains possible, even remotely, for a holder to prove the validity of a token by responding to a set of "challenge" questions; these questions can only be successfully answered by measuring an authentic token. The core behind this approach is to ensure that the "challenge" questions reveal no additional information about the quantum state of the token.

We now discuss a specific realization of such an approach, the classical verification quantum ticket (cv-qticket), and demonstrate its robustness against noise and operational imperfections. In contrast to the case of bare qtickets, a cv-qticket holder will be expected to answer "challenge" questions and hence to measure qubits himself. Our treatment will contemplate the possibility of a dishonest holder participating simultaneously in multiple remote verifications, which could in principle offer the counterfeiter an additional advantage with respect to the qticket scenario; in particular, certain measurement strategies may yield an increased likelihood for multiple successful authentications.

One example of a cv-qticket framework, is to utilize a set of eight possible two-qubit product states with each qubit being prepared as a polarization eigenstate along either X or Z directions (note that a single qubit framework is also possible):

$$\{|0,+\rangle, |0,-\rangle, |1,+\rangle, |1,-\rangle, |+,0\rangle, |-,0\rangle, |+,1\rangle, |-,1\rangle\}.$$

We then envision each cv-qticket to consist of n blocks, each containing r qubit pairs, and thus, a total of $n \times r \times 2$ qubits; as before, each of the qubit pairs is chosen uniformly at random from the allowed set above. A "challenge" question consists of requesting the holder to measure each block (of qubits) along a basis chosen randomly among either X or Z; naturally, as depicted in Table 1, a valid qubit pair (within a block) is one in which the holder correctly answers the state for the particular qubit (within the pair) which was prepared along the questioned basis. For a given tolerance threshold, an overall answer will only be deemed correct if at least $F_{\text{tol}}^{\text{cv}} r$ qubits within each of the n blocks are found valid. By analogy to the qticket case, honest users are exponentially likely to be verified so long as $F_{\text{exp}} > F_{\text{tol}}^{\text{cv}}$; in particular, since there now exist n blocks of qubits, each of which can be thought of as an individual qticket (with r qubits),

$$p_{\text{h}}^{\text{cv}} \geq \left(1 - e^{-rD(F_{\text{exp}} \| F_{\text{tol}}^{\text{cv}})}\right)^n. \tag{6.3}$$

The proof of cv-qticket security is based upon a generalized formalism of quantum retrieval games [44, 52], in combination with a generalized Chernoff-Hoeffding bound [61] (details

Table 6.1: Verification of a single cv-qticket. Here, we consider a cv-qticket with $n = 4$ and $r = 2$, totaling 8 qubit pairs and $F_{\text{tol}} = 3/4$ (for illustrative purposes only). The prepared qubit-pairs are chosen at random, as are the bank's requested measurement bases (for each block). The holder's answer has at most, a single error per block, which according to, $F_{\text{tol}} = 3/4$, is allowed. Secure cv-qtickets require $F_{\text{tol}} > 1/2 + 1/\sqrt{8}$ and a larger number of constituent qubits.

Prepare	$\|-,0\rangle$	$\|0,+\rangle$	$\|1,+\rangle$	$\|0,+\rangle$	$\|0,+\rangle$	$\|+,1\rangle$	$\|-,0\rangle$	$\|1,+\rangle$
B:Ask	Z				X			
H:Ans.	$0,0$	$0,1$	$1,1$	$0,1$	$-,+$	$+,-$	$-,+$	$+,-$
Correct	✓	✓	✓	✓	✓	✓	✓	×
Block	✓				✓			
B:Res.	Verified							

in supporting information). So long as $F_{\text{tol}}^{\text{cv}} > \frac{1+1/\sqrt{2}}{2}$, a dishonest user is exponentially unlikely to be authenticated by two independent verifiers. For two complementary "challenge" questions, one finds that on average, no more than $1+1/\sqrt{2} \approx 1.707$ can be answered correctly. Interestingly, the threshold $F_{\text{tol}}^{\text{cv}}$ corresponds exactly to that achievable by either covariant qubit cloning[24] or by measurement in an intermediate basis (Fig. 1b.), suggesting that both such strategies may be optimal [45]. Similar to the qticket case, one finds that a dishonest user is exponentially likely to fail,

$$p_{\text{d}}^{\text{cv}} \leq \binom{v}{2}^2 \left(1/2 + e^{-rD(F_{\text{tol}} \| \frac{1+1/\sqrt{2}}{2})}\right)^n, \tag{6.4}$$

where v represents the number of repeated verification attempts . Thus, so long as the hierarchy of fidelities is such that: $\frac{1+1/\sqrt{2}}{2} < F_{\text{tol}} < F_{\text{exp}}$, it is possible to prove both soundness and security of the cv-qtickets protocol (see supporting information for rigorous statement and proofs).

6.4 Applications

Next, we consider applications of the above primitives to practically relevant protocols. For instance, one might imagine a composite cv-qticket which allows for multiple verification

rounds while also ensuring that the token cannot be split into two independently valid subparts [44]. Such a construction may be used to create a quantum-protected credit card. Indeed, the classical communication which takes place with the issuer (bank) to verify the cv-qticket (via "challenge" questions) may be intentionally publicized to a merchant who needs to be convinced of the card's validity. By contrast to modern credit card implementations, such a quantum credit card would be unforgeable and hence immune to fraudulent charges (Fig. 2a).

An alternate advantage offered by the qticket framework is evinced in the case where verifiers may not possess a secure communication channel with each other. Consider for example, a dishonest user who seeks to copy multiple concert tickets, enabling his henchmen to enter at different checkpoint gates. A classical solution would involve gate verifiers communicating amongst one another to ensure that each ticket serial number is only allowed entry a single time; however, as shown in Fig. 2b., such a safeguard can be overcome in the event that communication has been severed. By contrast, a concert ticket based upon the proposed qticket primitive would be automatically secure against such a scenario; indeed, the security of qtickets is guaranteed even when verifiers are assumed to be isolated. Such isolation may be especially useful for applications involving quantum identification tokens, where multiple verifiers may exist who are either unable or unwilling to communicate with one another.

6.5 Discussion

While quantum primitives have been the subject of tremendous theoretical interest, their practical realization demands robustness in the face of realistic imperfections. Our above analysis demonstrates that such noise tolerance can be achieved for certain classes of unforgeable quantum tokens. Moreover, the derived tolerance thresholds are remarkably mild and suggest that proof of principle experiments are currently accessible in systems ranging from trapped ions [60, 81] and superconducting devices [127, 46] to solid-state spins [36, 93, 14, 90]. In particular, recent advances on single nuclear spins situated in a compact room-temperature solid, have demonstrated that ultra-long storage times can be attained in combination with high fidelity initialization and readout [90]; such advances suggest that quantum devices based upon single qubit quantum memories may be both practical and realistically feasible.

While our analysis has focused on describing a primitive based upon single tokens, natural

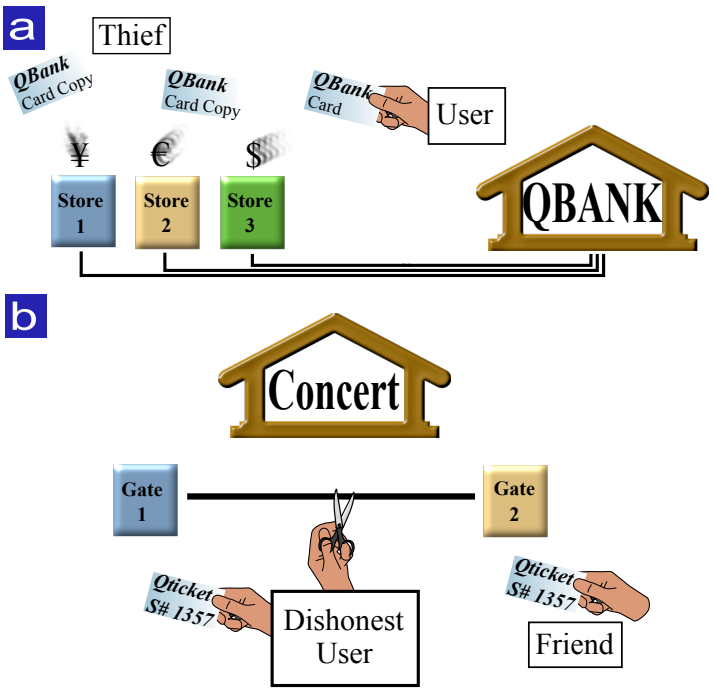

Figure 6.2: a) Depicts the possibility of using the cv-qticket framework to implement a quantum-protected credit card. Unlike its classical counterpart, the quantum credit card would naturally be unforgeable; this prevents thieves from being able to simply copy credit card information and perform remote purchases. b) Depicts a dishonest user who attempts to copy a concert qticket (e.g. same serial number), enabling his friend to enter at an alternate checkpoint gate. Naively, each verifier can communicate with one another to prevent such abusive ticket cloning. However, such a safeguard can be overcome in the event that the communication among verifiers is either unsecured, unavailable or severed (possibly by the dishonest user himself). The qticket is exempt from this type of attack since security is guaranteed even in the case of isolated verifiers.

extensions to the case of multiple identical quantum tokens open up the possibility of even more novel applications. In particular, as detailed in the supplementary information, it is possible to extend our threshold results to the case where c identical copies of the quantum token are issued. In this case, to ensure that the production of $c+1$ valid tokens is exponentially improbable, the required threshold fidelity must be greater than $1-\frac{1}{(c+1)(c+2)}$. The existence of such multiple identical tokens can provide a certain degree of anonymity for users and could be employed in primitives such as quantum voting. A crucial question that remains is whether a rigorous proof of anonymity can be obtained in a noisy environment. Furthermore, our proposed quantum tokens can also be seen as a basic noise tolerant building block for implementing more advanced application schemes; such schemes can range from novel implementations of quantum key distribution [16, 45, 49, 110] based upon physical qubit transport to complex one-time-entry identification cards. Beyond these specific applications, a number of scientific avenues can be explored, including for example, understanding whether an interplay between computational assumptions and quantum memories can yield fundamentally new approaches to encryption.

6.A Notation and external results

The following definitions and external results will be used extensively throughout the proofs and are included here to provide a self-contained presentation.

Definition A quantum state t-design is a probability distribution over pure quantum states $(p_i, |\,\psi_i\rangle)$ such that

$$\sum_i p_i \left(|\,\psi_i\rangle\langle\psi_i\,|\right)^{\otimes t} = \int_{\text{Haar}} \left(|\,\psi\rangle\langle\psi\,|\right)^{\otimes t} d\psi.$$

In other words, a quantum state t-design duplicates the properties of the unique unitarily invariant Haar measure over quantum states for all polynomials up to degree t. We will use the set of states

$$\tilde{Q} = \{|\,0\rangle, |\,1\rangle, |\,+\rangle, |\,-\rangle, |\,+i\rangle, |\,-i\rangle\} \tag{6.5}$$

with equal weights $p_i = 1/6$; this constitutes a quantum state 3-design over $\mathcal{H}_2$ [132].

The average fidelity for a channel quantifies how well the channel preserves quantum states.

Definition The Average fidelity of a map M is defined as

$$F(M) = \int_{\text{Haar}} \langle\psi \mid M\left(\mid \psi\rangle\langle\psi \mid\right) \mid \psi\rangle d\psi.$$

Note for example that the average fidelity of a map M is expressed as a Haar integral of a degree 2 polynomial expression in bras and kets and can thus be equated to a weighted average over a quantum state 2-design.

Throughout the text, boolean values $\mathcal{B} = \{True, False\}$ will be represented as $True := 1$, $False := 0$ and the negation $\bar{b} := 1 - b$. We will also use the variable $\vec{b}$ to denote boolean strings (i.e. ordered sequences of values in $\{0,1\}$) with $\text{len}(\vec{b})$ denoting the length or number of components of a sequence and $\text{tl}(\vec{b})$ denoting the string obtained from removing the last element from $\vec{b}$. We will denote by $\mathbf{Pr}[e]$ the probaility of an event e and $\mathbf{Exp}[v]$ the expectation value of an expression v. Note that according to our convention, if the expression is a boolean formula they may be used interchangeably.

The relative entropy is a distinguishability measure between two probability distributions. It will be used extensively (particularly among binary or Bernoulli distributions) and appears in the definition of auxiliary results. Let $0 \leq p, q \leq 1$, by abuse of notation, we take $D(p\|q) = p \ln \frac{p}{q} + (1-p) \ln \frac{1-p}{1-q}$, the relative entropy between two Bernoulli probability distributions with respective parameters p and q. Note that this definition satisfies $D(p\|q) \geq 2(p-q)^2$.

The following generalization of the Chernoff-Hoeffding bound derived by Panconesi and Srinivasan [102] provides the same thesis as a standard Chernoff bound while relaxing the hypothesis to allow dependent random variables.

Theorem 6.A.1 *(Generalized Chernoff-Hoeffding bound) Let $X_1, \ldots, X_n$ be Boolean $\{0,1\}$ random variables, such that for some δ_i and every $S \subseteq \{1, \ldots, n\}$, it holds that $\mathbf{Pr}\left[\bigwedge_{i \in S} X_i\right] \leq \prod_{i \in S} \delta_i$. Then for any $\gamma \in [\delta, 1]$ we have that $\mathbf{Pr}\left[\sum_{i=1}^n X_i \geq \gamma n\right] \leq e^{-nD(\gamma\|\delta)}$, with $\delta := n^{-1} \sum_{i=1}^n \delta_i$.*

A further generalization to real valued random variables will also be required. This is adapted to our purpose from theorem 3.3 of Impagliazzo and Kabanets [61].

Theorem 6.A.2 *Let $X_1, \ldots, X_n$ be real valued random variables, with each $X_i \in [0,1]$. Suppose that there is a $0 \leq \delta \leq 1$ s.t., for every set $S \subseteq \{1, \ldots, n\}$, $\mathbf{Exp}\left[\prod_{i \in S} X_i\right] \leq \delta^{|S|}$ and γ s.t. $\delta \leq \gamma \leq 1$ and $\gamma n \in \mathbb{N}$. Then we have that $\mathbf{Pr}\left[\sum_{i=1}^n X_i \geq \gamma n\right] \leq 2e^{-nD(\gamma\|\delta)}$.*

6.B Qtickets

We first provide a rigorous definition of qtickets and how they are verified. We then proceed to our claims, and the soundness, security and tightness of our security bound (accompanied with respective proofs). Namely, we show that qtickets may be successfully redeemed by an honest holder achieving a sufficiently good storage fidelity. We then show that a dishonest holder will have a negligible chance of producing two qtickets which are accepted by verifiers from a single valid qticket, even after repeated verification attempts. Finally we show how a simple counterfeiting strategy has a high probability of producing two such qtickets if the verification tolerance is set below the threshold value. As an extension, we consider how our results generalize to producing multiple identical qtickets.

6.B.1 Definition of qtickets

Each qticket consists of a serial number s and an N component pure product state $\rho^{(s)} = \bigotimes_{i=1}^{N} \rho_i^{(s)}$. For each serial number s, qticket components $\rho_i^{(s)}$ are chosen uniformly at random from $\tilde{Q}$. This means qtickets $\rho^{(s)}$ are taken uniformly at random from the set $Q = \tilde{Q}^{\otimes N}$ (where by abuse of notation, the elements of Q are N component pure product states in $\mathcal{H}_Q = \mathcal{H}_2^{\otimes N}$, with components taken from $\tilde{Q}$). The verifiers store a database containing, for each s, a classical description of $\rho^{(s)}$ kept secret from ticket holders and the general public. In order to simplify notation, the serial number s associated to individual qtickets will be omitted from now on.

In order to use qtickets, they are transferred to a verification authority who can either accept or reject them. In both cases however, the qticket is not returned, only the binary outcome of verification. The qticket protocol is additionally parametrized by the fraction F_{tol} of qubits that a verification authority requires to be correct in order for verification to succeed. In order to verify a submitted qticket $\tilde{\rho}$, a full measurement will be performed in the product basis associated to the original qticket ρ and the number of correct outcomes is then counted. If more than at least $F_{\text{tol}}N$ are correct, the (possibly noisy) submitted qticket $\tilde{\rho}$ is accepted, otherwise, it is rejected.

For any pure product state $\rho = \bigotimes_{i=1}^{N} \rho_i$ we define a projector $P_{\text{acc}}^{\rho} \in \mathcal{L}(\mathcal{H}_Q)$ associated to the subspace of states that would be accepted if ρ were a qticket (i.e. states coinciding with ρ in at least a fraction F_{tol} of the qubits). The projector P_{acc}^{ρ} offers a more abstract

interpretation and may be rigorously defined as

Acceptance projector Given a pure N qubit product state $\rho = \bigotimes_{i=1}^{N} \rho_i$ and a security parameter $0 \leq F_{tol} \leq 1$, we define the acceptance projector

$$P_{\text{acc}}^{\rho} = \sum_{\vec{b}:\sum b_i \geq F_{tol} N} \bigotimes_{i=1}^{N} \left(b_i \rho_i + \bar{b_i} \rho_i^{\perp} \right),$$

where $\vec{b} \in \{0,1\}^N$ is a boolean string.

By abused of notation, ρ_i and its orthogonal complement $\rho_i^{\perp} := \mathbb{1}_2 - \rho_i$ are used as rank 1 projectors in $\mathcal{L}(\mathcal{H}_2)$.

6.B.2 Soundness

The soundness result states that even under imperfect storage and readout fidelity, legitimate qtickets work well as long as the fidelity loss is not too severe. The completely positive trace preserving (CPTP) maps M_i will be assumed to represent the encoding, storage and readout of the i-th qubit component of the qticket. In this sense, the soundness statement takes place at the level of single qubits. This is necessarily the case, since legitimate qtickets are ruined if a significant fraction of the qubits fail in a correlated way. Given $F_i = F(M_i)$, the average fidelity of the qubit map M_i, we define $F_{\text{exp}} := N^{-1} \sum F_i$ to be the average qubit fidelity of the full map $M = \bigotimes_i M_i$ over all components. The probability that the "noisy" qticket resulting from this map is accepted as valid is given by $p_{\text{h}}(M) = \frac{1}{|Q|} \sum_{\rho \in Q} \mathsf{tr} \left[P_{\text{acc}}^{\rho} M(\rho) \right]$.

Theorem 6.B.1 *(Soundness of qtickets) As long as $F_{\text{exp}} > F_{\text{tol}}$, an honest holder can successfully redeem qtickets with a probability*

$$p_{\text{h}}(M) \geq 1 - e^{-N D(F_{\text{tol}} \| F_{\text{exp}})}.$$

Proof. Consider the boolean random variables $\vec{X} = (X_1, \ldots, X_N)$ with joint distribution given by

$$\mathbf{Pr}[\vec{X} = \vec{b}] = \frac{1}{|Q|} \sum_{\rho \in Q} \mathsf{tr} \left[M(\rho) \bigotimes_{i=1}^{N} \left(b_i \rho_i + \bar{b}_i \rho_i^{\perp} \right) \right]. \tag{6.6}$$

Since $M = \bigotimes_i M_i$, we may recast equation 2 as

$$\mathbf{Pr}[\vec{X} = \vec{b}] = \prod_{i=1}^{N} \frac{1}{6} \sum_{\rho_i \in \tilde{Q}} \mathsf{tr} \left[M_i(\rho_i)(b_i \rho_i + \bar{b}_i \rho_i^{\perp}) \right] \tag{6.7}$$

Since $\tilde{Q}$ is a quantum state 2-design over qubit space, each factor coincides with the definition of the average fidelity F_i of M_i if $b_i = 1$ and with $1-F_i$ if $b_i = 0$. Hence the X_i are independent boolean random variables with probability $\mathbf{Pr}[X_i] = F_i$. Moreover, according to definition 6.B.1, we have $\frac{1}{|Q|}\sum_{\rho\in Q} \mathsf{tr}[P^{\rho}_{acc} M(\rho)] = \mathbf{Pr}[\sum_{i=1}^{N} X_i \geq F_{\mathrm{tol}} N]$. Since the X_i are independent, a standard Chernoff-Hoeffding bound allows us to conclude. ■

6.B.3 Security

Consider the probability of producing two tokens, both passing verification by means of the most general possible transformation, a CPTP map T, applied on a single genuine qticket.

Definition (Counterfeiting fidelity) We define the average counterfeiting fidelity of a map $T \in \mathcal{H}_Q \to \mathcal{H}_Q^{\otimes 2}$ as

$$p_{\mathrm{d}}(T) = \frac{1}{|Q|}\sum_{\rho\in Q} \mathsf{tr}\left[(P^{\rho}_{\mathrm{acc}})^{\otimes 2}\, T\left(\rho\right)\right] \tag{6.8}$$

One of our main results states that as long as the verification threshold F_{tol} is set sufficiently high ($> 5/6$), a counterfeiter will have negligible (exponentially small in N) chances of producing two verified tokens from a single genuine original.

Theorem 6.B.2 *(Security of qtickets) For $F_{\mathrm{tol}} > 5/6$ and for any CPTP map $T \in \mathcal{H}_Q \to \mathcal{H}_Q^{\otimes 2}$ we have that*

$$p_{\mathrm{d}}(T) \leq e^{-ND(2F_{\mathrm{tol}}-1\|2/3)}. \tag{6.9}$$

Most of the work for proving this goes into excluding the possibility that a non-product counterfeiting strategy could perform significantly better than any product strategy such as performing optimal cloning on each individual qubit. That is, we take into account the fact that the map T need not factorize with respect to the different components of the qticket. Note also that $D(2F_{\mathrm{tol}} - 1\|2/3) = 0$ precisely for $F_{\mathrm{tol}} = 5/6$ and is positive otherwise. Finally, we prove that even if the holder of a qticket attempts to perform v succesive verification attempts (each time possibly using information learned from the acceptance/rejection of previous attempts) the chances of having two or more submitted qtickets accepted grows by no more than a factor of $\binom{v}{2}$.

Theorem 6.B.3 *(Security of qtickets with learning) If the holder of a valid qticket submits v tokens for verification, the probability of having two or more accepted is upper bounded by*

$$p_{\mathrm{d},v} = \binom{v}{2} e^{-ND(2F_{\mathrm{tol}}-1\|2/3)}.$$

Note that since $\binom{v}{2}$ is a polynomial of degree 2 in v, this bound still allows for an exponentially large number (in N) of qticket submissions v, while preserving exponentially good security.

Proof outline

We now outline the proof for theorems 6.B.2 and 6.B.3. First, the claim in theorem 6.B.2 is equated to an equivalent one, which averages over the set of all pure product states instead of Q. We then bound the average cloning probability by $(2/3)^N$ for the set of pure product states following the lines of R. F. Werner [128] for the optimal cloning of pure states. From there, the generalized Chernoff bound from theorem 6.A.1 for dependent random variables allows us to derive the desired result. The result of theorem 6.B.3 is obtained from a counting argument relating the security of multiple verification attempts with the static counterfeiting fidelity bound of theorem 6.B.2.

Equivalence with continuous statement

For the qticket protocol, drawing each component from a discrete set of states is required in order to provide an efficient classical description. However, certain statements are simpler to analyze over the full set of pure product states. This is the case for the counterfeiting fidelity, which can also be expressed as a uniform average over all pure product states.

Lemma 6.B.4 *(Counterfeiting fidelity) The average counterfeiting fidelity of a map T can be expressed as*

$$p_{\mathrm{d}}(T) = \int d\vec{\rho} \quad \mathsf{tr}\left[\left(P_{\mathrm{acc}}^{\vec{\rho}}\right)^{\otimes 2} T\left(\vec{\rho}\right)\right] \tag{6.10}$$

where $\int d\vec{\rho}$ represents N nested integrations on the Haar measure of qubit components and $\vec{\rho}$ the resulting product state.

Proof. Definition 6.B.1 may seem unnecessarily cumbersome, yet it serves to make explicit that the projector P_{acc}^{ρ} is a polynomial of degree 1 in each of the components ρ_i of the qticket ρ. Furthermore, note that regardless of what the multi-qubit map T is, its application $T(\rho)$

has degree 1 in each of the components ρ_i of ρ. Together this implies that the integrand of lemma 6.B.4 is a polynomial of degree at most 3 in each of the qubit components ρ_i of $\vec{\rho}$. We may conclude by observing that the average taken in definition 6.B.3 is equivalent to uniformly taking each component ρ_i from a qubit state 3-design. ■

Optimal cloning for pure product states

R. F. Werner [128] obtained a tight upper bound for the average probability of a CPTP map T producing m clones from n copies of an unknown pure quantum state $|\,\psi\rangle$. Our statement is that if one attempts to clone an N component pure product state, the optimal cloning probability is achieved by independently cloning each of the components; neither generating entanglement nor correlations may help with the cloning. We present this statement for the case of cloning two copies from a qubit product state, but the derivation is fully generalizable.

Lemma 6.B.5 *(Optimal cloning of pure product states) The average cloning fidelity over N qubit component pure product states of a CPTP map T is bounded by*

$$\int d\vec{\rho}\,\mathsf{tr}[\vec{\rho}^{\otimes 2}T(\vec{\rho})] \leq (2/3)^N\,.$$

Proof. One possible derivation of this lemma is by following the lines of the original proof for optimal cloning of pure states [128]. First one shows that if there is a CPTP map T achieving average cloning fidelity $F^\star$ then there is a covariant CPTP map $T^\star$ achieving the same average cloning fidelity. This map can be explicitly constructed as

$$T^\star(\vec{\rho}) = \int d\vec{g} \quad \vec{g}^{\dagger\otimes 2}T(\vec{g}\vec{\rho}\vec{g}^\dagger)\vec{g}^{\otimes 2}, \tag{6.11}$$

where the integral $\int d\vec{g}$ averages over all possible local rotations $\vec{g}$ on N subsystems. This covariant map achieves exactly the same cloning fidelity for any initial pure product state since all pure product states are equivalent up to local unitaries. Finally, we observe

$$0 \leq \mathsf{tr}[\vec{\rho}^{\otimes 2}T^\star(\mathbb{1}_{2^N} - \vec{\rho})] \tag{6.12}$$

since $\mathbb{1}_{2^N} - \vec{\rho}$ is positive and $T^\star$ positivity preserving. We then obtain

$$F^\star \leq \mathsf{tr}[\vec{\rho}^{\otimes 2}T^\star(\mathbb{1}_{2^N})] \tag{6.13}$$

and may now average this inequality over $\vec{\rho}$ and use

$$\int d\vec{\rho} \quad \vec{\rho}^{\otimes 2} = \frac{(S_2)^{\otimes N}}{3^N}, \tag{6.14}$$

where S_2 is the rank 3 projector onto the symmetric space of two qubits. The operator norm of this expression is $1/3^N$ whereas $\mathsf{tr}[T^\star(\mathbb{1}_{2^N})] \leq 2^N$ leading to $F^\star \leq (\frac{2}{3})^N$, as desired. ■

Pigeonhole argument and Chernoff bound

We are now ready to prove the first no-counterfeiting result for qtickets.

Proof of theorem 6.B.2. Consider the boolean random variables $\vec{E} = (E_1, \ldots, E_N)$ with joint distribution given by

$$\mathbf{Pr}[\vec{E} = \vec{b}] = \int d\vec{\rho} \mathsf{tr}\left[T(\vec{\rho}) \bigotimes_{i=1}^{N} \left(b_i \rho_i^{\otimes 2} + \bar{b}_i(\mathbb{1}_4 - \rho_i^{\otimes 2})\right)\right]. \tag{6.15}$$

Intuitively, the variable E_i represents the event of measuring the i-th component to be correctly cloned.

In order for the two qtickets to be accepted, there must be a total of at least $F_{\text{tol}}N$ components yielding the correct measured outcome in each qticket. By the pigeonhole principle, this means that there are at least $2F_{\text{tol}}N - N$ components which were measured correctly on both submitted qtickets,

$$p_{\text{d}}(T) \leq \mathbf{Pr}\left[\sum_{i=1}^{N} E_i \geq (2F_{\text{tol}} - 1)N\right]. \tag{6.16}$$

For arbitrarily chosen T, the E_i may be dependent variables. However, according to lemma 6.B.5, for any subset S of qubit components, we may bound

$$\mathbf{Pr}[\forall_{i \in S} E_i] \leq \left(\frac{2}{3}\right)^{|S|}. \tag{6.17}$$

Theorem 6.A.1, is now invoked to provide an upper bound on the RHS of eq. 6.16, yielding the thesis of theorem 6.B.2. ■

Combinatorial bound on learning

The bound on counterfeiting that we have provided assumes that two (possibly entangled) counterfeits are produced by applying a CPTP map on a single original copy. In contrast, a sequential strategy temporally orders the submitted qtickets where the production strategy

(CPTP map) for the later submissions can depend on whether previous submissions where accepted or not. The counterfeiter may learn valuable information about how to construct valid qtickets from the feedback provided by the verifiers. The content of theorem 6.B.3 is that even with a valid qticket and the information learned from v repeated submissions it is very unlikely for a counterfeiter to produce more than one accepted qticket.

Proof of theorem 6.B.3. According to theorem 6.B.2, the probability $p_{\mathrm{d}}(T)$ for any CP map T to produce two valid counterfeit copies from a single one, is upper bounded by $B = e^{-ND(2F_{\mathrm{tol}}-1\|2/3)}$. We bound the counterfeiting probability of an interactive strategy S submitting v tokens for verification by the sum of the counterfeiting fidelity of $\binom{v}{2}$ CP maps $T_{k,l}$. Each of these maps corresponds to the case in which a specific pair $\{k,l\}$ of the v submitted tokens are the first to be accepted by the verifiers.

Without loss of generality, we assume that in an interactive strategy the holder waits for the outcome of the j-th verification in order to decide how to continue and produce the $j+1$-th submission. We model a v step interactive strategy S as a collection of CPTP maps $\{S_{\vec{b}}\}$ with $\vec{b}$ a boolean string of length between 0 and $v-1$ representing what the counterfeiter does after receiving the first $\mathrm{len}(\vec{b})$ verification outcomes.

Each $S_{\vec{b}}$ is a CPTP map from $\mathcal{H}_H$ to $\mathcal{H}_Q \otimes \mathcal{H}_H$, where $\mathcal{H}_Q$ is a Hilbert space accommodating qtickets and $\mathcal{H}_H$ is a larger space representing the memory of the holder.

For any partial verification result $\vec{b}$ we may write the CPTP map which produces the $\mathrm{len}(\vec{b})$ submissions as $\tilde{S}_{\mathrm{tl}(\vec{b})}$, which is composed of successively applying $S_{\vec{b'}}$ for all initial substrings $\vec{b'}$ of $\vec{b}$. That is

$$\begin{aligned} \tilde{S}_{\emptyset} :=& S_{\emptyset} \\ \tilde{S}_{\vec{b}} :=& \left(\mathrm{id}_Q^{\otimes \mathrm{len}(\vec{b})} \otimes S_{\vec{b}}\right) \circ \tilde{S}_{\mathrm{tl}(\vec{b})}. \end{aligned} \tag{6.18}$$

For an interactive strategy S the probability that the first $\mathrm{len}(\vec{b})$ verification outcomes are given by $\vec{b}$ is expressed as

$$p_{\vec{b}}(S) = \frac{1}{|Q|} \sum_{\rho \in Q} \mathsf{tr}[\tilde{S}_{\mathrm{tl}(\vec{b})}(\rho) \bigotimes_{j=1}^{\mathrm{len}(\vec{b})} \left(b_j P^{\rho}_{\mathrm{acc}} + \bar{b}_j P^{\rho}_{\mathrm{rej}}\right) \otimes \mathbb{1}_H], \tag{6.19}$$

where $P^{\rho}_{\mathrm{rej}} := \mathbb{1}_Q - P^{\rho}_{\mathrm{acc}}$. The probability for the interactive strategy S to succeed at counterfeiting in v steps can be described as the sum of these probabilities over all possible full

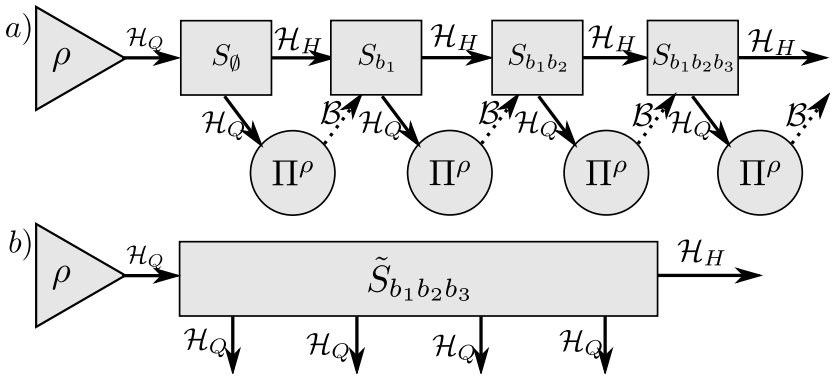

Figure 6.3: a) We schematically illustrate how a dynamical strategy S works. Each step of a strategy (grey rectangles) is a CPTP map $S_{\vec{b}}$ which depends on the classical outcome $\vec{b}$ of previous verifications. The first map $S_\emptyset$ takes an original qticket ρ as input, whereas subsequent steps rely on an internal memory state of the holder. The content of internal memory could range from no information at all, to a full original qticket and a detailed register of previous submissions. The verifiers have a fixed strategy Π^ρ which consists of applying the measurement $\{P^\rho_{\text{acc}}, P^\rho_{\text{rej}}\}$ and only returning the classical boolean measurement outcome. b) By fixing the classical input $\vec{b}$ to the strategy, a CPTP map $\tilde{S}_{\vec{b}} \in \mathcal{H}_Q \to \mathcal{H}_Q^{\otimes \text{len}(\vec{b})+1} \otimes \mathcal{H}_H$ is constructed, corresponding to one possible partial application of the strategy S. This CPTP map produces $\text{len}(\vec{b})+1$ possibly entangled outputs in $\mathcal{H}_Q$ from a single input qticket.

verification outcomes including at least two acceptances

$$p_{\text{d},v}(S) = \sum_{\substack{\vec{b}:\sum b_i \geq 2 \\ \text{len}(\vec{b})=v}} p_{\vec{b}}(S). \tag{6.20}$$

The key idea now is to use $p_{\vec{b}}(S) = p_{\vec{b}0}(S) + p_{\vec{b}1}(S)$ to provide an alternate expression for this sum. Namely, we combine verification outcomes starting in the same way into a single summand while avoiding the inclusion of failed counterfeiting attempts. Each full verification outcome containing two or more successful verifications has a unique shortest initial substring containing exactly two successful verifications. That a given substring is the shortest can be guaranteed by taking the last verification of the substring to be one of the two accepted.

$$p_{\text{d},v}(S) = \sum_{\substack{\vec{b}:\sum b_i = 2 \\ b_{\text{len}(\vec{b})}=1}} p_{\vec{b}}(S). \tag{6.21}$$

Each of the $\binom{v}{2}$ summands on the RHS of Eq. (S6.21), may be characterized by two indices k, l s.t.

$$\vec{b} = \overbrace{0\ldots0}^{k-1}1\overbrace{0\ldots0}^{l-k-1}1 \quad \text{for some } k < l \leq v. \tag{6.22}$$

For each one of these summands, we construct a static strategy $T_{k,l}(\rho) = \mathsf{tr}_{\setminus k,l}[\tilde{S}_{\mathrm{tl}(\vec{b})}(\rho)]$ which takes as input a single valid qticket ρ and submits exactly two tokens. The counterfeiting probability of this map on ρ is

$$\begin{aligned}
&\mathsf{tr}\left[(P^{\rho}_{\mathrm{acc}})^{\otimes 2}\, T_{k,l}(\rho)\right] \\
=&\mathsf{tr}\left[(P^{\rho}_{\mathrm{acc}})^{\otimes 2}\, \mathsf{tr}_{\setminus k,l}[\tilde{S}_{\mathrm{tl}(\vec{b})}(\rho)]\right] \\
=&\mathsf{tr}[\tilde{S}_{\mathrm{tl}(\vec{b})}(\rho) \bigotimes_{j=1}^{\mathrm{len}(\vec{b})} \left(b_j P^{\rho}_{\mathrm{acc}} + \bar{b}_j \mathbb{1}_Q\right) \otimes \mathbb{1}_H] \\
\geq&\mathsf{tr}[\tilde{S}_{\mathrm{tl}(\vec{b})}(\rho) \bigotimes_{j=1}^{\mathrm{len}(\vec{b})} \left(b_j P^{\rho}_{\mathrm{acc}} + \bar{b}_j P^{\rho}_{\mathrm{rej}}\right) \otimes \mathbb{1}_H].
\end{aligned} \tag{6.23}$$

By averaging over $\rho \in Q$ we obtain $p_{\vec{b}}(S) \leq p_{\mathrm{d}}(T_{k,l}) \leq B$ and invoking Eq. (S6.21) we obtain $p_{\mathrm{d},v}(S) \leq \binom{v}{2} B$. ■

6.B.4 Tightness

For $F_{tol} < 5/6$ applying an optimal qubit cloning map[128] $\Lambda(\rho) = \frac{1}{3}\rho \otimes \rho + \frac{1}{6}\rho \otimes \mathbb{1} + \frac{1}{6}\mathbb{1} \otimes \rho$ on each of the individual qubits of the qticket provides a good counterfeiting probability. The plot in Fig. S6.4 illustrates the probability of counterfeiter to actually get two qtickets accepted when taking this approach. For each of the two counterfeited qtickets, the probability of failing verification is the cumulant of a binomial distribution $B(N, 5/6)$ up to $F_{\mathrm{tol}}N$ and rejection probability may be upper bounded by $\frac{1}{2}\exp(-2N(5/6 - F_{\mathrm{tol}})^2)$ using Hoeffding's inequality. Even when failure of the two qtickets is anticorrelated, the probability of either of them failing verification can not excede the sum. This shows that a the scheme can not be made secure for $F_{\mathrm{tol}} < 5/6$. While such a scheme provides optimal forging probability when $(F_{tol} = 1)$, other schemes could in principle outperform it in terms of counterfeiting capability. Althought this is in principle possible, our security result shows that assymptotically in N, no other strategy may work for $F_{\mathrm{tol}} > 5/6$.

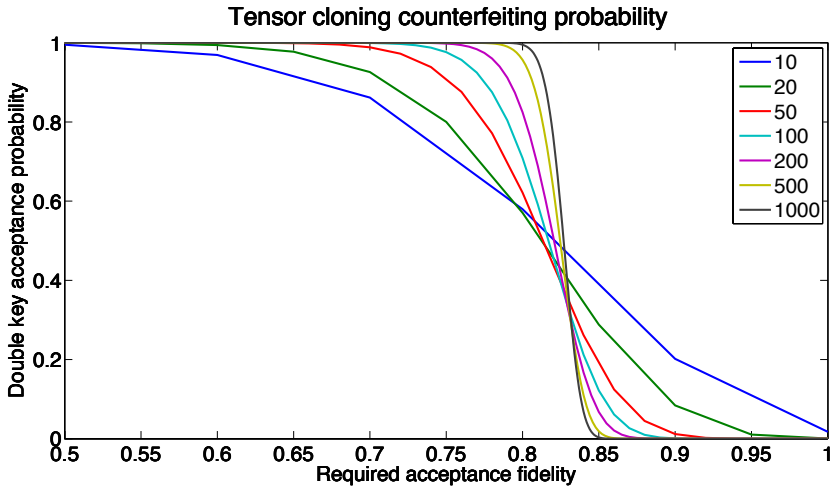

Figure 6.4: We numerically calculate the probability of accepting two copies of a qticket when the adversary strategy is assumed to be independently cloning each of the N qubits using an optimal cloning map. We see that the probability of producing two accepted qtickets approaches a step function at 5/6 with N.

6.B.5 Extension: Issuing multiple identical qtickets

Our results admit generalization to a scenario where the c identical copies of each qtickets are issued and succesful verification of $c+1$ is to be excluded. To obtain an analog of lemma 6.B.4 requires the individual qubits composing a qticket to be drawn at random from a state t-design with $t = c+(c+1)$ (for example $t = 5$ would already be needed if two identical copies are issued). The optimal $c \to c+1$ cloning probability for N component product states is in this case bounded by $\left(\frac{c+1}{c+2}\right)^N$. The threshold fidelity required to guarante security is then given by $F_{\text{tol}} > 1 - \frac{1}{(c+1)(c+2)}$ For such an F_{tol}, the analogous result to theorem 6.B.2 one obtained is

$$p_{c\to c+1}(T) \leq e^{-ND\left((c+1)F_{tol}-c\|\frac{c+1}{c+2}\right)}. \tag{6.24}$$

Finally, if $v > c+1$ verification attempts are allowed, the probability of counterfeiting can be proven not to grow faster than $\binom{v}{c+1}$. The proofs of these claims completely follow the lines that have been presented. Striving for legibility, we have limited the proof presented to $c = 1$, thus avoiding the notational burdon imposed by the extra indices required.

6.C CV-Qtickets

In this section we provide a proof that cv-qtickets are secure, not only against counterfeiting but also against any other possible double usage. We first present definitions for cv-qtickets and their verification. We then state the associated soundness and security guarantees and outline the security proof. Only the proof of the security statement is provided, since proving soundness for cv-qtickets requires no additional techniques as compared to soundness of qtickets.

6.C.1 CV-Qticket definition

Each cv-qticket is composed of $n \times r$ qubit pairs. Each qubit pair is prepared by choosing a state from

$$\{|0,+\rangle, |0,-\rangle, |1,+\rangle, |1,-\rangle, |+,0\rangle, |-,0\rangle, |+,1\rangle, |-,1\rangle\}$$

uniformly at random.

A full verification question for the cv-qticket will consist of n randomly chosen axes from $\{X, Z\}$ each corresponding to a specific block of r qubit pairs. In principle, the holder of the cv-qticket then measures the polarization of every qubit components along the corresponding requested axis and communicates the measurement outcomes to the verifier. The criteria to consider an answer correct is the following; within each of the n blocks, at least $F_{\text{tol}}r$ of the reported outcomes corresponding to qubits prepared in a polarization eigenstate of the inquired axis should be given correctly.

6.C.2 Soundness

The soundness result states that even under imperfect storage and readout fidelity, legitimate cv-qtickets work well as long as the fidelity loss is not too severe. Again, the completely positive trace preserving (CPTP) maps M_j will be assumed to represent the encoding, storage and readout of the j-th qubit component of the cv-qticket, with the full map over all components given by $M = \bigotimes_{j\in\{1,\ldots,2r\times n\}} M_j$. In the case of cv-qtickets, sufficiently many ($F_{\text{tol}}r$) correct answers should be provided within each block, demanding that a sufficiently good average fidelity be implemented for every single block. A random remapping of the Cartesian axes for each qubit component of a cv-qticket is also necessary, and can be achieved via a

random unitary (possibly from a unitary 2-design). This is required for example in the case where an actual physical polarization, say X, is lost faster than other components. In this case asking for the stored X polarization for all qubits in a block may yield a large failure probability even though the average storage fidelity among the qubits is sufficiently high. A random unitary remapping solves this and allows to connect with the average qubit storage fidelity, even in the case where only two nominal axes are used.

Given $F_j = F(M_j)$, the average fidelity of the qubit map M_j, we define $F_{\mathrm{exp},b} := N^{-1}\sum_{j:\lceil \frac{j}{2r} \rceil = b} F_j$ to be the average qubit fidelity within block $b \in \{1,\ldots,n\}$. Furthermore, to simplify the final expression, let us define $F_{\mathrm{exp}} = \min_b F_{\mathrm{exp},b}$.

Theorem 6.C.1 *(Soundness of cv-qtickets) As long as $F_{\mathrm{exp}} > F_{\mathrm{tol}}$, an honest holder implementing a map M can successfully redeems cv-qtickets with a probability*

$$p_{\mathrm{h}}^{\mathrm{cv}}(M) \geq \left(1 - e^{-rD(F_{\mathrm{exp}}\|F_{\mathrm{tol}})}\right)^n.$$

Observe that one may reduce this statement to n independent statements within each block which are completely analogous to the soundness for qtickets theorem 6.B.1.

6.C.3 Security

A naive security statement expresses that the holder of a single cv-qticket is unable to produce two copies from it, each with the potential of passing a verification. Since the verification of cv-qtickets is achieved by sending a classical message to a verifier, the security statement for cv-qtickets goes beyond this; it states that even with simultaneous access to two randomly chosen verification questions, the holder of a cv-qticket is exponentially unlikely to provide satisfactory answers to both. We further extend our security claim, to an even more adverse scenario; the holder of a cv-qticket has simultaneous access to v independent verification questions and may proceed to answer them in any chosen order. Moreover failing in verification attempts does not forbid the holder from further attempts which may possibly be performed relying on the information accumulated from previous verification outcomes.

Let S be a mathematical object denoting the counterfeiting strategy taken by the holder of a valid cv-qticket. We will denote by $p_{\mathrm{d},v}^{\mathrm{cv}}(S)$, the probability that strategy S leads to two or more successful verifications when engaging in v verification attempts with possibly independent verifiers. The probability is taken over the random generation of cv-qtickets, of

verification questions, and of measurement outcomes (Born's rule). The security statement is then

Theorem 6.C.2 *(Security of cv-qtickets) For any counterfeiting strategy S and tolerance parameter $F_{\text{tol}} > \frac{1+1/\sqrt{2}}{2}$ we have*

$$p^{\text{cv}}_{\text{d},v}(S) \leq \binom{v}{2}^2 \left(1/2 + e^{-rD(F_{\text{tol}}\|\frac{1+1/\sqrt{2}}{2})}\right)^n .$$

The proof of this statement goes as follows. Since abstractly cv-qtickets consist of a set of randomly produced states and questions requested on these states the formalism of quantum retrieval games (QRGs) provides adequate modeling. This framework is presented in a largely self-contained manner, since its generality and potential make it of independent interest. We first provide basic definitions for QRGs and derive some simple results. Then we present possible ways of composing QRGs together with associated quantitative bounds. The first results are then applied to the qubit pair constituents of cv-qtickets to bound the holders potential to provide answers to complementary question. Cv-qtickets are then modeled by a QRG for scenarios in which the holder of a cv-qticket wishes to simultaneously answer questions from two independent verifiers without any additional aid. Finally, a combinatorial bound, similar to the one used for qtickets, is used to provide an upper limit on how the double verification probability may increase with the number v of verification attempts.

6.C.4 Quantum retrieval games

Quantum retrieval games (QRGs), recently defined by Gavinsky [44] provide a framework to analyze protocols in which information is to be extracted from a state produced according to a classical probability distribution. We will here present a definition of QRGs following Gavinsky as well as some additional results derived which may be of independent interest.

Alice prepares a normalized state $\rho_s = \varrho(s)/p_s$ according to the probability $p_s := \mathsf{tr}[\varrho_s]$ and transfers it to Bob. Whereas Alice remembers the index s of the generated state, Bob is only provided with ρ_s and a full description of the distribution from which it was generated. Alice then asks Bob a question about s which Bob attempts to answer as best as possible. A simple possibility is for Alice to directly ask Bob the value of s. In general however, the set of possible answers A need not coincide with the set of indexes S over the possible prepared states. If each answer a is either correct or incorrect the question may be modeled

as $\sigma \in S \times A \to \{0,1\}$. This is, $\sigma(s,a) = 1$ iff the answer a is correct for state index s and $\sigma(s,a) = 0$ otherwise. This definition faithfully represents Gavinsky's QRGs. We extend this notion to weighted quantum retrieval games (WQRGs) to model situations where some answers are "more correct" than others. Here for each prepared state s and possible answer a the game will assign a non-negative real value $\sigma(s,a)$ associated to the utility function of answer a given input s (i.e. $\sigma \in S \times A \to \mathbb{R}_+$).

Bob needs to choose an answer $a \in A$ and may use his copy of state ρ_s to do so. The most general strategy that Bob can take according to the laws of quantum mechanics is to perform a positive operator valued measurement (POVM). We will consider post-selected POVMs, as opposed to a physical POVM, as those which may fail to produce a measurement outcome. This is, whereas a physical POVM always produces an outcome from the expected set, for post-selected POVM some "invalid" outcomes are discarded and excluded from statistics.

In order to express the random preparation of states by Alice we first define the notion of an indexed ensemble.

Indexed ensemble We will say that ϱ is an ensemble on $\mathcal{H}$ indexed over S iff $\forall s \in S : \varrho(s)$ is a positive operator on $\mathcal{H}$ and $\sum_{s\in S} \mathsf{tr}[\varrho(s)] = 1$.

Note that if ϱ is an indexed ensemble, then $\rho = \sum_s \varrho(s)$ is a normalized density matrix. Although Alice gives a specific state $\varrho(s)/\mathsf{tr}[\varrho(s)]$ to Bob, since Bob does not know s, he does not know which one has been received. The state $\rho = \mathsf{tr}_{Alice}[\sum_{s\in S} s \otimes \varrho(s)]$ will be called the reduced density matrix of ϱ since it corresponds to tracing out Alice's classically correlated subsystem containing the index s. Without loss of generality, ρ can be assumed to be full rank on $\mathcal{H}$.

In other words, a physical/selective projection $\mathcal{P}$ indexed over A is simply a physical/post-selected POVM equipped with an interpretation for each possible measurement outcome in terms of possible answers in $a \in A$.

Selective and physical projections We will say that $\mathcal{P}$ is a selective projection indexed over A iff $\forall a \in A$, $\mathcal{P}(a)$ are bounded positive semidefinite operators on $\mathcal{H}$. It will also be a physical projection iff $\sum_a \mathcal{P}(a) = \mathbb{1}$.

Note that no normalization has been imposed for selective projections since induced probability distributions are normalized a posteriori. An indexed ensemble and a projection on the

same Hilbert space induce a joint probability distribution over the indexes $S \times A$ of prepared states and provided answers.

Induced probability distribution Let ϱ be an ensemble on $\mathcal{H}$ indexed over S and let $\mathcal{P}$ be a projection on $\mathcal{H}$ indexed over A. Then

$$p(s_0, a_0) = \frac{\mathsf{tr}[\mathcal{P}(a_0)\varrho(s_0)]}{\sum_{s,a} \mathsf{tr}[\mathcal{P}(a)\varrho(s)]}. \tag{6.25}$$

is a probability distribution over $S \times A$ which will be denoted by $p = \langle \varrho, \mathcal{P} \rangle$ and is undefined unless $\sum_{s,a} \mathrm{Tr}[\mathcal{P}(a)\varrho(s)] > 0$.

Furthermore, note that for physical projections the denominator in Eq. (S6.25) is 1 and the marginal of the resulting distribution over S is $p(s) = \sum_a p(s, a) = \mathsf{tr}[\varrho(s)]$ which is independent of $\mathcal{P}$.

Weighted quantum retrieval games Let ϱ be an ensemble on $\mathcal{H}$ indexed over S. Consider a utility function $\sigma \in S \times A \to \mathbb{R}_+$. Then the pair $\mathcal{G} = (\varrho, \sigma)$ is a weighted quantum retrieval game. A WQRG is also a QRG when $\sigma \in S \times A \to \{0, 1\}$.

The value of a game $\mathcal{G}$ w.r.t. a projection $\mathcal{P}$ is the average utility obtained by Bob by using a certain measurement strategy $\mathcal{P}$. This value is given by the expectancy of the utility function σ over the joint distribution of prepared states and measurement outcomes.

Definition The value of game $\mathcal{G} = (\varrho, \sigma)$ w.r.t. projection $\mathcal{P}$ is defined as

$$\mathrm{Val}(\mathcal{G}, \mathcal{P}) := \sum_{s,a} p(s, a)\sigma(s, a) \tag{6.26}$$

where $p = \langle \varrho, \mathcal{P} \rangle$ is the induced probability distribution.

We now define the optimum value achievable by Bob for two distinct conditions depending on whether selective or physical projections are allowed.

Definition The selective (respectively physical) value of a game $\mathcal{G}$ are defined as

$$\mathrm{Sel}(\mathcal{G}) := \sup_{\mathcal{P} \in \text{Selective projections}} \mathrm{Val}(\mathcal{G}, \mathcal{P}) \tag{6.27}$$

$$\mathrm{Phys}(\mathcal{G}) := \sup_{\mathcal{P} \in \text{Physical projections}} \mathrm{Val}(\mathcal{G}, \mathcal{P}). \tag{6.28}$$

Note that according to this definition $\mathrm{Sel}(\mathcal{G}) \geq \mathrm{Phys}(\mathcal{G})$ since the supremum is taken over a larger set. However, for certain tailored games, the selective and physical values will coincide. The advantage of selective values is that they may be straightforwardly computed and are more amenable to compositional results. If Bob is forced to provide an answer, he can only achieve the physical value of a game. If Bob is allowed to abort the game after measuring his state ρ_s and aborted games are not considered when calculating his expected utility then he will be able to achieve the selective value.

The following result provides an explicit formula to calculate the selective value of a game. In this sense, it is a generalization of lemma 4.3 in [44].

Theorem 6.C.3 (Selective value of a game) *Let $\mathcal{G} = (\varrho, \sigma)$ be a WQRG with $\sum_s \varrho(s) = \rho$. Define $O(a) := \sum_s \sigma(s,a)\rho^{-1/2}\varrho(s)\rho^{-1/2}$. Then the selective value of $\mathcal{G}$ may be calculated as $\mathrm{Sel}(\mathcal{G}) = \max_a \|O(a)\|$, where $\|\cdot\|$ denotes the operator norm.*

Proof. We first use the definition of the value of a game $\mathcal{G}$ w.r.t. $\mathcal{P}$, expand the induced probability distribution and move the sum over s inside the trace

$$\mathrm{Val}(\mathcal{G}, \mathcal{P}) = \frac{\sum_a \mathrm{Tr}[\mathcal{P}(a) \sum_s \sigma(s,a)\varrho(s)]}{\sum_a \mathsf{tr}[\mathcal{P}(a) \sum_s \varrho(s)]}. \tag{6.29}$$

We define $\tilde{\mathcal{P}}$ such that $\tilde{\mathcal{P}}(a) = \rho^{1/2}\mathcal{P}(a)\rho^{1/2}$. Using this definition and that of ρ and O_a we may rewrite

$$\begin{aligned} \mathrm{Val}(\mathcal{G}, \mathcal{P}) &= \frac{\sum_a \mathrm{Tr}[\tilde{\mathcal{P}}(a)O(a)]}{\sum_a \mathrm{Tr}[\tilde{\mathcal{P}}(a)]} \\ &\leq \max_a \frac{\mathrm{Tr}[\tilde{\mathcal{P}}(a)O(a)]}{\mathrm{Tr}[\tilde{\mathcal{P}}(a)]} \\ &\leq \max_a \|O(a)\|. \end{aligned} \tag{6.30}$$

The first inequality uses the positivity of all summands. For the second inequality we note that $\tilde{\mathcal{P}}(a)$ must be positive semidefinite and the variational definition of operator norm of the positive semidefinite operator $O(a)$. Equality can be achieved by taking $\tilde{\mathcal{P}}(a_0)$ to be a projector onto the highest eigenvalue subspace of $O(a_0)$ if $\|O(a_0)\| = \max_a \|O(a)\|$ and taking $\tilde{\mathcal{P}}(a_0) = 0$ otherwise. ∎

The theorem provides an explicit construction of a projection achieving the selective value of a game. Furthermore, the proof allows us to derive a necessary and sufficient condition under which the selective and physical values of a game coincide.

Corollary 6.C.4 *Given a retrieval game $\mathcal{G}$, we have that* $\mathrm{Sel}(\mathcal{G}) = \mathrm{Phys}(\mathcal{G})$ *iff there exist positive* $\tilde{\mathcal{P}}(a)$ *such that*

$$O(a)\tilde{\mathcal{P}}(a) = \mathrm{Sel}(\mathcal{G})\tilde{\mathcal{P}}(a) \quad \text{and} \quad \sum_a \tilde{\mathcal{P}}(a) = \rho \tag{6.31}$$

We now turn to the systematic composition of retrieval games in the form of product and threshold games. This provides a way to construct more elaborate retrieval games together with bounds on their associated values. A natural definition of tensor product may be given for indexed ensembles, projections and utility functions.

$$(\varrho_1 \otimes \varrho_2)(s_1, s_2) = \varrho_1(s_1) \otimes \varrho_2(s_2) \tag{6.32}$$

$$(\mathcal{P}_1 \otimes \mathcal{P}_2)(a_1, a_2) = \mathcal{P}_1(a_1) \otimes \mathcal{P}_2(a_2) \tag{6.33}$$

$$(\sigma_1 \otimes \sigma_2)((s_1, s_2), (a_1, a_2)) = \sigma_1(s_1, a_1)\sigma_2(s_2, a_2) \tag{6.34}$$

These definitions have the property that the tensor product of physical projections is a physical projection and that the induced probability distribution of two tensor product is the tensor product of the individual induced probability distributions

$$\langle(\varrho_1 \otimes \varrho_2), (\mathcal{P}_1 \otimes \mathcal{P}_2)\rangle = \langle\varrho_1, \mathcal{P}_1\rangle \otimes \langle\varrho_2, \mathcal{P}_2\rangle$$

Tensor product WQRG Let $\mathcal{G}_1 = (\varrho_1, \sigma_1)$ and $\mathcal{G}_2 = (\varrho_2, \sigma_2)$. We define the tensor product WQRG $\mathcal{G}_1 \otimes \mathcal{G}_2$ as

$$\mathcal{G}_1 \otimes \mathcal{G}_2 = (\varrho_1 \otimes \varrho_2, \sigma_1 \otimes \sigma_2).$$

Proposition 6.C.5 (Tensor product selective value) *The selective value of a tensor product game is the product of the selective value of the independent games.*

$$\mathrm{Sel}(\mathcal{G}_1 \otimes \mathcal{G}_2) = \mathrm{Sel}(\mathcal{G}_1)\,\mathrm{Sel}(\mathcal{G}_2)$$

Proof. By using the definition of $O(a)$ in theorem 6.C.3 with respect to the WQRG involved we obtain

$$\|O(a_1, a_2)\| = \|O_1(a_1) \otimes O_2(a_2)\| = \|O_1(a_1)\|\|O_2(a_2)\|.$$

Maximizing over a_1 and a_2 on both sides theorem 6.C.3 provides the desired equality. ■

The selective value of the product game is attained by the tensor product of projections, each achieving the respective selective values.

Corollary 6.C.6 (Tensor product physical value) *If* $\mathrm{Phys}(\mathcal{G}_1) = \mathrm{Sel}(\mathcal{G}_1)$ *and* $\mathrm{Phys}(\mathcal{G}_2) = \mathrm{Sel}(\mathcal{G}_2)$ *then* $\mathrm{Phys}(\mathcal{G}_1 \otimes \mathcal{G}_2) = \mathrm{Sel}(\mathcal{G}_1 \otimes \mathcal{G}_2)$.

Given a direct product game and a projection for it one may consider the inverse procedure of defining a projection on one of the subcomponents of the game.

Restriction of a projection Let $\mathcal{P}$ be a projection on $\mathcal{H}_1 \otimes \mathcal{H}_2$ indexed over $A_1 \times A_2$. Furthermore, let ρ_2 be a normalized density matrix on $\mathcal{H}_2$. We define the restriction $\mathcal{P}_{|1}$ with respect to ρ_2 and A_2 as

$$\mathcal{P}_{|1}(a_1) = \sum_{a_2} \mathsf{tr}_2(\mathcal{P}(a_1, a_2)\mathbb{1} \otimes \rho_2).$$

By abuse of notation, if $\rho = \rho_1 \otimes \rho_2$ is a normalized product state in $\mathcal{H}_1 \otimes \mathcal{H}_2$ we may define the restriction of $\mathcal{P}$ with respect to the normalized tensor factors of ρ. This is the case for the reduced density matrix of product indexed ensembles. By restricting a projection one obtains a new projection which induces the same reduced probability distribution

Lemma 6.C.7 (Restriction of a projection) *Let* $\mathcal{P}_{|1}$ *be the restriction of* $\mathcal{P}$ *with respect to* ρ_2 *and* A_2*, where* ρ_2 *is the reduced density matrix of* ϱ_2*. Then*

$$\langle \varrho_1, \mathcal{P}_{|1} \rangle(s_1, a_1) = \sum_{s_2, a_2} \langle \varrho_1 \otimes \varrho_2, \mathcal{P} \rangle(s_1 s_2, a_1 a_2).$$

Theorem 6.C.8 (Selective value of threshold QRG) *Let* $\mathcal{G}_j = (\varrho_j, \sigma_j)$ *be WQRGs s.t.* $\sigma_j \in (S_j, A_j) \to [0, 1]$ *and* $\mathrm{Sel}(\mathcal{G}_j) = \delta_j$ *for all* $j \in \{1, \ldots, n\}$*. Furthermore take* $\delta = n^{-1} \sum_{j=1}^{n} \delta_j$ *and* $\delta \leq \gamma \leq 1$*. Define the QRG* $\mathcal{G}_\gamma = (\bigotimes_j \varrho_j), \sigma_\gamma)$ *with a tensor product ensemble distribution and boolean utility function*

$$\sigma_\gamma(\vec{s}, \vec{a}) = \left(\sum_{j=1}^{n} \sigma_j(s_j, a_j) \geq \gamma n \right).$$

Then we have $\mathrm{Sel}(\mathcal{G}_\gamma) \leq 2e^{-nD(\gamma \| \delta)}$.

Proof. The direct product indexed ensemble $\varrho = \bigotimes_j \varrho_j$ and projection $\mathcal{P}$ induce a normalized probability distribution over $\vec{S} \times \vec{A}$ given by

$$p(\vec{s}, \vec{a}) = \frac{\mathsf{tr}[\mathcal{P}(\vec{a})\varrho(\vec{s})]}{\sum_{\vec{s}\vec{a}} \mathsf{tr}[\mathcal{P}(\vec{a})\varrho(\vec{s})]}.$$

Define the dependent random variable X_j to be $\sigma_j(s_j, a_j)$ where s_j and a_j are taken according to this probability distribution. For any $S \subseteq \{1, \ldots, n\}$, we may define $\mathcal{P}_{|S}$ as the restriction

of the projection $\mathcal{P}$ to the subsystems specified by S with respect to $(\rho_{\vec{s}})$. By proposition 6.C.5 we have that

$$\mathbf{Exp}\left[\prod_{j\in S} X_j\right] = \mathrm{Val}\left(\bigotimes_{j\in S}\mathcal{G}_j, \mathcal{P}_{|S}\right) \leq \prod_{j\in S}\delta_j. \tag{6.35}$$

Using theorem 6.A.1 and definition 6.C.4 we obtain

$$\mathrm{Val}\left(\mathcal{G}_\gamma, \mathcal{P}\right) = \mathbf{Pr}\left[\sum_j X_j \geq \gamma n\right] \leq 2e^{-nD(\gamma\|\delta)}. \tag{6.36}$$

Since this is true for arbitrary $\mathcal{P}$ we conclude that $\mathrm{Sel}(\mathcal{G}_\gamma) \leq 2e^{-nD(\gamma\|\delta)}$. ∎

6.C.5 CV-Qticket qubit pair building block

Consider a game in which Alice transfers to Bob one of the following states chosen at random

$$S = \{|0,+\rangle, |0,-\rangle, |1,+\rangle, |1,-\rangle, |+,0\rangle, |-,0\rangle, |+,1\rangle, |-,1\rangle\},$$

each with probability 1/8. Alice then asks Bob for the Z polarization of both qubits, possible answers being $A = \{00, 01, 10, 11\}$. An answer is correct iff it coincides in the polarization of the qubit prepared in a Z eigenstate. Bob can always answer the question correctly by measuring both qubits in the Z basis.

The quantum retrieval game formalism applies to this problem although one must admit that it is like cracking a nut with a sledgehammer. We call this game $\mathcal{G}_Z = (\varrho, \sigma_Z)$ where we have $\sum_s \varrho(s) = \rho = \mathbb{1}_4/4$, and $\mathsf{tr}[\varrho(s)] = 1/8$ for all $s \in S$. A formal definition of the utility function σ_Z can be given as $\sigma_Z(s,a) = (s_1 \equiv a_1 \,\mathrm{or}\, s_2 \equiv a_2)$. We first define the operators $O(a)$ from theorem 6.C.3. Due to symmetry we may restrict to considering one such operator

$$O(00) = 4\left(\varrho(0,+) + \varrho(0,-) + \varrho(+,0) + \varrho(-,0)\right) \tag{6.37}$$

and find that $\|O(00)\| = 1$ which is a non degenerate eigenvalue for all $O(a)$. The fact that the four corresponding eigenspaces are orthogonal confirms that 1 is also the physical value of the game.

The same trivial value of 1 can be achieved for the game in which Alice requests the X direction polarization of the states. We will call this game $\mathcal{G}_X = (\varrho, \sigma_X)$. The problem becomes interesting if Bob is requested provide a guess for both complementary polarizations. There are two relevant possibilities, both of which will require Bob to give an answer twice as

long as before. The first scenario describes the best case probability of Bob answering both questions correctly and may be modeled by a QRG with utility function

$$\mathcal{G}_\wedge = (\varrho, \sigma_\wedge) \quad \sigma_\wedge(s, a_X a_Z) = \sigma_X(s, a_X) \wedge \sigma_Z(s, a_Z).$$

In the second scenario we are interested in the average number of questions answered correctly when two complementary questions are posed and may be modeled by the WQRG with utility function

$$\mathcal{G}_{\text{avg}} = (\varrho, \sigma_{\text{avg}}) \quad \sigma_{\text{avg}}(s, a_X a_Z) = \frac{\sigma_X(s, a_X) + \sigma_Z(s, a_Z)}{2}.$$

Thanks to symmetries one need only calculate a single $\|O(a)\|$ and for concreteness we choose $O(++00)$. For the conjunction QRG we obtain

$$O(++00) = 4\left(\varrho(0,+) + \varrho(+,0)\right) \text{ and } \|O_{++00}\| = 3/4.$$

For the average WQRG we obtain

$$\begin{aligned} O(++00) =& 2[2\varrho(0,+) + 2\varrho(+,0) + \varrho(0,-) \\ &+ \varrho(-,0) + \varrho(+,1) + \varrho(1,+)] \end{aligned} \tag{6.38}$$

and $\|O_{++00}\| = 1/2 + 1/\sqrt{8} \approx 0.8536$. This is precisely the optimal fidelity for covariant qubit cloning (i.e. cloning of equatorial qubits). On the other hand, if Bob is asked the same question twice instead of complementary questions it is clear that he will be able to repeat two correct answers. All in all, if Bob is asked complementary question half of the time and coinciding questions half of the time he will be able to emulate an average fidelity of $3/4 + \sqrt{2}/8 \approx 0.927$.

Indeed, once we have defined a concrete WQRG, calculating its selective value becomes an exercise thanks to theorem 6.C.3. Furthermore, if the game has sufficient symmetry it will be possible to prove a coinciding physical values for the game.

6.C.6 CV-Qticket retrieval games

We will first bound the probability of answering two of these randomly chosen questions by bounding the selective value of the corresponding retrieval game. To do this, we bound the value of a game where r complementary questions are asked on r qubit pairs (this is precisely

the case for one block when the two random questions are complementary).

$$\begin{aligned}\sigma^{(X)}_{F_{\text{tol}}}(\vec{s},\vec{a}^{(X)}) &= \left(\sum_{j=1}^{r}\sigma^{(X)}_{j}(s_j,a^{(X)}_j)\geq F_{\text{tol}}r\right)\\ \sigma^{(Z)}_{F_{\text{tol}}}(\vec{s},\vec{a}^{(Z)}) &= \left(\sum_{j=1}^{r}\sigma^{(Z)}_{j}(s_j,a^{(Z)}_j)\geq F_{\text{tol}}r\right)\\ \sigma^{\wedge}_{F_{\text{tol}}}(\vec{s},(\vec{a}^{(X)},\vec{a}^{(Z)})) &= \sigma^{(X)}_{F_{\text{tol}}}(\vec{s},\vec{a}^{(X)})\wedge\sigma^{(Z)}_{F_{\text{tol}}}(\vec{s},\vec{a}^{(Z)})\end{aligned} \tag{6.39}$$

We will not calculate the selective value exactly but give a bound in terms of theorem 6.C.8. In order for the two block answers to be correct, among the two, at least $2F_{\text{tol}}r$ answers should have been provided correctly for individual qubit pairs. This is a weaker condition since it only imposes that the sum among the two block answers be sufficiently large, not necessarily implying that they are both above threshold.

$$\sigma^{\wedge}_{F_{\text{tol}}}(\vec{s},(\vec{a}^{(X)},\vec{a}^{(Z)}))\leq\left(\sum_{j=1}^{r}\sigma^{avg}_{j}(s_j,(a^{(X)}_j,a^{(Z)}_j))\geq F_{\text{tol}}r\right) \tag{6.40}$$

The description on the right hand side has precisely the form required for theorem 6.C.8. We conclude that the selective value and hence the probability within any strategy of providing valid answers to two complementary questions for the same block is upper bounded by $2\exp[-rD(F_{\text{tol}}\|1/2+1/\sqrt{8})]$ (for $F_{\text{tol}}>1/2+1/\sqrt{8}$).

Given two randomly chosen questions for a block there is a probability of $1/2$ that they will coincide and a probability $1/2$ that they will be complementary. Taking this into account, the probability for a dishonest holder to correctly answer two such randomly chosen block questions is upper bounded by $1/2+\exp[-rD(F_{\text{tol}}\|1/2+1/\sqrt{8})]$. By taking r sufficiently large, this value can be guaranteed to be smaller then 1. Hence, the probability of correctly answering n such randomly chosen threshold question pairs will be upper bounded by $B:=(1/2+\exp[-rD(F_{\text{tol}},1/2+1/\sqrt{8})])^n$ which can be made exponentially close to 1 in n.

6.C.7 Combinatorial bound on choosing and learning

The formulation presented adequately models a scenario in which the holder of a cv-qticket does not receive any feedback from the verifiers. However, if the holder of a cv-qticket can engage in several verification protocols, new possibilities arise which should be taken into account.

Firstly, by simultaneously engaging in several (v) verification protocols with different verifiers, the holder may simultaneously have access to v challenge questions. The holder may then for instance, choose the most similar questions and attempt to answer these. Furthermore, by successively participating in v verification protocols the holder can choose to perform verifications sequentially and wait for the outcome of the k-th before choosing which question to answer as the $k+1$-th and providing an answer for it.

In general, if the holder engages in v verification attempts, he will receive v random questions providing no additional information on the cv-qticket. There are $\binom{v}{2}$ possible question pairs among these, each of which can be seen as randomly chosen. Thus if no feedback is used the probability of answering at least one of these pairs correctly is upper bounded by $\binom{v}{2}B$. An example scenario where this bound is relatively tight is when r is very large and n is relatively small. In this case, the probability of answering two randomly chosen questions is well approximated by the collision probability 2^{-n} (i.e. the probability that two questions coincide) which grows precisely as $\binom{v}{2}$ if the holder has access to v independently drawn questions and may choose to answer any pair.

Suppose now, that the answers to the verifiers are provided sequentially, so that the decision of which answer to produce for each verifier may be made dependent on the outcome of previous verifications. We can safely assume that the answers to challenge questions are then provided sequentially, each after receiving the acceptance or rejection of the previous ones. We can then apply a similar argument to the one exposed for the proof of qticket security in section 6.B.3. This yields an additional factor of $\binom{v}{2}$ corresponding to the possible feedback scenarios up to the point of the second accepted answer, each of which can be simulated statically (i.e. by assuming the given feedback and fixing a corresponding POVM to generate answer up to that point). Hence the total probability for an interactive strategy with v verification attempts of producing two or more accepted answers is upper bounded by $\binom{v}{2}^2 B$.

It may seem artificial for verifiers to select a random question each time. Randomness is important in order to avoid revealing information about the issued cv-qticket. However, the verifier may choose a random question once and for all and ask it until it is answered correctly. Once it has been answered correctly, the verifier knows that the cv-qticket has already been redeemed and can thus reject all subsequent verification attempts. This is similar to the kind

of scheme used for prepaid telephone cards discussed in the applications section. However, the quantum case provides an advantage since one may have multiple verifiers which do not communicate. In a simple example with two verifiers, two composite questions may be chosen such that they are complementary on every qubit pair (i.e. one question is chosen at random and uniquely determines the other).

6.D Applications

Our quantum information application attempts to reduce quantum requirements to a minimum. However, even prepare and measure qubit memories remain technologically challenging. For problems admitting a classical solution, such an approach is likely to be technologicaly less demanding. In other words, relevant applications for prepare and measure quantum memories will be those solving problems for which no classical solutions are known. In this section we discuss some problems with classical solutions and propose refinement of such problems for which no classical solution is possible.

6.D.1 Enforcing single usage with a single verifier

For some applications, the no cloning of quantum information is only an apparent advantage. Our qticket and cv-qticket constructions can guarantee an exponentially small double usage probability. However, this is not an impresive feat for scenarios where there is a single verifier or if the verifiers have acces to realtime communication with a centralized database. In this case, a randomly chosen classical ticket has equaly good properties. After a ticket is succesfully redeemed once, it can be removed from the central database, making it invalid for any succesive verification attempt. In fact this classical strategy is widely used for crediting prepaid phone lines with a client calling a toll free number and typing the purchased ticket number in order to credit a telephone account. Thus in such scenarios, the quantum strategy does not provide additional protection with respect to a classical solution.

6.D.2 Multiple non communicating verifiers

In scenarios with multiple non communicating verifiers, (cv-)qtickets provide a soution to a problem where all classical approaches fail. We describe a *witness protection program* as an

example of how such a scenario might look like.

In a witness protection program, a governmental institution decides to give asylum to a key eye witness to whom an unforgeable quantum token is issued. This token can be used by the witness (holder) to claim asylum in any of a set of participating hotels (verifiers). The issuer also provides all hotels with the necessary information to verify the tokens. When using the token, neither the eye-witness nor the chosen hotel wish to divulge the locale where the witness is hosted, thus protecting both from being targets of an attack. This includes suspending communication between participating hotels as well as with the issuing authority. Any classical solution can not prevent a sufficiently resourceful holder from making copies of the received token, thus hotels are forced to communicate in order to avoid its double use. In this case, a quantum solution based on unforgeable tokens is the sole possibility to satisfy these unique constraints.

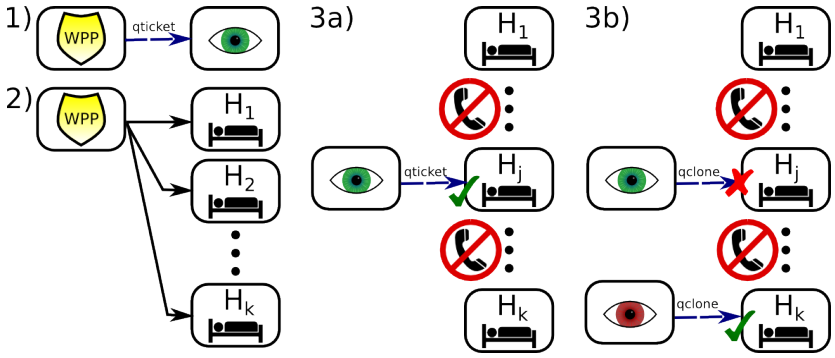

Figure 6.5: 1) The issuing entity hands a qticket to the key witness. 2) It provides the hotels with the secret classical description which will be used to verify it. 3a) An honest witness choses a hotel and physically transfer the qticket for verification. It will be accepted as long as the level of accumulated noise is below threshold. 3b) A dishonest witness will fail to counterfeit his/her qticker to provide acomodation for an additional guest. However, there is no way of avoiding a valid qticket from changing hands.

6.D.3 Reduced availability under sporadic verification

In principle, a centralized database may guarante that classical ticket are only redeemed once. However, there are situations where the ticket should be available only to one holder at a time and the non-clonable nature of a qticket allows enforcing this. One such example is

the sporadic control of tickets required for a given service. For concreteness, imagine a qticket which is valid for making use of a public transportation network. Commuters are sporadically controled, at which point if they are found to have a invalid qticket they are charged an important fine, whereas if they are found to hold a valid qticket, they are provided with a fresh substitute. If the transportation tickets are classical, sporadic control can not avoid counterfeited copies in the hands of coluding commuters from circulating simultaneously. The deceiving commuters need only communicate classicaly among each other before and after they are controled, effectively sharing a single classical ticket to make use of the service multiple times[1]. In contrast the unavailability of long distance quantum comunication would disallows them to share a qticket in such a way (i.e. each valid qticket may only be at one place at a time).

6.D.4 The quantum credit card

Having developed a single verification, noise tolerant, non-forgeable token, such as the cv-qticket, it is now possible to examine generalizations to interesting composite protocols. For instance, Gavinsky's proposal[44] allows for multiple verification rounds to be performed on a single token, while also ensuring that the token can not be split into two independently valid subparts. Such a construction may be seen as a quantum credit card. Indeed, the classical communication which takes place with the issuer (bank) to verify the cv-qticket (via "challenge" questions) may be intentionally publicized to a merchant who needs to be convinced of the card's validity. An alternate possibility is to follow the original interpretation as a quantum cash token where verification is performed by the receiver each time the "money" changes hands.

6.D.5 Excluding eavesdropers

While qtickets do not provide additional advantage against dishonest holder in the scenario of a single verifier quantumness may provide an advantage against eavesdroping and untrusted communication. In order to make online banking more secure, Banks routinely use TANs (transaction authentication numbers) as an additional security measure. The bank sends its client a list of TANs via postal service in addition to an online password which is set up via

[1] If the classical ticket is not renewed upon control even communication is unnecesary.

another channel. Each time a bank transaction is requested online by the client, the bank requests a TAN from the list to guarantee the authenticity of the transaction. An impostor then needs to know both a secret password used by the user and some TANs, thus increasing the difficulty to succesfully impersonate a transaction with respect to any single security measure. However, since TANs are classical objects it is conceivable that an eavesdroper may learn them while remaining undetected (imagine an eavesdroper taking xray pictures of the correspondence). This means that with some effort of the eavesdroper the additional security measure becomes ineffective.

This problem can be straightforwardly resolved by using quantum prepare and measure memories. Even if a cv-qticket is sent via an untrusted optical fiber or postal service, the receiver may openly communicate with the issuer and sacrifice some of the received qubits in order to obtain a bound on how much information could have leaked to eavesdropers. This is precisely the approach taken in QKD to obtain a statistical bound on the information that has leaked out. Gavinsky's $\mathcal{Q}$ scheme, allowing multiple verification rounds may be reinterpreted as quantum TAN lists. The holder of a quantum TAN list may verify its validity, and perform a transaction by publicly communicating with the bank. If the quantum TAN list is verified to be legitimate, then the probability of an eavesdroper getting verified by using the leaked information will be negligible (exponentially small). In turn, the cv-qtickets described in the main text and appendix may be used as basic building blocks for such a scheme in the presence of noise.

References

[1] S. Aaronson: *Quantum Copy-Protection and Quantum Money*, In *24th Annual IEEE Conference on Computational Complexity, 2009.*. IEEE (July 2009) pages 229–242.

[2] V.M. Acosta, E. Bauch, M.P. Ledbetter, A. Waxman, L. Bouchard and D. Budker, *Phys. Rev. Lett.* **104** (2010), 070801.

[3] D. Aharonov and M. Ben-Or, *quant-ph/9611025* (1996).

[4] D. Aharonov, M. Ben-Or, R. Impagliazzo and N. Nisan, *quant-ph/9611028* (1996).

[5] C. Ahn, A.C. Doherty and A.J. Landahl, *Phys. Rev. A* **65** (2002), 042301.

[6] C.S. Ahn: *Extending quantum error correction: new continuous measurement protocols and improved fault-tolerant overhead.* Pasadena, CA, Caltech, Dissertation, 2004.

[7] R. Alicki and M. Fannes, *Phys. Rev. A* **79** (2009), 012316.

[8] R. Alicki, M. Fannes and M. Horodecki, *arXiv:0810.4584* (2008).

[9] R. Alicki, M. Horodecki, P. Horodecki and R. Horodecki, *arXiv:0811.0033* (2008).

[10] P.W. Anderson, *Phys. Rev. Lett.* **18** (1967), 1049.

[11] D. Bacon, *Phys. Rev. A* **73** (2006), 012340.

[12] D. Bacon, *Phys. Rev. A* **78** (2008), 042324.

[13] M.V. Balabas, T. Karaulanov, M.P. Ledbetter and D. Budker, *Phys. Rev. Lett.* **105** (2010), 070801.

[14] G. Balasubramanian, P. Neumann, D. Twitchen, M. Markham, R. Kolesov, N. Mizuochi, J. Isoya, J. Achard, J. Beck, J. Tissler, V. Jacques, P.R. Hemmer, F. Jelezko and J. Wrachtrup, *Nat. Materials* **8** (2009), 383.

[15] P. Benioff, *Journal of Statistical Physics* **29** (1982), 515.

[16] C.H. Bennet and G. Brassard: *Quantum Cryptography: Public Key Distribution and Coin Tossing*, In *Proceedings of the IEEE International Conference on Computers, Systems & Signal Processing, Bangalore, India*. IEEE, New York (1984) pages 175–179.

[17] C.H. Bennett, *IBM Journal of Research and Development* **17** (1973), 525.

[18] K. Binder and E. Stoll, *Phys. Rev. Lett.* **31** (1973), 47.

[19] S. Bravyi, D.P. DiVincenzo, D. Loss and B.M. Terhal, *Phys. Rev. Lett.* **101** (2008), 070503.

[20] S. Bravyi and M.B. Hastings, *arXiv:1001.4363* (2010).

[21] S. Bravyi, M.B. Hastings and S. Michalakis, *Jour. Math. Phys.* **51** (2010), 093512.

[22] S. Bravyi and B. Terhal, *New Jour. Phys.* **11** (2009), 043029.

[23] K.R. Brown, *Phys. Rev. A* **76** (2007), 022327.

[24] D. Bruss, M. Cinchetti, G. Mauro D'Ariano and C. Macchiavello, *Phys. Rev. A* **62** (2000), 012302.

[25] H.J. Carmichael: *Statistical Methods in Quantum Optics 1: Master Equations and Fokker-Planck Equations (Theoretical and Mathematical Physics)*. Springer, November 1998.

[26] S. Chesi, D. Loss, S. Bravyi and B.M. Terhal, *New Jour. Phys.* **12** (2010), 025013.

[27] S. Chesi, B. Röthlisberger and D. Loss, *arXiv:0908.4264* (2009).

[28] A.M. Childs and W. van Dam, *arXiv:0812.0380* (2008).

[29] M. Christandl, N. Datta, A. Ekert and A.J. Landahl, *Phys. Rev. Lett.* **92** (2004), 187902.

[30] E. Cirillo and J. Lebowitz, *Jour. Stat. Phys.* **90** (1998), 211.

[31] C. Cohen-Tannoudji, J. Dupont-Roc and G. Grynberg: *AtomPhoton Interactions: Basic Processes and Applications.* 1. ed. Wiley-Interscience, March 1992.

[32] E. Dennis, A. Kitaev, A. Landahl and J. Preskill, *Jour. Math. Phys.* **43** (2002), 4452.

[33] D. Deutsch, *Proceedings of the Royal Society A Mathematical Physical and Engineering Sciences* **400** (1985), 97.

[34] S. Diehl, A. Micheli, A. Kantian, B. Kraus, H.P. Bchler and P. Zoller, *Nature Phys.* **4** (2008), 878.

[35] L. Duan and C. Monroe, *Rev. Math. Phys.* **82** (2010), 1209.

[36] M.V.G. Dutt, L. Childress, L. Jiang, E. Togan, J. Maze, F. Jelezko, A.S. Zibrov, P.R. Hemmer and M.D. Lukin, *Science* **316** (2007), 1312 .

[37] A.K. Ekert, *Phys. Rev. Lett.* **67** (1991), 661.

[38] E. Farhi, D. Gosset, A. Hassidim, A. Lutomirski, D. Nagaj and P. Shor, *Phys. Rev. Lett.* **105** (2010), 190503.

[39] E. Farhi, D. Gosset, A. Hassidim, A. Lutomirski and P. Shor, *arXiv:1004.5127* (2010).

[40] R.P. Feynman, *International Journal of Theoretical Physics* **21** (1982), 467.

[41] P. Gács, *Jour. Stat. Phys.* **103** (2001), 45.

[42] A. Gali, *Phys. Rev. B* **79** (2009), 235210.

[43] A. Gali, M. Fyta and E. Kaxiras, *Phys. Rev. B* **77** (2008), 155206.

[44] D. Gavinsky, *arXiv:1109.0372* (2011).

[45] N. Gisin, G. Ribordy, W. Tittel and H. Zbinden, *Rev. Math. Phys.* **74** (2002), 145.

[46] S. Gladchenko, D. Olaya, E. Dupont-Ferrier, B. Doucot, L.B. Ioffe and M.E. Gershenson, *Nature Phys.* **5** (2009), 48.

[47] D. Gottesman, *Phys. Rev. A* **57** (1998), 127.

[48] D. Gottesman, *arXiv:0904.2557* (2009).

[49] D. Gottesman and H. Lo, *IEEE Transactions on Information Theory* **49** (2003), 457.

[50] L.F. Gray. In *Perplexing Problems in Probability*, 1. ed. Birkhauser Verlag AG (August 1999), pages 331–354.

[51] G. Grinstein, *IBM J. Res. & Dev.* **48** (2004).

[52] G. Gutoski and J. Watrous: *Toward a general theory of quantum games*, In *Proceedings of the thirty-ninth annual ACM symposium on Theory of computing*STOC '07. ACM, New York, NY, USA (2007) page 565?574.

[53] A. Hamma, C. Castelnovo and C. Chamon, *Phys. Rev. B* **79** (2009), 245122.

[54] A. Hamma and D.A. Lidar, *Phys. Rev. Lett.* **100** (2008), 030502.

[55] J.W. Harrington: *Analysis of quantum error-correcting codes: symplectic lattice codes and toric codes.* Caltech, Thesis, 2004.

[56] A.W. Harrow, A. Hassidim and S. Lloyd, *Phys. Rev. Lett.* **103** (2009), 150502.

[57] M.B. Hastings and X.G. Wen, *Phys. Rev. B* **72** (2005), 045141.

[58] W. Hoeffding, *Journal of the American Statistical Association* **58** (1963), 13.

[59] M. Horodecki, P.W. Shor and M.B. Ruskai, *Rev. Math. Phys.* **15** (2003), 629.

[60] D.B. Hume, T. Rosenband and D.J. Wineland, *Phys. Rev. Lett.* **99** (2007), 120502.

[61] R. Impagliazzo and V. Kabanets. *Constructive Proofs of Concentration Bounds.* Technical report 072, Electronic Colloquium on Computational Complexity, 2010.

[62] V. Jacques, P. Neumann, J. Beck, M. Markham, D. Twitchen, J. Meijer, F. Kaiser, G. Balasubramanian, F. Jelezko and J. Wrachtrup, *Phys. Rev. Lett.* **102** (2009), 7.

[63] L. Jiang, M.V.G. Dutt, E. Togan, L. Childress, P. Cappellaro, J.M. Taylor and M.D. Lukin, *Phys. Rev. Lett.* **100** (2008), 073001.

[64] S.P. Jordan and E. Farhi, *Phys. Rev. A* **77** (2008), 062329.

[65] S.P. Jordan, E. Farhi and P.W. Shor, *Phys. Rev. A* **74** (2006), 052322.

[66] P. Karbach, *Phys. Rev. A* **72** (2005), 030301.

[67] A. Kay, *Phys. Rev. Lett.* **102** (2009), 070503.

[68] A. Kay, *arXiv:0903.4274* (2009).

[69] A. Kay and R. Colbeck, *arXiv:0810.3557* (2008).

[70] A. Kay and M. Ericsson, *New Jour. Phys.* **7** (2005), 143.

[71] N. Khaneja, R. Brockett and S.J. Glaser, *Phys. Rev. A* **63** (2001), 032308.

[72] C. King, *Information Theory, IEEE Transactions on* **49** (2003), 221.

[73] A.Y. Kitaev, *Physics-Uspekhi* **44** (2001), 131.

[74] A.Y. Kitaev, *Annals of Physics* **303** (2003), 2.

[75] E. Knill, R. Laflamme and W.H. Zurek, *Science* **279** (1998), 342.

[76] H. Krauter, C.A. Muschik, K. Jensen, W. Wasilewski, J.M. Petersen, J.I. Cirac and E.S. Polzik, *Phys. Rev. Lett.* **107** (2011), 080503.

[77] D. Kribs, R. Laflamme and D. Poulin, *Phys. Rev. Lett.* **94** (2005), 180501.

[78] C. Kurtsiefer, S. Mayer, P. Zarda and H. Weinfurter, *Phys. Rev. Lett.* **85** (2000), 290.

[79] T.D. Ladd, D. Maryenko, Y. Yamamoto, E. Abe and K.M. Itoh, *Phys. Rev. B* **71** (2005), 014401.

[80] R. Laflamme, C. Miquel, J.P. Paz and W.H. Zurek, *Phys. Rev. Lett.* **77** (1996), 198.

[81] C. Langer, R. Ozeri, J.D. Jost, J. Chiaverini, B. DeMarco, A. Ben-Kish, R.B. Blakestad, J. Britton, D.B. Hume, W.M. Itano, D. Leibfried, R. Reichle, T. Rosenband, T. Schaetz, P.O. Schmidt and D.J. Wineland, *Phys. Rev. Lett.* **95** (2005), 060502.

[82] D.A. Lidar, *Phys. Rev. Lett.* **100** (2008), 160506.

[83] E.H. Lieb and D.W. Robinson, *Comm. Math. Phys.* **28** (1972), 251.

[84] G. Lindblad, *Comm. Math. Phys.* **48** (1976), 119.

[85] A. Lutomirski, *arXiv:1107.0321* (2011).

[86] A. Lutomirski, S. Aaronson, E. Farhi, D. Gosset, A. Hassidim, J. Kelner and P. Shor, *arXiv:0912.3825* (2009).

[87] H. Mabuchi, *New Jour. Phys.* **11** (2009), 105044.

[88] N.B. Manson, J.P. Harrison and M.J. Sellars, *Physical Review B* **74** (2006), 104303.

[89] S. Massar and S. Popescu, *Phys. Rev. Lett.* **74** (1995), 1259.

[90] P.C. Maurer, G. Kucsko, C. Latta, L. Jiang, N.Y. Yao, S.D. Bennett, F. Pastawski, D. Hunger, N. Chisholm, M. Markham, D.J. Twitchen, J.I. Cirac and M.D. Lukin, *Science* **336** (2012), 1283.

[91] M. Mehring: *Principles of High Resolution Nmr in Solids.* 2. ed. Springer-Verlag, February 1983.

[92] G.E. Moore, *Electronics* **38** (1965), 2005.

[93] J.J.L. Morton, A.M. Tyryshkin, R.M. Brown, S. Shankar, B.W. Lovett, A. Ardavan, T. Schenkel, E.E. Haller, J.W. Ager and S.A. Lyon, *Nature* **455** (2008), 1085.

[94] M. Mosca and D. Stebila, *arXiv:0911.1295* (2009).

[95] P. Neumann, J. Beck, M. Steiner, F. Rempp, H. Fedder, P.R. Hemmer, J. Wrachtrup and F. Jelezko, *Science* **329** (2010), 542 .

[96] P. Neumann, R. Kolesov, V. Jacques, J. Beck, J. Tisler, A. Batalov, L. Rogers, N.B. Manson, G. Balasubramanian, F. Jelezko and J. Wrachtrup, *New Journal of Physics* **11** (2009), 013017.

[97] P. Neumann, R. Kolesov, B. Naydenov, J. Beck, F. Rempp, M. Steiner, V. Jacques, G. Balasubramanian, M.L. Markham, D.J. Twitchen, S. Pezzagna, J. Meijer, J. Twamley, F. Jelezko and J. Wrachtrup, *Nature Phys.* **6** (2010), 249.

[98] M.A. Nielsen, *Phys. Lett. A* **303** (2002), 249.

[99] Z. Nussinov and G. Ortiz, *Phys. Rev. B* **77** (2008).

[100] Z. Nussinov and G. Ortiz, *Ann. of Phys.* **324** (2009), 977.

[101] O. Oreshkov and T.A. Brun, *Phys. Rev. A* **76** (2007), 022318.

[102] A. Panconesi and A. Srinivasan, *SIAM Journal on Computing* **26** (1997), 350.

[103] F. Pastawski, A. Kay, N. Schuch and I. Cirac, *Phys. Rev. Lett.* **103** (2009), 080501.

[104] F. Pastawski, A. Kay, N. Schuch and I. Cirac, *Quant. Inform. and Comp.* **10** (2010), 0580.

[105] J.P. Paz and W.H. Zurek, *Proc. R. Soc. A* **454** (1998), 355.

[106] H.L. Richards, S.W. Sides, M.A. Novotny and P.A. Rikvold, *J. Magn. Magn. Mater.* **150** (1995), 37.

[107] R.L. Rivest, A. Shamir and L. Adleman, *Communications of the ACM* **21** (1978), 120.

[108] T. van der Sar, Z.H. Wang, M.S. Blok, H. Bernien, T.H. Taminiau, D.M. Toyli, D.A. Lidar, D.D. Awschalom, R. Hanson and V.V. Dobrovitski, *Nature* **484** (2012), 82.

[109] M. Sarovar and G.J. Milburn, *Phys. Rev. A* **72** (2005), 012306.

[110] V. Scarani and R. Renner, *Phys. Rev. Lett.* **100** (2008), 200501.

[111] P. Shor: *Fault-tolerant quantum computation*, In *Proceedings of the 37th Annual Symposium on Fundamentals of Computer Science*. IEEE Computer Society Press, Burlington, VT, USA (1996) pages 56–65.

[112] P.W. Shor, *Proceedings 35th Annual Symposium on Foundations of Computer Science* **35** (1994), 124.

[113] P.W. Shor, *Phys. Rev. A* **52** (1995), R2493.

[114] P.W. Shor, *SIAM J. Comput.* **26** (1997), 1484.

[115] P. Spinicelli, A. Drau, L. Rondin, F. Silva, J. Achard, S. Xavier, S. Bansropun, T. Debuisschert, S. Pezzagna, J. Meijer, V. Jacques and J. Roch, *New Jour. Phys.* **13** (2011), 025014.

[116] M. Steiner, P. Neumann, J. Beck, F. Jelezko and J. Wrachtrup, *Phys. Rev. B* **81** (2010), 035205.

[117] C.J. Terblanche, E.C. Reynhardt and J.A. van Wyk, *Solid State Nuclear Magnetic Resonance* **20** (2001), 1. PMID: 11529416.

[118] E. Togan, Y. Chu, A.S. Trifonov, L. Jiang, J. Maze, L. Childress, M.V.G. Dutt, A.S. Sorensen, P.R. Hemmer, A.S. Zibrov and M.D. Lukin, *Nature* **466** (2010), 730.

[119] A. Toom, *Problems of Information Transmission* **10** (1974), 239.

[120] D.M. Toyli, C.D. Weis, G.D. Fuchs, T. Schenkel and D.D. Awschalom, *Nano Lett.* **10** (2010), 3168.

[121] A.M. Tyryshkin, S. Tojo, J.J.L. Morton, H. Riemann, N.V. Abrosimov, P. Becker, H. Pohl, T. Schenkel, M.L.W. Thewalt, K.M. Itoh and S.A. Lyon, *Nat. Materials* **advance online publication** (2011).

[122] P. Vaidya: *Geometry helps in matching*, In *Proceedings of the twentieth annual ACM symposium on Theory of computing*STOCS. ACM (1988) pages 422–425.

[123] L.M.K. Vandersypen and I.L. Chuang, *Rev. Math. Phys.* **76** (2005), 1037.

[124] L.C. Venuti and P. Zanardi, *Phys. Rev. Lett.* **99** (2007), 095701.

[125] F. Verstraete, M.M. Wolf and J.I. Cirac, *Nature Phys.* **5** (2009), 633.

[126] G. Waldherr, J. Beck, M. Steiner, P. Neumann, A. Gali, T. Frauenheim, F. Jelezko and J. Wrachtrup, *Phys. Rev. Lett.* **106** (2011), 157601.

[127] G. Wendin, *Proc. R. Soc. A* **361** (2003), 1323 .

[128] R.F. Werner, *Phys. Rev. A* **58** (1998), 1827.

[129] S. Wiesner, *ACM SIGACT News* **15** (1983), 78.

[130] M.M. Wolf, *Nature Phys.* **4** (2008), 834.

[131] N.Y. Yao, L. Jiang, A.V. Gorshkov, P.C. Maurer, G. Giedke, J.I. Cirac and M.D. Lukin, *arXiv:1012.2864* (2010).

[132] H. Zhu and B. Englert, *Phys. Rev. A* **84** (2011), 022327.

List of Figures

Acknowledgements

I am greatly indebted to my supervisor, Ignacio Cirac, for proposing exciting research programs and providing the appropriate environment to carry them out. Throughout these years he has been very generous in providing time for discussion and guidance, while also offering me the freedom to develop my scientific independence.

I would like to thank Alastair Kay, Norbert Schuch, Lucas Clemente, Peter Maurer, Georg Kucsko, Norman Yao, Liang Jiang and Mikhail Lukin for their fruitful and constructive collaboration on the different research projects pursued during this thesis.

I also would like to acknowledge the people who have been especially generous with their guidance. Miguel Aguado, was a true mentor and introduced me to the notions required for understanding the topological approach to quantum memory and computing. Eric Kessler has provided invaluable help in guiding my dive into the literature of Nitrogen Vacancy centres. I should also thank, Geza Giedke, Mari Carmen Banuls, Maarten van den Nest and Thomas Schulte-Herbrüggen for their valuable advice and stimulating discussion.

Special thanks go to Heike and Anika without whom this thesis would be lost in translation. Thank you for always bringing good mood into the office and for the good advice. I would also like to thank, Leonardo, Oriol, Gemma, Matteo, Martin Schütz, Bierger, Tassilo, Sébastien, Michael, Oliver and the rest of my colleagues and friends at MPQ for their company through many fun side activities such as football, jam sessions, poker, hikes and grilling. It was a great fun.

To my parents for their support from the distance.

Finally, I would like to thank Leonore, for her support and bearing through the swinging effects of research on my moods during my time at MPQ.

I should also acknowledge the financial support of the Elitenetzwerk Bayern through the "Quantum Computation Communication and Control" and of the Max-Planck Society.

Curriculum Vitae

Fernando Pastawski born January 5^{th} 1982 in Córdoba, Argentina.

Education

2008-20012	Max-Planck-Institut für Quantenoptik *Ph.D. research*
2000-2008	Universidad Nacional de Córdoba *Physics master GPA 9.62 of 10*
2000-2005	Universidad Nacional de Córdoba *Computer Science master GPA 9.76 of 10*
1995-1999	Academia Argüello Highschool (Córdoba - Argentina)

Scholarships

2006	Fundación Deloite Scholarship
2005-2006	Conciencia scholarship from the Science Agency of Córdoba
1997-1998	Bernardo Houssay Scholar

Experience

2007	Universidad de Buenos Aires (UBA). *Teaching assistant*
Mar-Aug 2006	INRIA Everest group Sophia-Antipolis France. *Research intern*, Topic: "Type Theory and Result Certification"
Apr-Aug 2004	INRIA Everest group Sophia-Antipolis France. *Research intern*, Topic: "Type Based Termination"
2002-2004	Universidad Nacional de Crdoba *Undergraduate teaching assistant*
2003	Chemistry Department Universidad Nacional de Córdoba *programmer* Control and data acquisition software for a dye-laser.

Awards

2004	2^{nd} highest average of the National University of Córdoba
2004	2^{nd} in ACM programming competition South American regional
2004	1^{st} place Paenza University Mathematics Competitions (Argentina)
1998 & 1999	Bronze medal in the International Mathematical Olympiads (IMO)
1999 & 2000	Gold medal in Iberoamerican Mathematical Olympiads (OIM)